MuRF3 binds to the retromer subunit SNX5 inhibiting its MuRF2-mediated degradation and leading to its stabilization

Dissertation

zur Erlangung des akademischen Grades
doctor rerum naturalium (Dr. rer. nat.)
im Fach Biologie

eingereicht an der
Lebenswissenschaftlichen Fakultät der Humboldt-Universität zu Berlin
von

Diplom Biologin Jida Hamati

Präsident der Humboldt-Universität zu Berlin: Prof. Dr. Jan-Hendrik Olbertz
Dekan der Lebenswissenschaftlichen Fakultät: Prof. Dr. Richard Lucius

Gutachter: 1. Prof. Dr. Thomas Sommer

2. PD Dr. med. Jens Fielitz

3. Prof. Dr. Oliver Daumke

Tag der mündlichen Prüfung: 01.12.2015

Table of Contents

List of Figures

List of Tables

Abstract

Muscle specific RING-Finger ubiquitin E3 ligases MuRF1, MuRF2 and MuRF3 have been implicated in several cellular functions. MuRF1 and MuRF3 have been shown to bind and degrade muscle contractile and structural proteins via the ubiquitin proteasome system (UPS), thus playing an important role in the maintenance of skeletal and cardiac muscle structure and function. MuRF1 is considered an atrophy marker since its expression increases during muscle atrophy. MuRF2 and MuRF3 are involved in myocyte differentiation. In addition, both proteins bind to and stabilize microtubules. Nevertheless, many aspects of the functions of the MuRF-family are unknown. The domain structure of the MuRF family implicates several highly conserved domains involved in protein-protein interaction. Accordingly, one way to better understand the role of MuRF proteins in myocyte function and protein homeostasis is to identify and characterize their interactome. Therefore, quantitative mass spectrometric analysis was used to identify novel interaction partners and target proteins of MuRF1, MuRF2 and MuRF3.

In this study, the mammalian retromer subunit sorting nexin 5 (SNX5), which plays an important role in subcellular trafficking pathways, was identified as a novel interaction partner of MuRF3. SNX5 interacted via its Bin/Amphiphysin/Rvs (BAR)-domain with MuRF3. SNX5 and MuRF3 co-localized and associated with early endosomes, connecting the microtubule-binding MuRF3 to structures of subcellular trafficking pathway. SNX5 was also identified as a substrate of MuRF2, which interacted with and ubiquitinated SNX5 *in vivo*, mediating its degradation in a UPS-dependent manner. Interestingly, this MuRF2-mediated degradation was inhibited by MuRF3, which stabilized SNX5.

The role of MuRF2 and MuRF3 in stabilizing microtubules has been reported only in relation to muscle differentiation and contraction. In this study, MuRF2 and MuRF3 were linked for the first time with a subcellular trafficking protein, SNX5, which is directly associated with microtubules and functionally dependent on a stable microtubule network. Therefore, results may suggest a possible regulatory role of MuRF2 and MuRF3 in microtubule-dependent subcellular trafficking pathways.

Keywords: MuRF, UPS, SNX5, microtubules

Zusammenfassung

Die muskelspezifischen RING-Finger Ubiquitin E3 Ligasen MuRF1, MuRF2 und MuRF3 wurden mit verschiedenen zellulären Prozessen in Verbindung gebracht. MuRF1 und MuRF3 beteiligen sich zum Beispiel am Abbau mehrerer Muskelstrukturproteine über das Ubiquitin Proteasom System (UPS) und spielen somit eine wichtige Rolle bei der Aufrechterhaltung der Skelett- und Herzmuskelstruktur und -funktion. MuRF1 wurde als Atrophie-Marker identifiziert, da seine Expression während der Muskelatrophie ansteigt. Darüber hinaus wirken MuRF2 und MuRF3 bei der Stabilisierung von Mikrotubuli und Differenzierung von Myozyten mit. Dennoch sind bisher viele Aspekte der Funktion von MuRF-Proteinen ungeklärt. Die Domänenstruktur der MuRF-Proteinfamilie zeigt mehrere hochkonservierte Domänen, die sich an Protein-Protein Interaktionen beteiligen. Die Identifizierung und Charakterisierung ihres Interaktoms ermöglicht ein besseres Verständnis ihrer Funktionen. Aus diesem Grund wurden quantitative massenspektrometrische Analysen durchgeführt, um neue Interaktionspartner und Substrate für MuRF1, MuRF2 und MuRF3 zu identifizieren.

In der vorliegenden Arbeit wurde sorting nexin 5 (SNX5), eine Untereinheit des Retromer-Komplexes in Säugetieren, als Interaktionspartner von MuRF3 identifiziert. SNX5, das eine wichtige Rolle in subzellulären Transport-Signalwegen spielt, interagiert über seine BAR-Domäne mit MuRF3. Außerdem wurde gezeigt, dass SNX5 und MuRF3 co-lokalisieren und mit vesikulären Strukturen des subzellulären Transport-Signalweges assoziieren. Des Weiteren wurde SNX5 als Substrat von MuRF2 identifiziert. MuRF2 bindet und ubiquitiniert SNX5 *in vivo* und vermittelt damit dessen Abbau über das UPS. Interessanterweise stabilisierte MuRF3 SNX5 und inhibierte dessen MuRF2-vermittelten Abbau.

Die Rolle von MuRF2 und MuRF3 bei der Stabilisierung von Mikrotubuli wurde bisher nur in Bezug auf Muskeldifferenzierung und Kontraktion beschrieben. In dieser Studie konnten sie zum ersten Mal mit einem in subzellulärem Transport aktiven Protein in Verbindung gebracht werden, das direkt mit Mikrotubuli assoziiert und funktionell von einem stabilen Mikrotubuli-Netzwerk abhängig ist. Dies legt eine mögliche regulatorische Rolle von MuRF2 und MuRF3 in Mikrotubuli-abhängigen subzellulären Transportwegen nahe.

Schlagwörter: MuRF, UPS, SNX5, Mikrotubuli

1 Introduction

1.1. The skeletal muscle

The skeletal muscle is the largest body compartment and the most abundant tissue in adult vertebrates, comprising 40-50% of total body mass. Its main function is maintaining the integrity of the skeleton and generating force for motion. In addition, skeletal muscle is the primary target of glucose uptake and by undergoing size - remodeling, it represents the determining factor of endurance, physical strength and performance (Fanzani A. *et al*., 2012). Furthermore, skeletal muscle is the largest protein reservoir of the body. Through protein degradation, skeletal muscle serves as a source of amino acids which can be used for energy production by various organs including the heart, liver and brain. This is essential not only in extreme situations like stress, inflammation and fasting, but also during longer catabolic periods, such as in cancer, sepsis, burn injury, heart failure and AIDS (Karagounis L.G. and Hawley J.A., 2010, Bonaldo P. and Sandri M., 2013).

1.1.1. Structure and composition

Muscle cells, or myocytes, are formed through the fusion of developmental myoblasts (embryonic progenitor cells) in a process known as myogenesis. These long cylindrical cells, also called myofibers, contain multiple nuclei, mitochondria and sarcomeres, and are the contractile units of the skeletal muscle (Fig. 1). Muscle fibers are each surrounded by a thin layer of connective tissue called the endomysium, and 20-80 of them are bundled together in a parallel arrangement to form the muscle fascicle. Muscle fascicles are each encapsulated by the perimysium, and a large number of them are enveloped by a thick collagenous external layer extending from the tendons, called the epimysium, to form a single skeletal muscle (Fig. 1; Boron W.F. and Boulpaep E.L., 2009, Korthuis R.J., 2011).

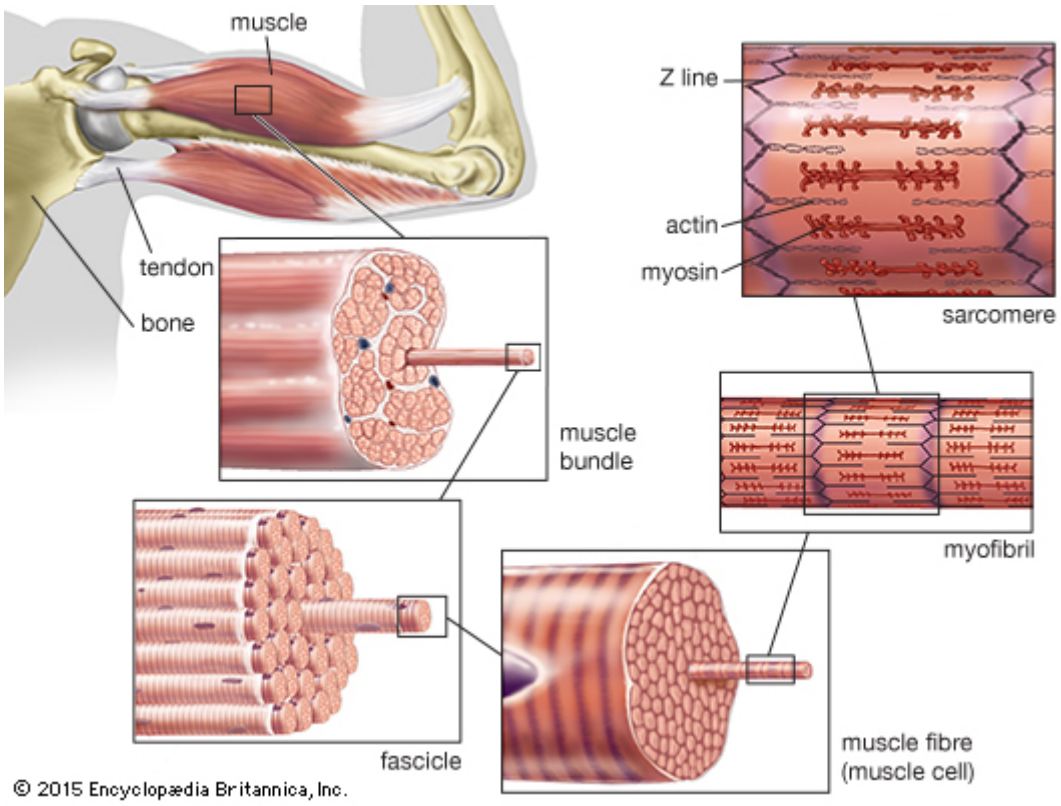

Figure 1: The anatomy and composition of the striated skeletal muscle. Muscle cells or fibers are enveloped by a thin collagenous layer, the endomysium. A bundle of parallelly arranged myofibers form the muscle fascicle, which is surrounded by the perimysium. A large number of muscle fascicles, encapsulated by a thick collagenous layer extending from the tendon called epimysium, form the skeletal muscle. Skeletal muscles are supplied by a large number of blood vessels and nerves. By courtesy of Encyclopaedia Britannica, Inc., copyright 2015; used with permission.

Different muscle fibers are classified not only by their histology, but also by the rapidity of their contraction, the ability to resist fatigue and the expression of specific myosin heavy chain (MHC) isoforms. The rate of contraction in the different muscle fiber types is related to the ATPase activity of the specific MHC isoform expressed in this particular muscle fiber type (Korthuis R.J., 2011). Type I fibers are slow-twitch red myofibers, which are thinner and contain a dense capillary network and a large amount of the oxygen-binding protein myoglobin. They are resistant to fatigue, contain high amounts of mitochondria and oxidative enzymes and low glycogen levels and glycolytic enzyme activity, thus relying on oxidative metabolism for energy production. Type II fibers are fast-twitch myofibers, which are sub-classified into red type IIa and white type IIb fibers. Type IIa myofibers are fatigue-resistant, contain myoglobin, high amounts of mitochondria and rely on oxidative metabolism. Type IIa muscle fibers are also glycogen-abundant. Type IIb myofibers contain less mitochondria, oxidative enzymes and myoglobin and therefore rely on the energy stored in glycogen and phosphocreatine. They are less resistant to fatigue (Armstrong R.B., 1996; Boron W.F. and

Boulpaep E.L., 2009). In humans three muscle fiber types were classified as I, IIa and IIx (Gundersen K., 2010; Schiaffino S. and Reggiani C., 2011). Fiber type IIx was previously known as IIb, and was shown to express a *MHC* gene homologous to the IIx gene of a fourth isoform discovered in rodents (Schiaffino S. and Reggiani C., 1996; Ennion S. *et al*., 1995; Smerdu V. *et al*., 1994). Fascicles are composed of two or more fiber types, but usually one of these fiber types predominates in the different muscle types (Korthuis R.J., 2011).

The plasma membrane of the muscle cell is known as sarcolemma. It surrounds the myofibrils and generates specialized invaginations, called T-tubules, which penetrate into the muscle interior. T-tubules communicate with the calcium reservoir, stored in the sarcoplasmic reticulum. Calcium is released from the sarcoplasmic reticulum upon nerve stimulation to initiate muscle contraction. In addition to the T-tubules, there are further specialized regions of the sarcolemma, such as the neuromuscular junctions (NMJs), where motor neurons contact the muscle, the digit-like projections that form myotendinous junctions (MTJs), which are major force transmission sites, and sites of myoblast fusion during myogenesis and muscle repair (Clark K.A. *et al*., 2002; Sanes J.R. *et al*., 1999; Burden S.J. *et al*., 2002). An intact membrane trafficking system to and from these unique membrane regions of the muscle cell is essential for maintaining muscle structure and function, as well as muscle myogenesis and regeneration (Towler M.C. *et al.,* 2004 a).

1.1.2. Skeletal muscle physiology - the sarcomere

The sarcomere is the smallest functional contractile unit of the muscle fiber (McComas A.J. *et al*., 1996). It comprises of the myofibrillar proteins myosin (the thick filament), actin and its associated proteins (the thin filament). The interaction between myosin and actin allows the muscle to contract (Plowman S.A. *et al*., 1997). Myosin is a very large protein which is composed of six polypeptides: two heavy chains and four light chains, of which two are regulatory and two are alkali. One regulatory and one alkali light chain are associated with one of the heavy chains. The head region of the MHC is not only the domain which interacts with actin allowing the muscle to contract, but it also contains an adenosine triphosphate (ATP) binding site and functions as an ATPase for hydrolyzing ATP into adenosine diphosphate (ADP) and inorganic phosphate (PI), providing the necessary energy for muscle contraction (Plowman S.A. *et al*., 1997). The thin filament consists of actin and two regulatory proteins, troponin and tropomyosin (McComas A.J. *et al*., 1996).

Muscle contraction occurs when the muscle fiber receives a stimulus in the form of an action potential, which leads to the release of calcium from the sarcoplasmic reticulum. Calcium then binds to troponin, a small globular protein with three subunits (TnT, TnI, TnC), which as a result undergoes a conformational change and pulls tropomyosin from its blocking position on the actin filament, exposing the myosin binding sites and allowing myosin heads to interact with actin. Myosin pulls the thin filament along the thick filament, which leads to the shortening of the sarcomere and contraction of the muscle. In the presence of Ca^{2+} and ATP, the myosin heads will attach to the actin molecules, pull the actin, release, and reattach. This process is known as cross-bridge cycling (Plowman S.A. *et al*., 1997; Scott W. *et al.*, 2001).

A third filament system in the sarcomere is composed of one single molecule, titin, the largest vertebrate protein identified to date (Maruyama K. *et al*., 1977; Wang K. *et al*., 1979). While actin-containing thin filaments are anchored in the so-called Z-lines and extend toward the middle of the sarcomere where they interact with myosin to drive contraction, the large titin filaments span half sarcomeres, with their N-termini overlapping the Z-lines and C-termini overlapping the M-lines, thus forming a continuous filament system between adjacent myofibrils. Based on its assembly and structure, titin is proposed to function as a template for myofibrillogenesis (Obermann W.M. *et al*., 1997; Gregorio C. *et al*., 1998, 2005; Mues A. *et al*., 1998).

1.2. Skeletal muscle atrophy

The skeletal muscle makes up a very large proportion of the total body mass, and in particular total body protein. Under normal physiological conditions, the protein homeostasis of the muscle fiber is guaranteed by a well coordinated balance between protein degradation and protein synthesis, which in turn has a significant effect on the general protein homeostasis of the body (Schiaffino S. *et al*., 2013). Skeletal muscle atrophy takes place when this homeostasis is disrupted and protein degradation exceeds protein synthesis, leading to a decrease in muscle mass. Muscle atrophy can be physiological (i.e. as a consequence of aging) or pathological. Age-related muscle atrophy, or sarcopenia, is defined as the presence of both low muscle mass and low muscle function (Cruz-Jentoft A.J. *et al*., 2010), which leads to decrease in the individual's mobility and life quality. Other triggers of muscle atrophy are malnutrition, severe burns, as well as muscle disuse (i.e. long periods of immobilization or bed rest, denervation, or spaceflight; Thomas, D. R., 2007).

Moreover, muscle atrophy represents the severe clinical syndrome known as cachexia, which accompanies many chronic illnesses such as chronic heart failure (CHF), chronic obstructive pulmonary disease (COPD), chronic kidney disease (CKD), cancer, AIDS, sepsis, immune disorders, myopathies and dystrophies (Thomas, D. R., 2007). Cachexia is defined as weight loss greater than 5% or weight loss greater than 2% and a body mass index (BMI) lower than 20 (Fearon K. *et al*., 2011). This complex metabolic syndrome is characterized by excessive loss of muscle mass and body fat, weakness and increase in morbidity and mortality (Bonaldo P. and Sandri M., 2013).

Regardless of the triggering factor, the main characteristics of muscle atrophy are a decrease in protein content, a reduction of the cross-sectional area of myofibers, decreased muscle strength and fatigue resistance (Vandervoort A.A., 2002). The clinical consequence of muscle atrophy, whether caused by physiological or pathological conditions, is similar, namely a severe deterioration of life-quality and the inability to manage daily activities (Fanzani A. *et al*., 2012).

The different types of conditions inducing muscle atrophy are an indication for different types of molecular triggers and signaling pathways for muscle atrophy. Indeed, many different catabolic factors, such as cytokines (e.g. tumor necrosis factor (TNF)-α, interleukin-1, interleukin-6), the transforming growth factor (TGF)-family (e.g. TGF-β, myostatin, activin), glucocorticoids, angiotensin II, low insulin-like growth factor (IGF)-1, but also stress stimuli and DNA damage, activate different signaling pathways, which in turn activate proteolytic pathways leading to muscle atrophy. The two major protein degradation pathways in eukaryotic cells are the ubiquitin-proteasome system (UPS) and the autophagy lysosome pathway. Under physiological conditions the UPS is responsible for the degradation of short-lived proteins, and the autophagy lysosome pathway regulates the levels of long-lived proteins and cell-organelles. Both pathways have been shown to crosstalk and play important roles in muscle atrophy (Jagoe R.T. *et al*., 2002; Glass D.J. *et al*., 2005; Jackman R.W. and Kandarian S.C., 2004; Fanzani A. *et al*., 2012).

1.3. Ubiquitin proteasome system

The UPS is responsible for the highly specific recognition and degradation of a large number of target proteins, which in turn control and regulate numerous cellular processes such as cell cycle, transcription and protein quality control (i.e. the degradation of misfolded or damaged proteins). The UPS comprises about 1000 components and is subjected to stringent regulation

at different steps of the cascade. Aberrations in its function can lead to different diseases such as myopathies (i.e. limb girdl muscular dystrophy, protein aggregate myopathy, hypertrophic cardiomyopathy; Mathews K.D. and Moore S.A., 2003; Predmore J.M., 2010), cancer, inflammatory and neurodegenerative disorders (Hershko A. and Ciechanover A, 1998; Weissman A.M., 2011).

Ubiquitin is a heat-stable, abundant and highly conserved 8-kDa polypeptide, which is ubiquitously expressed in eukaryotic cells. It is effective only by covalent attachment to other proteins in the ATP-dependent process of ubiquitination, which results in mono- or polyubiquitinated proteins (Ciechanover A. *et al*., 1980 a; Ciechanover A. *et al*., 1980 b). Within the polyubiquitin chain, the single molecules are connected through isopeptide bonds, formed between the C-terminal glycine 76 of one molecule and a lysine residue of the other ubiquitin molecule. Ubiquitin exhibits seven lysine residues (Lys 6, 11, 27, 29, 33, 48 and 63), but Gly76-Lys48 linked ubiquitin chains are the predominant recognition signal for subsequent proteasomal degradation (Glickman M. H. and Ciechanover A., 2002; Wilkinson K. D., 2000).

The addition of polyubiquitin (at least four molecules) to a substrate protein as a recognition signal for subsequent degradation at the proteasome is a reversible and regulated multistep reaction, which requires three distinct enzymatic components; an E1 ubiquitin-activating enzyme, an E2 ubiquitin-conjugating enzyme and an E3 ubiquitin-ligating enzyme (Hershko A. *et al.*, 1983; Hershko A. and Ciechanover A., 1998; Weissman A.M., 2001). In mammals, two E1-, approximately 40 E2- and several hundred E3-enzymes are known (Pickart C.M., 2001; Weissman A.M., 2011). Substrate specificity of the UPS is mediated by the E3 ubiquitin ligase. There are two major groups of E3 ubiquitin ligases which differ in their mechanism of action; the homologous to E6 associated protein C- terminus (HECT) domain E3 ligases, and the RING (Really Interesting New Gene) finger domain E3 ligases. The latter can function as a single enzyme or a multi-subunit protein complex. Single-subunit E3 enzymes mediate ubiquitination using the RING domain for E2 enzyme binding and a different domain to bind the substrate. Multi-subunit RING E3 ligases, such as the SCF (Skp-Cullin-F-box) complex, contain a cullin protein family member as scaffold, RING finger protein as E3 ligase and additional proteins as adaptors for substrate recognition and E2-enzyme binding (Kandarian S.C. and Stevenson E.J., 2002; Pickart C.M., 2004; Ciechanover A. and Iwai K., 2004; Deshaies R.J. and Joazeiro C.A., 2009).

The ubiquitin-proteasome cascade starts with the ATP-dependent activation of ubiquitin by the E1-enzyme, which uses ATP to form a high energy labile E1-thiol ester intermediate. The activated ubiquitin is then transferred to the E2-enzyme to generate a similar thiol ester intermediate. The activated ubiquitin can then either be transferred directly from E2 to an internal lysine residue of a substrate protein, which is already bound to a RING finger domain containing - E3- ligase, or it can be transferred from the E2 to a HECT domain - containing E3 ligase to form a third labile thiol ester intermediate. It is then transferred to the substrate protein, where a stable isopeptide bond between the activated ubiquitin and an internal lysine residue in the substrate is formed. Ubiquitin-conjugated substrates bind to the proteasome either directly or through shuttling proteins, where they are degraded to short peptides by the 26S proteasome. The ubiquitin chain is then disassembled by deubiquitinating enzymes (DUBs), which can also function as antagonists for E3s (Fig. 2; Hershko A. *et al.*, 1983; Glickman M.H. and Ciechanover A., 2002; Pickart C.M., 2000; Weissman A.M. *et al.,* 2011).

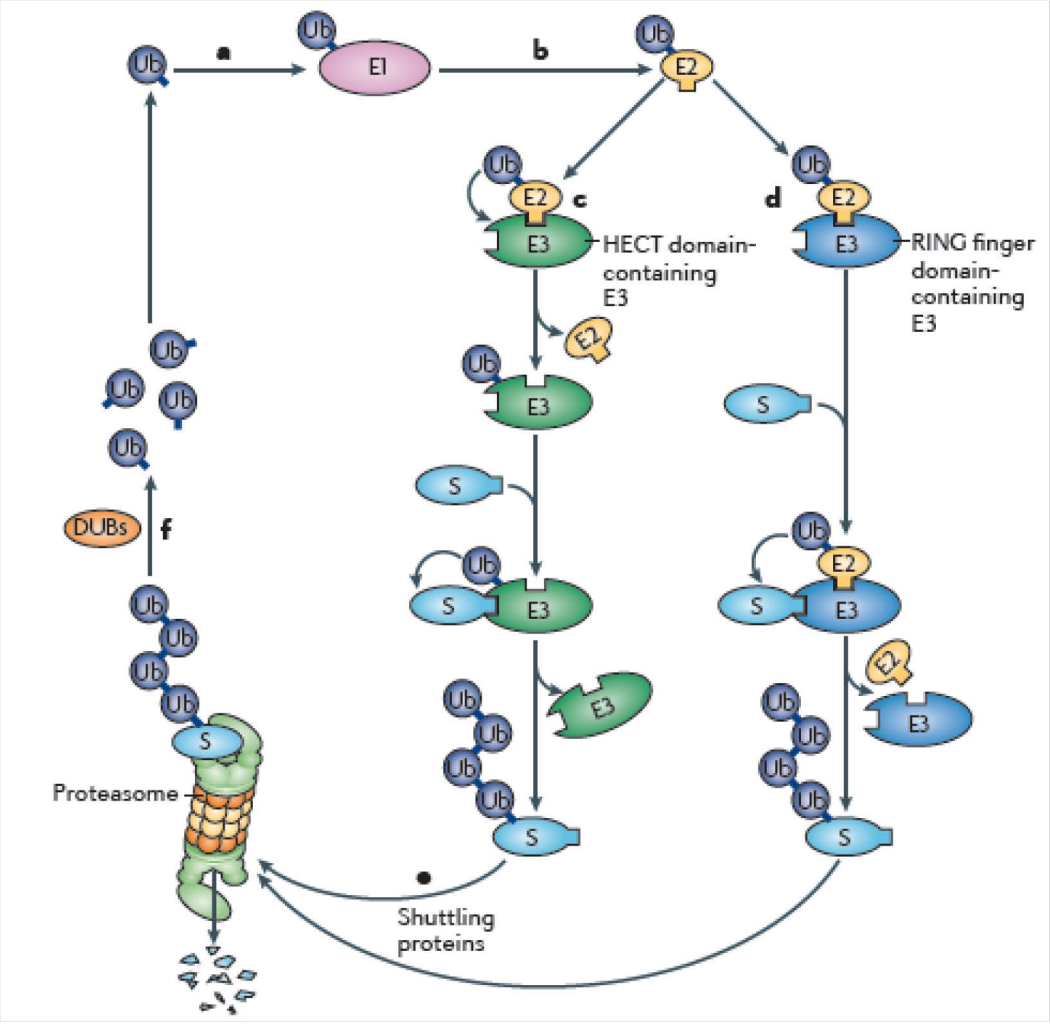

Figure 2: Schematic illustration of the ubiquitin-proteasome system. (a) Ubiquitin-activating enzyme (E1) activates ubiquitin (Ub) in an ATP-dependent step, forming a high-energy, labile E1-thiol ester intermediate. **(b)**

A similar thiol ester intermediate is formed when the activated ubiquitin is transferred to an ubiquitin-conjugating enzyme (E2). **(c)** Activated ubiquitin can then be transferred to a HECT domain-containing ubiquitin-protein ligase (E3) to form a third labile thiol ester intermediate. Ubiquitin is then transferred to the substrate (S), where a stable isopeptide bond is formed. A polyubiquitin chain is generated when additional ubiquitin moieties are added. **(d)** Alternatively, activated ubiquitin can be transferred directly from E2 to the Lys residue of a substrate that is already bound to a RING finger domain-containing ubiquitin ligase. **(e)** Ubiquitin-conjugated substrates bind directly or through shuttling proteins to the 26S proteasome, where they are degraded to short peptides. **(f)** Polyubiquitin chains are mostly disassembled by de-ubiquitinating enzymes (DUBs). Adapted by permission from Macmillan Publishers Ltd: Nature reviews molecular cell biology, Weissman A.M. *et al*., copyright 2011 http://www.nature.com/nrm/index.html

Protein degradation in the UPS is mediated by the 26S proteasome, a large protein complex composed of two sub-complexes: the catalytic active 20S core particle (CP) and the 19S regulatory particle (RP). The CP consists of four stacked heptameric rings, outer α- and inner β- rings, giving it a barrel-shaped structure. Three of the β- subunits display proteolytic activity. The RP consists of two sub-complexes, called lid and base, with the base sub-complex associating with the outer α- rings of the CP. The RP is the subunit responsible for substrate recognition, recruitment, de-ubiquitination and translocation into the CP, where it is subsequently degraded (Finley D., 2009; Schmidt M. and Finley D., 2013; Weissman A.M. *et al.,* 2011).

1.4. Muscle specific ubiquitin E3 ligases

Muscle-specific RING-finger (MuRF) proteins were identified by Spencer *et al*. (Spencer J.A. *et al*., 2000) while searching for interaction partners of the serum response factor (SRF). MuRF-proteins are expressed specifically in cardiac and skeletal muscle and possess ubiquitin ligase activity (Spencer J.A. *et al*., 2000). They belong to the RING-B-box-coiled-coil (RBCC) subclass of RING-finger proteins, which are characterized by an NH_2-terminal RING-finger followed by a zinc-finger domain (B-box), two leucine-rich coiled-coil domains and a C-terminal acidic region (Spencer J.A. *et al*., 2000; Centner T. *et al*., 2001; Dai K.S. and Liew C.C., 2001). The tripartite organization of the RBCC domains is highly conserved, which explains the important functional role of this protein structure. The RING-finger domain is a zinc-binding cysteine-histidine protein motif found in numerous proteins involved in signal transduction, gene transcription, differentiation, morphogenesis and ubiquitination of target proteins as ubiquitin E3 ligases (Borden K.L., 1998; Centner T. *et al*., 2001).

1.4.1. Muscle specific RING finger protein 1 (MuRF1)

MuRF1, which is encoded by the gene *Trim63* (tripartite motif containing 63), was characterized as a muscle specific ubiquitin E3 ligase in 2001 by Bodine *et al*., together with

the muscle specific F-box protein Atrogin 1/MAFbx (muscle atrophy F-box), as both proteins were shown to be upregulated during skeletal muscle atrophy caused by denervation, hindlimb suspension and immobilization in rats (Bodine S.C. *et al*., 2001; Gomes M.D. *et al*., 2001). Both were later shown to be also upregulated in multiple animal models of muscle atrophy, such as sepsis- and starvation-induced atrophy (Wray C.J. *et al*., 2003; Kee A.J. *et al*., 2003). Interestingly, knockout mice for either *Trim63* or *Fbxo32* are phenotypically normal. However, these mice are resistant to muscle atrophy induced by denervation (Bodine S.C. *et al*., 2001). *Trim63* knockout mice are also resistant to dexamethasone-induced muscle atrophy (Baehr L.M. *et al*., 2011). Therefore, MuRF1 and MAFbx are used as early markers for skeletal muscle atrophy, aiding in the diagnosis of muscle disease (Bodine S.C. *et al*., 2001).

MuRF1 interacts with and controls the half-life of several important muscle structural proteins, including troponin I (Kedar V. *et al*., 2004), myosin heavy chains (Clarke B.A. *et al*., 2007; Fielitz J. *et al*., 2007b), actin (Polge C. *et al*., 2011), myosin binding protein C and myosin light chains (Cohen S. *et al*., 2009). Furthermore, MuRF1 binds to titin at the M-band of the sarcomere, which has been shown to maintain the stability of the sarcomeric M-line region (Centner T. *et al*., 2001; McElhinny A.S. *et al*., 2002; Gotthardt M. *et al*., 2003). MuRF1 has been implicated in cardiac hypertrophy (Willis M.S. *et al.,* 2007).

1.4.2. Muscle specific RING finger protein 2 (MuRF2)

MuRF2 is encoded by the gene *Trim55* (tripartite motif containing 55). MuRF2 is expressed in at least four isoforms generated by two distinct differential splicing mechanisms. Three splice variants share the common N-terminal RING-finger and B-box domains and end in a common C-terminal sequence. They encode peptides of 27, 50 and 60 kDa, and are also referred to as MuRF2A. The smallest MuRF2 isoform, MuRF2A p27, is cardiac specific. The forth isoform, MuRF2B p60, has an alternative C-terminus, which is generated by alternative reading frame use due to a frameshift of the last coding exon, a novelty in muscle proteins (Pizon V. *et al*., 2002; McElhinny A.S. *et al*., 2004).

A recent study by Pizon *et al.* (Pizon V. *et al*., 2013) showed that the expression ratio between MuRF2A and MuRF2B isoforms changes during differentiation of skeletal muscle cells, and that this shift in isoform expression follows the sequential activation of the autophagic or the proteasomal degradation pathway. Furthermore, MuRF2B interacts with microtubule-associated protein 1A/1B light chain 3A (LC3), a protein needed for autophagic vesicles

formation (Pizon V. *et al*., 2013), whereas MuRF2A isoforms can form complexes with the autophagic proteins p62 and neighbor of BRCA1 gene 1 (NBR1) in myogenic cells. These two proteins act as cargo receptors for the degradation of ubiquitinated substrates by autophagy (Musa H. *et al*., 2006; Lange S. *et al*., 2005).

MuRF2 expression analysis during mouse embryonic cardiac and skeletal muscle development shows that expression of MuRF2A p50 and p60 isoforms is developmentally regulated, with the expression shifting from the embryonic predominant p50 isoform to the p60 isoform, which dominates postnatally. Furthermore, MuRF2A expression during embryonic development parallels that of the autophagic proteins LC3, p62 and NBR1 (Perera S. *et al*., 2011; Perera S. *et al*., 2012). MuRF2B isoform was also shown to be developmentally controlled (Pizon V. *et al*., 2013).

During atrophic stress, MuRF2 is briefly translocated to the nucleus and nuclear lamina in cardiomyocytes (Lange S. *et al*., 2005; Pizon V. *et al*., 2002), and in skeletal muscle *in vivo* (Lange S. *et al*., 2005; Ochala J. *et al*., 2011), suggesting a role in the transcription program during myocyte differentiation.

In mature cardiac myocytes, endogenous MuRF2 associates with the M-band of the sarcomere (Pizon V. *et al*., 2002). Apart from titin and myosin, it has been shown to interact with nebulin, troponin I and T, myotilin and T-cap in yeast two-hybrid assays (Witt S.H. *et al*., 2005). To date, very little is known about the E3 ligase function of MuRF2, and no MuRF2 substrate proteins have been identified thus far.

1.4.3. Muscle specific RING finger protein 3 (MuRF3)

MuRF3 is encoded by the gene *Trim54* (tripartite motif containing 54). It was the first MuRF-protein to be identified and characterized. Two human and one mouse isoforms for MuRF3 have been identified. It associates with and stabilizes microtubules, and is required for skeletal myocyte differentiation and development and formation of cellular microtubular networks (Spencer J.A. *et al*., 2000; Centner T. *et al*., 2001). MuRF3 is upregulated only postnatally (Perera S., *et al*., 2011).

MuRF3, like MuRF1 and 2, localizes to the M-line and Z-disc of the sarcomere, forms homodimers and heterodimers with the other two MuRF-proteins (Centner T. *et al*., 2001; McElhinny A.S. *et al*., 2004; Gregorio C., 2005), and exhibits an E3 ligase activity (Kedar V. *et al*., 2004). It has been shown to play an important role in maintaining cardiac integrity and

function after acute myocardial infarction, by regulating the turnover of its target proteins four-and-a-half LIM domain (FHL2) and γ-filamin. FHL2 and γ-filamin are sarcomere associated proteins, FHL2 interacts with the M-band portion of titin and γ-filamin localizes to the Z-discs and functions as actin-cross-linking protein. Mice lacking *Trim54* showed diminished cardiac function and susceptibility to ventricular rupture after acute myocardial infarction (Fielitz J. *et al.,* 2007 a).

MuRF3 and MuRF1 are the two key E3 ubiquitin ligases for the UPS-dependent turnover of contractile sarcomeric proteins. They mediate the ubiquitination and degradation of MHCIIa and β/slow MHC, with UbcH5a, -b or -c functioning as E2 ubiquitin-conjugating enzymes. Combined deficiency in both *Trim63* and *Trim54* in double knockout mice results in a protein aggregate myopathy, characterized by subsarcolemmal MHC accumulation in skeletal and cardiac myocytes, accompanied by skeletal muscle myopathy, reduced maximal force development, hypertrophic cardiomyopathy and decreased cardiac function, indicating their importance in the maintenance of skeletal and cardiac muscle structure and function (Fielitz J. *et al.,* 2007 b).

1.4.4. Association of MuRF2 and MuRF3 with microtubules

MuRF2 plays an important role in the earliest steps of heart and skeletal muscle differentiation. During myogenic differentiation, glutamylated microtubules are transiently formed, while the dynamic pool of tyrosinated tubulin is simultaneously reduced (Gundersen G. *et al*., 1989). These glutamylated microtubules seem to be involved in the active transport of sarcomeric proteins to the sites of myofibrillogenesis (Pizon V. *et al*., 2002). Through its transient association with stable glutamylated microtubules, MHC and titin during early myofibrillogenesis MuRF2 acts as an adaptor between the sarcomeric proteins and the microtubule network. During this complex, dynamic and extremely precise process, MuRF2 first binds microtubules at the exclusion of tyrosinated tubulin. Through transient association with sarcomeric myosin and A-band titin, these MuRF2-associated microtubules are suggested to play a regulatory role in the subsequent incorporation of myosin into nascent sarcomeres and the elongation of titin when non-striated myofibrils differentiate into mature sarcomeres (Pizon V. *et al*., 2002). However, MuRF2 is excluded from the mature skeletal sarcomeres, which is in agreement with the very weak expression in adult cardiac and skeletal tissues, and its down-regulation during myocyte differentiation (Centner T. *et al*., 2001; Pizon V. *et al*., 2002).

MuRF3 also associates with microtubules, thus regulating their dynamics. Like MuRF2, it associates with the stable glutamylated microtubules during myofibrillar assembly (Pizon V. *et al*. 2002; Spencer J.A. *et al*., 2000). The leucine-rich coiled coil domain of MuRF3 is necessary and sufficient for this interaction. However, amino acids 168-211 are required for optimal association, and the RING-finger domain is required for continuous binding along and stabilization of microtubules *in vivo* (Spencer J.A. *et al*., 2000). Therefore, MuRF3 plays a role in establishing and maintaining a stable microtubule array which is required for muscle differentiation (Gundersen G. *et al*., 1989; McElhinny A.S. *et al*., 2004).

1.5. Membrane trafficking pathways in skeletal muscle

Skeletal muscle cells exhibit the usual housekeeping membrane trafficking pathways for the sorting of newly synthesized proteins, internalizing cell surface receptors for hormones and nutrients and mediating membrane repair. However, due to the unique muscle-specific membrane structures, the special metabolic requirements, and the high demand for membrane repair in a tissue which is constantly under mechanical stress, these trafficking pathways are further specialized (Towler M.C. *et al*., 2004 a). One example is the muscle-specific regulation of glucose transporter type 4 (GLUT4) trafficking, which is critical for glucose metabolism in this energy-demanding tissue (Rudich A. *et al*., 2003). Another example is the identification of increasing numbers of muscle-specific isoforms of proteins (e.g. muscle-specific clathrin heavy chain 22) known to play a role in trafficking pathways, as well as novel muscle-specific proteins, which seem to be involved in tissue-specific aspects of muscle membrane trafficking (Liu S.H. *et al*., 2001). Although membrane repair occurs in all eukaryotic cells, it appears to be more complex in muscle, where mechanical stress continuously challenges membrane integrity. Thus, specialized proteins such as dysferlin are required for maintaining mechanical integrity of the muscle. Dysferlin is associated with the sarcolemma and plays a role in muscle membrane traffic. Mutations in human dysferlin are linked to slow progressive forms of muscular dystrophy and dysferlin-null mice have a defect in muscle membrane repair pathways (Bansal D. *et al*., 2003).

In the last two decades, great progress has been made in skeletal muscle research which focused mainly on structural and cytoskeletal proteins. However, it has become obvious that these alone cannot coordinate a functional unit, and that the orchestration of the multi-functional events in skeletal muscle requires additional signaling and membrane trafficking proteins. Moreover, a large number of hereditary myopathies are caused by mutations in genes encoding for proteins involved in the organization of muscle membrane and the

coordination of interactions between internal muscle structures, muscle membrane and the extracellular matrix (ECM; reviewed in Towler M.C. *et al*., 2004 a). Therefore, a better understanding of specialized muscle membrane trafficking pathways is important for gaining insights into muscle disease and processes critical for muscle development and repair.

1.5.1. Endosomal trafficking pathway

The endosomal network comprises a series of interconnected tubulovesicular membranous compartments that begins at the plasma membrane with the internalization of cargo through endocytosis, where it enters the early endosome (EE; Mayor S. and Pagano R.E., 2007). The EE is a dynamic compartment with a high homotypic fusion capacity, high contents of phosphatidylinositol 3-monophosphate (PtdIns(3)P), and a characteristic morphology of vacuolar and tubular subdomains (Cullen P.J., 2008). It displays a complex and pleiomorphic structure which consists of a central cisternal region (referred to as *cis* region which receives incoming vesicles from the plasma membrane and the *trans*-Golgi network) from which tubular and vesicular elements emanate (the *trans* region of the organelle; Fig. 3; Gruenberg J. and Howell K.E., 1989; Mukherjee S. and Maxfield F.R., 2000).

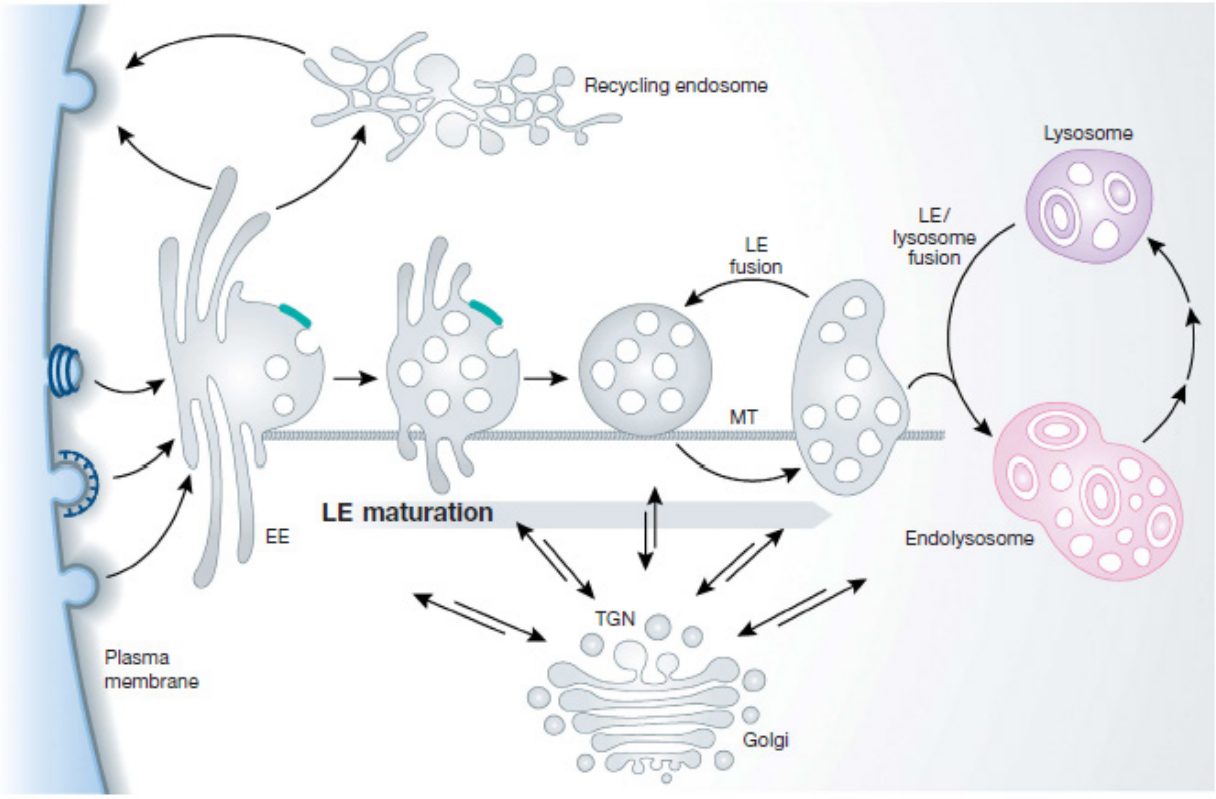

Figure 3: The endosomal trafficking pathway. Endosomal cargo export pathways originate from multiple, functionally distinct gateways along the entire endosome maturation pathway. Endocytic vesicles deliver their contents and membranes to early endosomes (EEs) in the peripheral cytoplasm. During endosome maturation, endosomes move towards the perinuclear space along microtubules (MT), leading to the formation of late

endosomes (LEs), which inherit the vacuolar domains of the EE network with endocytosed cargo combined with newly synthesized lysosomal hydrolases and membrane components from the secretory pathway. During maturation, endosomes undergo homotypic fusion, grow in size and acquire more intraluminal vesicles (ILVs), before they finally fuse with a lysosome, generating a transient hybrid organelle, the endolysosome, which is subsequently converted to the classical dense lysosome. Adapted by permission from John Wiley & Sons Inc.: The EMBO Journal, Huotari J. and Helenius A., copyright 2011 http://emboj.embopress.org/

EEs represent the first and main cargo sorting station in the pathway, primarily into two distinct pathways, which are very well separated, both topologically and functionally: the endosomal-lysosomal degradative pathway, one major function of which is the down-regulation of signaling receptors, and several distinct retrieval and recycling pathways, such as recycling toward the plasma membrane or retrograde transport toward the trans-Golgi network (TGN; Cullen P.J. and Korswagen H.C., 2013). Although the different compartments of these pathways can be easily identified due to their characteristic organization and topology, the boundaries between two distinguishable compartments in the same pathway are blurred at the molecular level. This is partially because key proteins which regulate membrane transport are often found in more than one compartment (Fig. 3; Gruenberg J., 2001).

In higher eukaryotic cells, endocytosis of proteins and lipids is mainly mediated by clathrin-coated vesicles. The common clathrin is a large protein which comprises three heavy and three light chains and polymerizes into a triskelion. Clathrin-triskelions assemble into polyhedral lattices to form clathrin coats (Mayor S. and Pagano R.E., 2007). After cargo is endocytosed into the mildly acidic lumen (pH ≈ 6.2) of EEs, its efficient sorting occurs. Recycling receptors are rapidly segregated away from their ligands and transported in recycling endosomes (REs) to the plasma membrane, whereas ligands, together with down-regulated receptors, follow the endosomal-lysosomal degradation pathway (Gruenberg J., 2001; Maxfield F.R. and McGraw T.E., 2004). Quantitatively, endocytosis and recycling back cargo to the plasma membrane represent the major membrane trafficking pathways of mammalian cells. Therefore, membrane lipids and proteins must be recycled in an efficient and accurate manner (Howes M.T. *et al*., 2010). REs differ from EEs in their acidification properties and the selective subset of proteins and lipids they contain, including the Rab GTPases (Scott C.C. and Gruenberg J., 2011; Hsu V.W, and Prekeris R., 2010). Small GTPases of the Rab family are selectively associated with each compartment, and provide the most important identity markers and master regulators in the cytotic pathway. While Rab5 and its effectors determine the functions of EEs, such as membrane fusion, recycling of receptor molecules to the plasma membrane occurs either directly and rapidly in a Rab4-controlled pathway, or indirectly via REs in a Rab11-dependent manner (Chavrier P. *et al*.,

1990; Ullrich O. *et al*., 1994; Galvez T. *et al.,* 2012). Another recycling pathway is the retrograde transport pathway of cargo from EEs to the TGN. Retrograde sorting to the TGN is mediated by the retromer complex (Seaman M.N., 2012; Burd C. and Cullen P.J., 2014), which will be discussed later in detail.

1.5.2. Endosome maturation

The transport from early to late endosomes (LEs), a pathway also known as endosome maturation, is also accompanied by major protein and lipid remodeling and changes in the endosomal luminal milieu. The limiting membrane of LEs contains lysosomal membrane proteins such as lysosomal-associated membrane protein 1 (LAMP1) and the lumen contains a complement of acid hydrolases causing a decrease in luminal pH values from ≈ 6.2 in EE to ≈ 5.5/5.0 in LEs (Scott C.C. and Gruenberg J., 2011). In addition, endosome maturation involves a conversion from Rab5 (in EEs) to Rab7 (in LEs), a so-called Rab switch, which also appears to control recruitment of the retromer to endosomal membranes (Rojas R. *et al*., 2008; Seaman M.N., 2012). Rab7 and its effectors regulate the functions of LEs and lysosomes (Rink J. *et al*., 2005; Jovic M. *et al.,* 2010). Endosome maturation begins with the sorting of proteins that need to be degraded, such as activated signaling receptors, into luminal invaginations of the EE membrane, which branch off as free cargo-containing intraluminal vesicles (ILVs), a step which controls signaling. These ILVs then detach from EEs and become free multivesicular bodies (MVBs), or endosomal carrier vesicles (ECVs). Once formed, MVB/ECVs rapidly acidify and mediate microtubule-dependent transport toward LEs, with which they eventually fuse, delivering their protein and lipid cargo. Just like EEs, LEs show high homotypic fusion activity, and contain multivesicular regions and highly dynamic tubulo-cisternal elements. They serve as a second trafficking hub and sorting station in the endocytic pathway. ILVs and their cargo can either be packaged into lysosomes for degradation, or sorted toward other destinations, e.g. they can be released extracellularly as exosomes upon endosome fusion with the plasma membrane (Fig. 3; Bissig C. and Gruenberg J., 2013; Huotari J. and Helenius A., 2011; Raposo G. and Stoorvogel W., 2013). LEs also function at a crossroad with the autophagy pathway, which provides an additional entry route into the endocytic pathway for the degradation of cytosolic components and organelles at the lysosome (Sandri M., 2011; Lamb C.A. *et al*., 2013). LEs and lysosomes undergo rapid fusion events of their membranes (kiss and run fusion), forming a transient hybrid organelle, the endolysosome, and allowing interchange of cargo and enzymes. Endolysosomes are then

converted into the classical lysosomes (Fig. 3; Luzio J.P. *et al*., 2007; Huotari J. and Helenius A., 2011; Scott C.C. *et al*., 2014).

1.5.3. Retrograde and recycling pathways and the Retromer - complex

In the past years, a lot has been reported about the signals and mechanisms of cargo sorting into the endo-lysosomal degradative pathway. Nevertheless, understanding recycling pathways, and how cargo is retrieved from lysosomal degradation, is still limited. While the main cargoes of retrograde pathways are sorting receptors and molecules whose functions depend on continual retrieval from the endosomal system back to the biosynthetic pathway, plasma membrane recycling cargoes include nutrient transporters, signaling and cell adhesion receptors, and are therefore more diverse in structure. Retrieval of cargoes is mediated by the assembly of coat complexes, which recognize specific cargoes, drive membrane remodeling and elicit scission to form cargo-enriched carriers which bud from the endosomes into the cytoplasm (Bonifacino J.S. and Rojas R., 2006; Johannes L. and Popoff V., 2008; Grant B.D. and Donaldson J.G., 2009; Maxfield F.R. and McGraw T.E., 2004). In recent years, the protein family of sorting nexins (SNX) has been shown to play very important roles as coat complexes in multiple endosomal recycling pathways, prominently as subunits of the retromer-complex (Fig. 4; Cullen P.J., 2008; Cullen P.J. and Korswagen H.C., 2013; Burd C. and Cullen P.J., 2014).

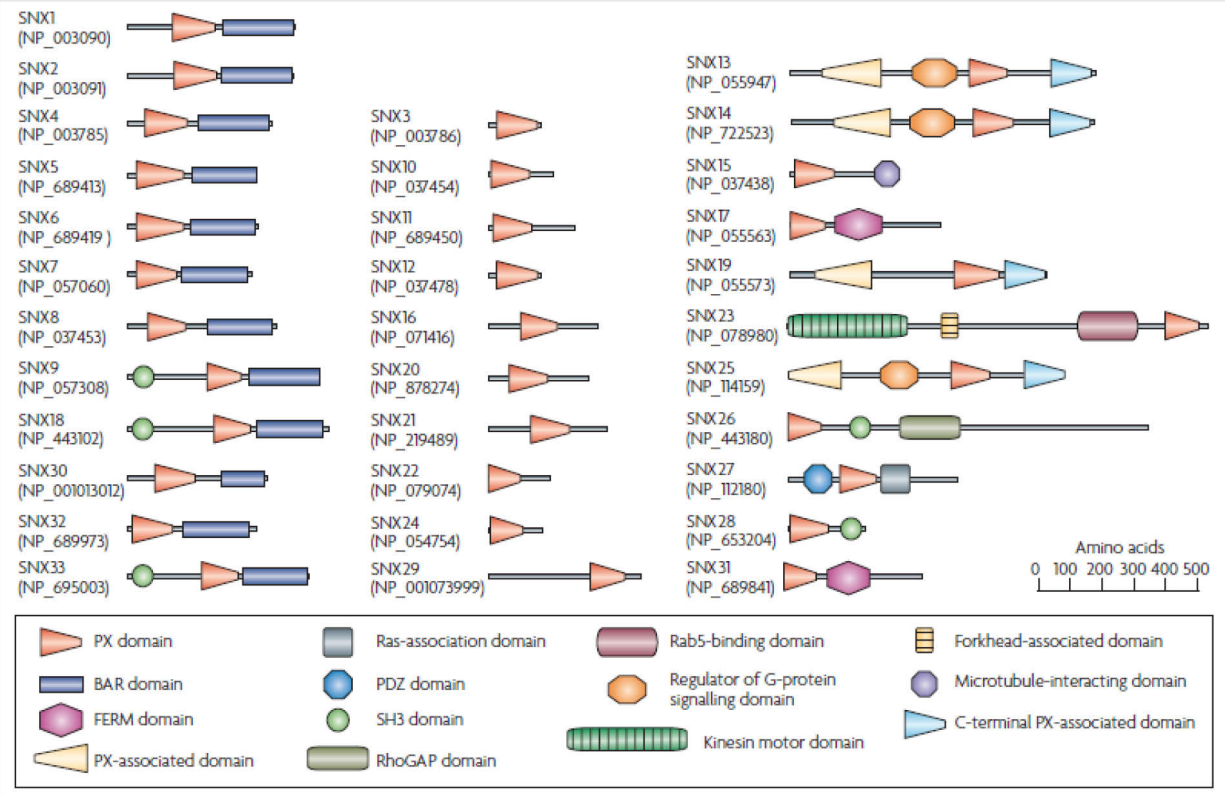

Figure 4: Domain architecture of the mammalian sorting nexins. A depiction of the 33 mammalian sorting nexins known to date, which are classified into 3 subfamilies: those which only an isolated SNX-PX domain (middle); those which contain a C-terminal BAR domain in addition to the SNX-PX domain (SNX-BAR, left); and those which contain other recognized domainsin addition to the SNX-PX domain (right). FERM= protein4.1, ezrin, radixin, moesin; PDZ= postsynaptic density protein-95, Discs-large, Zona-occludens-1; RhoGap= Rho GTPase-activating protein; SH3= Src- homology-3. Adapted by permission from Macmillan Publishers Ltd: Nature reviews molecular cell biology, Cullen P.J., copyright 2008 http://www.nature.com/nrm/index.html

SNXs are an evolutionarily conserved family of proteins classified by the presence of a unique type of a PtdIns(3)P-binding phox-homology (PX) domain, the SNX-PX domain. SNXs are associated with PtdIns(3)P-enriched elements of the endosomal pathway, and play roles in diverse processes such as endocytosis, endosomal sorting and signaling. Based on the presence of a C-terminal Bin/Amphiphysin/Rvs (BAR) domain, several SNXs have been classified as the SNX-BAR subfamily (Fig. 4; Teasdale R.D. *et al*., 2001; Carlton J.G. *et al*., 2004; Cullen P.J., 2008).

The retromer is an endosomal coat multi-protein complex which was first identified in yeast, where it mediates the retrieval of a TGN sorting receptor (Vps10) from the endosome to the TGN. It is formed through the association of two sub-complexes: the first is a highly conserved and stable heterotrimeric complex of the subunits Vps26, Vps29 and Vps35, which recognizes cargo proteins and is therefore called the cargo selective complex (CSC). The CSC does not have an intrinsic membrane binding activity and relies on the association with the

second sub-complex for endosome recruitment (Seaman M.N. *et al*., 1997; 1998). The second sub-complex contains a heterodimer of the SNX-BAR-proteins Vps5 and Vps17, which induce and/or stabilize the formation of membrane tubules (van Weering J.R. *et al*., 2012 a; 2012 b; Burd C. and Cullen P.J., 2014). In mammals, Vps5 has two orthologs, SNX1 and SNX2, whereas Vps17 has the orthologs SNX5, SNX6 and possibly SNX32. Heterodimerization occurs when one Vps5 ortholog dimerizes with one Vps17 ortholog (Wassmer T. *et al*., 2007; van Weering J.R. *et al.,* 2010; Koumandou V.L. *et al*., 2011). In addition to these two sub-complexes, the retromer recruits additional proteins that mediate further cargo capture and packaging, such as SNX3 and SNX27 (Strochlic T.I. *et al*., 2007; Temkin P. *et al.,* 2011), as well as accessory proteins like EHD1 which regulates maturation and scission of the retromer tubules (Gokool S. *et al*., 2007; Gomez T.S. and Billadeau D.D., 2009; Harbour M.E. *et al*., 2010; Seaman M.N. *et al*., 2009; Wassmer T. *et al*., 2009).

Cargo selection sub-complex

The core component of the CSC is Vps35, which forms a horseshoe-shaped α-helix onto which Vps26 and Vps29 independently bind at either distal end (Norwood S.J. *et al*., 2011; Hierro A. *et al*., 2007). Most retromer cargoes possess at least one hydrophobic motif, F/W-L-M/V, which is required for retromer-dependent sorting, and their interaction with the CSC is of low affinity (Seaman M.N., 2007). Although little is known about the manner by which the CSC recognizes cargo, it is assumed that multiple direct and indirect cargo-recognition mechanisms exist (Cullen P.J. and Korswagen H.C., 2013).

SNX-BAR-sub-complex and membrane remodeling

The PX domain of SNX1 and SNX2 has been shown to associate with endosomal PtdIns (3)P and phosphatidylinositol 3,5-bisphosphate (PtdIns(3,5)P_2) (Cozier G.E. *et al.,* 2002). Upon dimerization with SNX5 and SNX6 through their BAR-domains, a positively charged crescent-shaped surface is formed, which has the ability to sense, and through electrostatic interactions, bind membrane curvature (Peter B.J. *et al*., 2004; Carlton J. *et al*., 2004; 2005). In addition, SNX1 and SNX2 are capable of inducing membrane remodeling which leads to membrane tubulation. Both of them contain amphipathic helixes in their N-BAR domains that form in the cytosol-lipid interface causing surface tension between the leaflets of the bilayer, which the membrane accommodates by generating positive curvature (i.e. bends into the cytosol). This membrane curvature is stabilized by the curvature-sensing properties of the BAR-domains (Frost A. *et al*., 2009; Bhatia V.K. *et al*., 2009). Recently, it has been

suggested that the retromer SNX-BARs switch between curvature-sensing and curvature-inducing modes, thus driving the formation of endosomal tubules (van Weering J.R. *et al*., 2010).

Retromer-mediated sorting is initiated when the CSC concentrates cargo into the SNX-BAR defined membrane tubule prior to a fission event that generates the endosome-to-TGN carriers. This is followed by multiple fission and fusion events, which progressively enrich retromer-labeled endosomes with specific cargo as they migrate from the cell periphery towards the TGN in the perinuclear region (Wassmer T. *et al*., 2009).

1.5.4. Endosome motility along microtubules

Endosome maturation is a dynamic process, in which endosome movement and location in the cytoplasm are tightly linked to their stage of maturation, size, cargo contents and function. During the formation of EEs in the cell periphery, they are subjected to slow short-range back and forth movements along microtubules, but as they mature, they undergo long-range saltatory oscillations with a net movement towards the perinuclear region, where the majority of lysosomes are localized (Nielsen E. *et al*. 1999; Bananis E. *et al*., 2000; 2004; Driskell O.J. *et al*., 2007; Loubery S. *et al*., 2008). The centripetal movement along microtubules that radiate out from the microtubule organizing center (MTOC) is mediated by kinesin and dynein motor proteins, which provide opposing forces that move endosomes in opposite directions (Murray J.W. *et al*., 2000; Soppina V. *et al*., 2009). Kinesins constitute a large family of mainly plus-end-directed motor proteins, some of which, like KIF16B and KIF3A, have been implicated in EE and LE motility. KIF16B is a kinesin-3 motor protein and a member of the SNX family. It is also known as SNX23 (Fig. 4). It attaches to EEs through its PtdIns(3)P binding PX domain when Rab5 is activated, and seems to alter the balance between degradation and recycling of cargo; its depletion leads to a block of cargo recycling and an increase in cargo degradation whereas its overexpression has the opposite effect (Hirokawa N. *et al*., 2009; Hoepfner S. *et al.*, 2005; Brown C.L. *et al*., 2005). On the other hand, dynein-dependent, minus-end-directed endosome motility brings cargo to the proximity of lysosomes in the perinuclear area (Bananis E. *et al*., 2004). Organelles bind to dynein motors either directly or indirectly through adaptor protein complexes, such as the dynactin multiprotein complex (Huotari J. and Helenius A., 2011). This motor activity is required for fission of EEs, sorting of cargo into recycling and degradative compartments and fusion of endosomes during endosome maturation (Bananis E. *et al*., 2000; Driskell O.J. *et al*., 2007).

Recent studies have shown that SNX5 and SNX6 are functionally and mechanistically associated with the microtubule cytoskeleton through their interaction with the dynactin component p150^{glued} (also known as dynactin subunit 1, DCTN1), an activator of the minus-end-directed microtubule motor dynein. By recruiting the dynein/dynactin motor complex, the SNX-BAR retromer subcomplex coordinates cargo sorting and tubular-based carrier formation at the donor endosomal membrane with long-range minus-end-directed microtubule-based transport and carrier recognition at the recipient TGN membrane. This association regulates the dynamic spatial organization of the endosomal network, which is required for efficient retromer-mediated endosomal protein sorting along the microtubules towards the MTOC where the TGN is localized (Cullen P.J., 2008; Wassmer T. *et al*., 2009; Hong Z. *et al*., 2009).

1.6. Sorting nexin 5 (SNX5)

SNX5 was identified as a new member of the SNX-BAR subfamily by Otsuki *et al.* when it was reported to bind the Fanconi anemia complementation group A protein (FANCA; Otsuki T. *et al*., 1999). As a product of the *sorting nexin 5* gene, SNX5 is 46.8 kDa and consists of one phosphoinositide-binding PX-domain and one BAR-domain, which contains three coiled coil domains (Fig. 4; Worby C.A. and Dixon J.E., 2002; Hara S. *et al.,* 2008). SNX5 interacts with SNX1 and SNX2 and shares 66% amino-acid identity with SNX6, suggesting they might share cellular functions (Worby C.A. and Dixon J.E., 2002; Wassmer T. *et al*., 2007; Bonifacino J.S. and Hurley J.H., 2008).

SNX5 plays a role in the retrograde transport of the cation-independent mannose 6-phosphate receptor (CI-MPR)/ insulin-like growth factor II receptor (IGF2R; Seaman M.N., 2005; Hara S. *et al.*, 2008; Wassmer T. *et al*, 2007), the endosomal trafficking of epidermal growth factor receptor (EGFR), and E-Cadherin (Liu H. *et al*., 2006; Merino-Trigo A. *et al*., 2004; Sun Y. *et al*., 2013; Schill N.J. *et al*., 2014). SNX5 binds to type I gamma phosphatidylinositol phosphate 5-kinase i5 (PIPKIγi5), an enzyme which synthesizes PtdIns4,5P_2, and they both prevent the ubiquitination of the Hrs protein which facilitates its association with EGFR, thus leading to EGFR sorting into ILVs and its degradation (Sun Y. *et al*., 2013). However, SNX5 can also act antagonistically to PIPKIγi5, preventing the lysosomal degradation of E-Cadherin (Schill N.J. *et al*., 2014).

In addition, SNX5 functions as modulator of macropinocytosis by playing an essential role in macropinosome biogenesis. Macropinocytosis mediates the endocytosis of solute molecules,

nutrients and antigens, and is therefore important in functions associated with immune responses (Kerr M.C. *et al*., 2006; Lim J.P. *et al*., 2008; Wang J.T. *et al*., 2010; Lim J.P. *et al.,* 2012). Furthermore, SNX5 interacts with Mind bomb-1 (Mib1), an E3 ubiquitin ligase which is a key regulator of ligands of the Notch signaling pathway, and is suggested to regulate the functions of Mib1 and therefore plays an essential role in cell fate determination in mammalian early development (Yoo K.W. et al., 2006; Weinmaster G. and Fischer J.A., 2011). A recent *in vivo* study of SNX5 showed that mice lacking the *Snx5* gene exhibited partial perinatal mortality, with approximately 40% of the animals dying within a day of birth. Neonatal mice lacking the *Snx5* gene showed significant breathing defects associated with cyanosis and reduced pulmonary air space at birth, and histological analysis revealed they had reduced alveolar epithelial type I cells, indicating that *Snx5* is necessary for the differentiation of these cells during perinatal murine lung development (Im S.K. *et al.,* 2013).

1.7. SNX5 and the GLUT4 trafficking pathway

In a study by Towler *et al*. in 2004, SNX5 was identified as an interaction partner of the muscle specific isoform of clathrin heavy chain, CHC22 (Towler M.C. *et al.,* 2004 b). CHC22 was discovered during the human genome project analysis of chromosome 22 (Kedra D. *et al*., 1996; Long K.R. *et al*., 1996; Sirotkin H. *et al*., 1996). It is expressed at high levels in skeletal muscle, somewhat lower levels in cardiac muscle and testes, and only at low levels in other tissues. Although the sequences of CHC22 and the ubiquitously expressed CHC17, which forms the clathrin coated vesicles, are 85% identical, initial studies showed that the two CHCs have different intracellular distributions, some distinct biochemical properties and are apparently regulated differently (Liu S.H. *et al*., 2001; Towler M.C. *et al.,* 2004 b). While each CHC17 subunit in the clathrin triskelion is bound by a regulatory light chain (LC), CHC22 trimerizes but does not bind clathrin LCs. Instead, SNX5 binds to the region in CHC22 where the light chain would normally bind to CHC17 for negative regulation of clathrin assembly (Brodsky M. *et al*., 2001). SNX5 does not bind CHC17 indicating a muscle tissue-specificity for the function of both CHC22 and SNX5. In addition, CHC17 and CHC22 bind different subsets of adaptor proteins (Towler M.C. *et al*., 2004 a). In mature muscle CHC22 is preferentially concentrated at neuromuscular and myotendinous junctions, suggesting a role at sarcolemmal contacts with extracellular matrix. CHC22 expression is increased during myoblast differentiation and also in regenerating muscle fibers, indicating a role in muscle repair (Towler M.C. *et al*., 2004 b).

In a recent study, CHC22, which exists in mice only as a pseudogene, exhibiting species-specificity (Wakeham D.E. *et al*., 2005), has been shown to play an important role in human glucose metabolism (Vassilopoulus S. *et al*., 2009). In muscle and fat tissues, the intracellular trafficking of glucose transporter GLUT4, the major GLUT isoform responsible for glucose translocation in mammalian skeletal muscle, is triggered during the body's response to insulin and exercise. GLUT4 is then exported from the intracellular GLUT4 storage compartments (GSCs) to the plasma membrane to clear glucose from the bloodstream (Bryant N.J. *et al*., 2002; Hou J.C. *et al*., 2007; Huang S. *et al*., 2007). GLUT4 membrane trafficking is disrupted in some forms of human type 2 diabetes leading to expanded and defective GSCs and increased intracellular sequestration (Garvey W.T. *et al*., 1998; Maianu L. *et al*., 2001). CHC22 was shown to be involved in the biogenesis of insulin-responsive GSCs in human muscle and adipocytes, independent from CHC17, and it exhibits high levels in the expanded GSCs in muscle from type 2 diabetic patients (Vassilopoulus S. *et al*., 2009). CHC22 mediates an intermediate stage of retrograde endosomal sorting of GLUT4 to the perinuclear TGN, which occurs after the CHC17-dependent step required for retrograde cargo exit from EEs, and is essential for its subsequent transport to GSCs. This CHC22-mediated sorting of GLUT4 requires the recruitment of retromer through binding to SNX5 and does not overlap with CHC17 function (Esk C. *et al*., 2010). It has also been shown to require dynein/dynactin motor activity on microtubules and an intact microtubule-network (Guilherme A. *et al*., 2000; Shigematsu S. *et al*., 2002; Ishiki M. and Klip A., 2005).

The expression of both CHC22 and GLUT4 is elevated in regenerating rat muscle, as well as regenerating skeletal muscle fibers from patients with inflammatory and other myopathies, implicating a role of the GLUT4 transport pathway in muscle regeneration (Towler M.C. *et al*., 2004 b; Hoshino S. *et al*., 2013).

1.8. Aim of the study

The aim of this study was using quantitative mass spectrometric analyses for the identification and characterization of novel interaction partners and target proteins of MuRF1, MuRF2 and MuRF3. This experimental approach allowed the investigation of different cellular conditions and the changes in MuRF protein-interactions which occur during a specific cellular process such as myocyte differentiation or atrophy of myotubes. Furthermore, it enabled the comparison between the interactomes of the different MuRF-proteins. By identifying and characterization of MuRF-interaction partners and target proteins, this technique was expected to offer a better understanding of the functions of MuRF proteins as ubiquitin E3 ligases, and the role they play in protein homeostasis, stabilizing of microtubules and myocyte differentiation.

2 Materials and Methods

2.1. Materials and instruments

2.1.1. Equipment and instruments

Table 1: Equipment and instruments used in this study

Instrument	Company
-80°C refrigerator ultra low	Sanyo, München, Germany
6 well plates	BD Biosciences, Heidelberg, Germany
Agarose gel chamber BlueMarine™ 200	SERVA Electrophoresis GmbH, Heidelberg, Germany
Bacteria hood	BDK Luft- und Reinraumtechnik GmbH, Sonnenbühl-Genkingen, Germany
Balance	FAUST GmbH, Meckenheim, Germany
Cell culture hood FAZ3	Waldner Electronics GmbH & Co., Gräfelfing, Germany
Cell culture flasks	BD Biosciences, Heidelberg, Germany
Cell scrapers	TPP Techno Plastic Products AG, Trasadingen, Switzerland
Centrifuge 1K15	SIGMA Laborzentrifugen GmbH, Osterode am Harz, Germany
Centrifuge 3K10	Laborzentrifugen GmbH, Osterode am Harz, Germany
Ceramic spheres	PEQLAB Biotechnology GmbH, Erlangen, Germany
CT15RE Centrifuge	VWR, Darmstadt, Germany
Development machine Curix 60	Agfa-Gevaert N.V., Mortsel, Belgium
Dissecting instruments	Fine Science Tools GmbH, Heidelberg, Germany
DNA/RNA UV-Cleaner UVT-S-AR	Biolabo Scientific Instruments, châtel-St-Denis, Switzerland
Electrophoresis Power Supply EPS 301	GE Healthcare GmbH, Solingen, Germany
FastPrep®-24 Instrument	MP Biomedicals GmbH, Eschwege, Germany
Fluo Star optima	BMG Labtech GmbH, Ortenberg, Germany
Fluorescence microscope	Leica Microsystems GmbH, Wetzlar, Germany
Gene pulser cuvettes 0.1 cm	Bio-Rad Laboratories GmbH, München, Germany
High performance chemiluminescence films	GE Healthcare GmbH, Solingen, Germany
Incubator	Thermo Fischer Scientific inc., Waltham, USA
Invers microscope	Nikon GmbH, Düsseldorf, Germany

Instrument	Company
KS 4000i Control Incubator Shaker	IKA®-Werke GmbH & Co. KG, Staufen, Germany
MicroAmp® Fast Optical 96-Well Reaction Plate	Life Technologies Corporation, Carlsbad, California, USA
Micro wave	SEVERIN Elektrogeräte GmbH, Sundern, Germany
MicroPulser Electroporator	Bio-Rad Laboratories GmbH, München, Germany
Mini Centrifuge	ROTH, Karlsruhe, Germany
Mini Trans-Blot Cell	Bio-Rad Laboratories GmbH, München, Germany
Mini-PROTEAN Tetra Electrophoresis System	Bio-Rad Laboratories GmbH, München, Germany
Nanodrop1000	Thermo Fischer Scientific inc., Waltham, USA
peqSTAR 96 Universal Gradient PCR machine	PEQLAB Biotechnology GmbH, Erlangen, Germany
Photometer Gene quant	GE Healthcare GmbH, Solingen, Germany
Pipets	Eppendorf AG, Hamburg, Germany
PowerPac Basic Power Supply	Bio-Rad Laboratories GmbH, München, Germany
Refrigerators	Liebherr-International Deutschland GmbH, Biberach an der Riss, Germany
Roll mixer RM5	NeoLab, Heidelberg, Germany
Safety hood	Köttermann GmbH & Co KG, Uetze/Hänigsen, Germany
Sanyo CO_2 incubator	Cotech Vertriebs GmbH, Berlin, Germany
Software LAS	Leica Microsystems GmbH, Wetzlar, Germany
Software LAS AF	Leica Microsystems GmbH, Wetzlar, Germany
SPE Confocal Microscope	Leica Microsystems GmbH, Wetzlar, Germany
Step one Plus Real-Time PCR System	Life Technologies Corporation, Carlsbad, California, USA
Thermomixer comfort	Eppendorf AG, Hamburg, Germany
UV-transilluminator	Phase, Lübeck, Germany
Vacusafe comfort Integra	Biosciences GmbH, Fernwald, Gemany
Vortex-Genie 2	ROTH, Karlsruhe, Germany
Water bath	GFL Gesellschaft für Labortechnik mbH, Burgwedel, Germany

2.1.2. Reagents and chemicals

Table 2: Reagents and chemicals used in this study

Reagent	Company
1 kb DNA marker	ROTH, Karlsruhe, Germany
100 bp DNA marker	ROTH, Karlsruhe, Germany
2-mercaptoethanol	ROTH, Karlsruhe, Germany
2-propanol	ROTH, Karlsruhe, Germany
Acetic acid	ROTH, Karlsruhe, Germany
Acrylamide 30 %	Merck KGaA, Darmstadt, Germany
Advantage® HD Polymerase	Clontech, Mountain View, USA
Agarose	ROTH, Karlsruhe, Germany
Albumin Fraction V (Bovine Serum Albumin)	ROTH, Karlsruhe, Germany
Ammonium peroxodisulphate (APS)	ROTH, Karlsruhe, Germany
Ampicillin	Sigma-Aldrich Chemie GmbH, München, Germany
Amylose Resin	New England Biolabs GmbH, Frankfurt/Main, Germany
Anti FLAG M2 Affinity Gel	Sigma-Aldrich Chemie GmbH, München, Germany
BCA Protein Assay Reagent	Thermo Fischer Scientific inc., Waltham, USA
Bromophenol blue	Sigma-Aldrich Chemie GmbH, München, Germany
Buffer P1	Qiagen, Hilden, Germany
Buffer P2	Qiagen, Hilden, Germany
Buffer P3	Qiagen, Hilden, Germany
Chloroacetamide	Sigma-Aldrich Chemie GmbH, München, Germany
Chloroform	ROTH, Karlsruhe, Germany
cOmplete, EDTA-free Protease Inhibitor Cocktail Tablets	Roche Deutschland Holding GmbH, Grenzach-Wyhlen, Germany
Cycloheximide	Sigma-Aldrich Chemie GmbH, München, Germany
dFBS (dialyzed FBS)	Sigma-Aldrich Chemie GmbH, München, Germany
Developer solution G153	Agfa-Gevaert N.V., Mortsel, Belgium
Dexamethasone	Sigma-Aldrich Chemie GmbH, München, Germany
D-glucose	Sigma-Aldrich Chemie GmbH, München, Germany
DMEM, low glucose (1 g/l), with L glutamine	PAA Laboratories GmbH, Pasching, Austria

Reagent	Company
DMEM, high glucose (4.5 g/l), with L glutamine	PAA Laboratories GmbH, Pasching, Austria
dNTP-Set	PEQLAB Biotechnology GmbH, Erlangen, Germany
Di-methyl-sulfoxide (DMSO)	Sigma-Aldrich Chemie GmbH, München, Germany
Dulbecco's PBS (1x) w/o Ca & Mg (D-PBS)	PAA Laboratories GmbH, Pasching, Austria
EDTA	Sigma-Aldrich Chemie GmbH, München, Germany
Ethanol 99 %	ROTH, Karlsruhe, Germany
Ethidium bromide 1 %	ROTH, Karlsruhe, Germany
Fetal bovine serum (FBS)	PAA Laboratories GmbH, Pasching, Austria
Fixer solution G354	Agfa-Gevaert N.V., Mortsel, Belgium
Fugene6 Transfection Reagent	Roche Deutschland Holding GmbH, Grenzach-Wyhlen, Germany
G-418 Sulfat (Neomycin)	PAA Laboratories GmbH, Pasching, Austria
GST-E1	R & D Systems
GST-UbcH5a	R & D Systems
Glycerol	Merck KGaA, Darmstadt, Germany
Glycine	ROTH, Karlsruhe, Germany
Hybond ECL Nitrocellulose Membrane	GE Healthcare GmbH, Solingen, Germany
Kanamycin acid sulphate	Sigma-Aldrich Chemie GmbH, München, Germany
L-Arginine	Sigma-Aldrich Chemie GmbH, München, Germany
LB-Agar (Lennox)	ROTH, Karlsruhe, Germany
LB-Medium (Lennox)	ROTH, Karlsruhe, Germany
L-glutamine 200 mM	PAA Laboratories GmbH, Pasching, Austria
LiChrosolv Water for Chromatography	Merck KGaA, Darmstadt, Germany
Lipofectamine Transfection Reagent	Life Technologies Corporation, Carlsbad, California, USA
Liquid nitrogen	Linde AG, Pullach, Germany
LysC endopeptidase	Waco, Osaka, Japan
L-Lysine	Sigma-Aldrich Chemie GmbH, München, Germany
L-Lysine4-isotope	Cambridge Isotope Laboratories, Inc.
L-Lysine8-isotope	Cambridge Isotope Laboratories, Inc.
Magnesium chloride ($MgCl_2$)	ROTH, Karlsruhe, Germany
Magnesium sulphate ($MgSO_4$)	ROTH, Karlsruhe, Germany

Reagent	Company
Maltose monohydrate	Sigma-Aldrich Chemie GmbH, München, Germany
Methanol	ROTH, Karlsruhe, Germany
MG132 protease inhibitor	Merck KGaA, Darmstadt, Germany
Milk powder	ROTH, Karlsruhe, Germany
N-Ethylmaleimide (NEM)	Thermo Fischer Scientific inc., Waltham, USA
Ni-Sepharose-6 Fast Flow	GE-Healthcare GmbH, Solingen, Germany
Nonidet P-40	Sigma-Aldrich Chemie GmbH, München, Germany
Nuclease free water	Qiagen, Hilden, Germany
NucleoBond® Xtra Maxi	MACHEREY-NAGEL GmbH & Co. KG, Düren, Germany
NucleoSpin® Gel and PCR Clean-up	MACHEREY-NAGEL GmbH & Co. KG, Düren, Germany
PageRuler prestained protein ladder	Thermo Fischer Scientific inc., Waltham, USA
Paraformaldehyde	Merck KGaA, Darmstadt, Germany
Penicillin/Streptomycin (100x)	PAA Laboratories GmbH, Pasching, Austria
Phenylmethanesulfonyl fluoride (PMSF)	Sigma-Aldrich Chemie GmbH, München, Germany
Phusion™ Hot Start High-Fidelity DNA polymerase	New England Biolabs GmbH, Frankfurt/Main, Germany
PLUS Reagent	Life Technologies Corporation, Carlsbad, California, USA
Power SYBR Green Master Mix	Life Technologies Corporation, Carlsbad, California, USA
ProLong® Gold antifade reagent with DAPI	Life Technologies Corporation, Carlsbad, California, USA
Random primers	Life Technologies Corporation, Carlsbad, California, USA
RNase A	Qiagen, Hilden, Germany
RNaseOUT Recombinant Ribonuclease Inhibitor	Life Technologies Corporation, Carlsbad, California, USA
SILAC DMEM	PAA Laboratories GmbH, Pasching, Austria
SNX5 recombinant protein	Enzo Life Sciences
Sodium chloride (NaCl)	ROTH, Karlsruhe, Germany
Sodium deoxycholate	Sigma-Aldrich Chemie GmbH, München, Germany
Sodium dodecylsulphate (SDS) Pellets	ROTH, Karlsruhe, Germany

Reagent	Company
Sodium ethylendiamine Tetraacetate (Na_2-EDTA)	ROTH, Karlsruhe, Germany
Sodium orthovanadate (Na_3VO_4)	Sigma-Aldrich Chemie GmbH, München, Germany
Superscript II Reverse Transcriptase	Life Technologies Corporation, Carlsbad, California, USA
T4 DNA ligase	New England Biolabs GmbH, Frankfurt/Main, Germany
TEMED	ROTH, Karlsruhe, Germany
Tetracycline	ROTH, Karlsruhe, Germany
Triton X-100	Sigma-Aldrich Chemie GmbH, München, Germany
Tris	Sigma-Aldrich Chemie GmbH, München, Germany
Tris-HCl	ROTH, Karlsruhe, Germany
TRIzol® Reagent	Life Technologies Corporation, Carlsbad, California, USA
Trypsin/EDTA (1x)	PAA Laboratories GmbH, Pasching, Austria
Tween 20	ROTH, Karlsruhe, Germany
Urea	Sigma-Aldrich Chemie GmbH, München, Germany
WEST-ZOL plus Western Blot Detection	HiSS Diagnostics GmbH, Freiburg, Germany
Whatman filter paper	VWR, Darmstadt, Germany
Yeast extract	ROTH, Karlsruhe, Germany

2.1.3. Antibodies

Table 3: Primary antibodies used for western blot (WB) and immunocytochemistry (ICC)

Antibody	Species	Dilution (WB/ICC)	Company
Anti-GAPDH (clone 6C5)	Mouse	1:30,000/ -	Millipore GmbH
Anti-DYKDDDDK tag (Anti-FLAG tag)	Rabbit	1:1000/ 1:250	Cell Signaling Technology
Anti-Myc tag (polyclonal)	Rabbit	1:1000/1:250	Millipore GmbH
Anti-c-Myc tag (monoclonal)	Mouse	1:1000/1:250	Sigma-Aldrich Chemie GmbH
Anti-His tag (monoclonal)	Mouse	1:1000/ 1:250	Novagen
Anti-SNX5	Rabbit	1:1000/1:250	Protein Tech
Anti-myosin (SLOW) (clone NOQ7.5.4D)	Mouse	1:1000/ -	Sigma-Aldrich Chemie GmbH

Antibody	Species	Dilution (WB/ICC)	Company
Anti-Myogenin	Mouse	1:1000/ -	Sigma-Aldrich Chemie GmbH
			Santa Cruz Biotechnology
Anti-Ubiquitin	Rabbit	1:1000/ -	BD Biosciences
Anti EEA1	Mouse	- / 1:250	BD Biosciences
Anti LAMP1	Mouse	- / 1:250	Generated at AG Fielitz lab
Anti MuRF2	Rabbit	1:300/ 1:50	Generated at AG Fielitz lab
Anti MuRF3	Rabbit	1:300/ 1:50	

Table 4: Secondary antibodies used for western blot (WB) and immunocytochemistry (ICC)

Antibody	Species	Dilution (WB/ICC)	Company
Anti-mouse IgG HRP linked	Horse	1:2000/ -	Cell Signaling Technology
Anti-rabbit IgG HRP linked	Goat	1:2000/ -	Cell Signaling Technology
Anti-mouse Alexa Fluor®488	Goat	- / 1:500	Life Technologies Corp.
Anti-rabbit Alexa Fluor®488	Goat	- / 1:500	Life Technologies Corp.
Anti-mouse Alexa Fluor®555	Goat	- / 1:500	Life Technologies Corp.
Anti-rabbit Alexa Fluor®555	Goat	- / 1:500	Life Technologies Corp.
Anti-mouse Alexa Fluor®647	Goat	- / 1:500	Life Technologies Corp.

2.1.4. Primers

Table 5: Primers used for cloning-, mutagenesis- and RT- PCR-reactions. Restriction enzymes used for cloning are included in the name of the primer (i.e. EcoRI, XbaI, KpnI, HindIII etc.).

Primer	Sequence (5'-3')
Mm MuRF1 His/Myc EcoRI for	CAGAATTCATGGATTATAAATCTAGCCTG
Mm MuRF1 His/Myc KpnI rev	CTTGGTACCTTGGTGTTCTTCTTTACCCTC
Mm MuRF2 His/Myc XhoI for	GACTCGAGATGAGCACTTCTCTGAATTAC
Mm MuRF2 His/Myc KpnI rev	CTTGGTACCTTCATTTAGGGAATTCAACCAG
Mm MuRF3 His/Myc XbaI for	TCTAGACTATGAACTTCACGGTGGGTTTCAA
Mm MuRF3 His/Myc KpnI rev	GGTACCGTGCAGGCCTGAGCCTTCTGGCAC
Mm MuRF1 pMal EcoRI for	CCGGAATTCGATTATAAATCTGGCCTGATTC
Mm MuRF1 pMal XbaI rev	GCTCTAGATCATTGGTGTTCTTCTTTAC
Mm MuRF2 pMal salI for	GCGTCGACAGCACTTCTCTGAATTACAAG
Mm MuRF2 pMal HindIII rev	CGAAGCTTTTATTCATTTAGGGAATTCAAC
Mm MuRF3 pMal EcoRI for	CCGGAATTCAACTTCACGGTGGGTTTCAAG
Mm MuRF3 pMal XbaI rev	GCTCTAGATCAGTGCAGGCCTGAGCCTTC

Primer	Sequence (5'-3')
Mm MuRF1 Flag EcoRI for	GCGAATTCGATTATAAATCTAGCCTGA
Mm MuRF1 Flag ApaI rev	GCGGGCCCTCATTGGTGTTCTTCTTT
Mm MuRF2 Flag ClaI for	GCATCGATAGCACTTCTCTGAATTACAAGTCTT
Mm MuRF2 Flag ApaI rev	GCGGGCCCTTATTCATTTAGGGAATT
Mm MuRF3 Flag EcoRI for	GCGAATTCAACTTCACGGTGGGTTTCAA
Mm MuRF3 Flag ApaI rev	GCGGGCCCTCAGTGCAGGCCTGAGCCTTC
Mm MuRF2 C42S His/Myc for	GCCTGTGGTCATTCTCCCTAGCCAGCACAA
Mm MuRF2 C42S His/Myc rev	TTCGTGAACATCTCTAGGCAGATGGGACAG
Mm MuRF2 C50S His/Myc for	GCACAACCTGTGCAGGAAAAGTGCCAGTGACATC
Mm MuRF2 C50S His/Myc rev	TGGCAAGGGAGAATGACCACAGGCTTCGTGAACA
Mm Snx5 His/Myc BamHI for	CGGGATCCATGGCCGCGGTTCCCGAGTT
Mm Snx5 His/Myc KpnI rev	GGGGTACCGTTGTTCTTGAATAAGTCGATGCAGCTC
Mm Snx5 Flag ClaI for	CCATCGATGCCGCGGTTCCCGA
Mm Snx5 Flag XbaI rev	GCTCTAGATCAGTTGTTCTTGAATAAGTCGATGC
Mm Snx5 BAR Flag ClaI for	CCATCGATCAGGATCTAAGTGTTAGACG
Mm Snx5 PX Flag XbaI rev	GCTCTAGAATCATATTCCAAGAAAACATGAAA
Mm Snx5 BARΔHelix1 for	GAAGAACCCACAGTCATCAAAAAGT
Mm Snx5 BARΔHelix1 rev	CACCTCCTTAACTCCAGAAAAAAGG
Mm Snx5 BARΔHelix2 for	AAGGCCCGGTTAAAAAGCAAAGATGTCAAG
Mm Snx5 BARΔHelix2 rev	GACTGTGGGTTCTTCCAAGGCCAGG
Mm Snx5 BARΔHelix3 for	ATCGACTTATTCAAGAACAACTGA
Mm Snx5 BARΔHelix3 rev	CTGATGAGTCTCTGCCAACT
Mm Snx5 Sybr for	GTTCCCGAGTTGCTGGAG
Mm Snx5 Sybr rev	GCGATGGGTCAACATTCAG

2.1.5. Expression plasmids

Table 6: Expression plasmids used in this study

Vector	Selection marker	Company
pcDNA3.1 (+) FLAG	Ampicillin	Life Technologies Corporation
pcDNA3.1 (-)A- Myc$(His)_6$	Ampicillin	Life Technologies Corporation
pMAL-c4E	Ampicillin	New England Biolabs
pmCherry-N1	Kanamycin/Neomycin	Clontech

2.2. Molecular biological methods

2.2.1. Polymerase chain reaction (PCR)

Amplification of DNA was performed using a PCR reaction according to the program in table 8. For amplification from cDNA, 20-30 ng of DNA template were used, whereas 5-10 ng of plasmid DNA were sufficient. For DNA analysis, the advantage® High Fidelity (HD)

polymerase was used with its corresponding PCR buffer supplied by the manufacturer (Table 7).

Table 7: Components of a PCR reaction

Components	Volume for one reaction [µl]
DNA template	X
5x adv. HD Buffer	10
5µM forward primer	4
5µM reverse primer	4
dNTPs (10 mM)	1
Adv. HD-polymerase	0.5
H_2O	ad 50 µl

PCR was carried out in a PCR- thermocycler. The Standard PCR reaction program (Table 8) was adjusted according to the quantity and quality of template DNA, the length and G/C content of the primers and the length of the amplified sequences. A list of PCR primers used in this study can be found in table 5. PCR products were purified by using the NucleoSpin® Gel and PCR Clean-up Kit according to manufacturer's protocol and as described in 2.2.9.

Table 8: Standard program of a PCR reaction

PCR reaction step	Temperature [°C]	Time [min]	Cycles
1 Initial denaturation	95	5	1
2 Denaturation	95	0.5-1	
3 Annealing	50-70	1	35 x steps 2-4
4 Elongation	72	1-3	
5 Terminal elongation	72	10	1

2.2.2. Site - directed mutagenesis PCR

With the Phusion™ Site-Directed Mutagenesis Kit, point mutations and deletions were introduced in plasmid DNA by using the highly processive Phusion™ Hot Start High-Fidelity DNA polymerase. PCR amplification of target plasmid was performed with two phosphorylated primers, which were designed so that they would anneal back to back to the plasmid. For point mutations, they were created by designing one or two base-mismatches in the forward primer, whereas deletions were created by designing primers that border the deleted area on both sides while being perfectly matched on their entire length. A list of primers can be found in table 5. Primers were phosphorylated at the 5' end to eliminate the need for a separate phosphorylation step before direct ligation. Phosphorylation was carried out using T4 Polynucleotide Kinase and its 10xT4 Polynucleotide Kinase Buffer and by

adding ATP to the reaction according to manufacturer's protocol. The reaction was carried out for 30 min at 37°C. Mutagenesis PCR was performed using 20-30 ng of template plasmid DNA. Components of the reaction are listed in table 9.

Table 9: Components of a site-directed mutagenesis PCR reaction

Components	Volume for one reaction [µl]
DNA template	X
5xPhusion ™HF Buffer	10
5µM phosphor. forward primer	4
5µM phosphor. reverse primer	4
dNTPs (10 mM)	1
Hot-Start DNA-polymerase	0.5
H_2O	ad 50 µl

PCR was carried out in a PCR- thermocycler according to the PCR reaction program shown in table 10. Annealing temperature was adjusted according to the length and G/C content of the primers and elongation time according to the length of the linearized plasmid DNA to be mutated (point mutations), or the linearized plasmid DNA without the deleted segment (in the case of deletion mutations).

Table 10: Program of a site-directed mutagenesis PCR reaction

PCR reaction step	Temperature [°C]	Time	Cycles
1 Initial denaturation	98	30 sec	1
2 Denaturation	98	10 sec	
3 Annealing	50-70	10-30 sec	25 x steps 2-4
4 Elongation	72	3-4 min	
5 Terminal elongation	72	10 min	1

Following the reaction, PCR product was digested with the restriction enzyme DpnI. This digest is crucial because DpnI only cleaves at methylated sites, so it digests the template plasmid but not the PCR product. Since the transformation efficiency of the template plasmid is much better than the circularized PCR product, without the DpnI digest a large number of colonies would be the parental DNA. DpnI restriction digestion was carried out by adding 1µl (20 U) of DpnI enzyme to the PCR product and incubating it at 37°C for 1 h. PCR products were purified by using the NucleoSpin® Gel and PCR Clean-up Kit according to manufacturer's protocol and as described in 2.2.9. Mutated PCR products were circularized by using T4 DNA ligase as described in 2.2.6.

2.2.3. Transformation of competent bacteria with DNA

- SOC medium: 2% (w/v) bacto tryptone, 0.5% (w/v) yeast extract, 10 mM NaCl, 2.5 mM KCl, 10 mM $MgCl_2$, 10 mM $MgSO_4$, 20 mM glucose

Transformation of chemically competent bacteria

For transformation of *E.coli* with plasmid DNA 100 µl of chemically competent bacteria were taken out of the -80°C freezer and thawed carefully on ice. Bacteria were mixed with 10µl of ligation reaction or 50ng of plasmid DNA preparation and incubated for 30 minutes on ice. A brief heat shock (42°C, 45 sec) was followed by incubation on ice for 10 min. 500 µl of SOC medium were added and after incubation for 1h at 37°C and 250rpm, cell suspension was streaked on LB agar plates, containing the suitable antibiotic (100 µg/ml ampicillin or 50 µg/ml kanamycin). Plates were incubated at 37°C overnight. The bacteria strain *E.coli XL1-Blue* was used for all cloning experiments and DNA preparation, and *E.coli BL21* was used for expression of recombinant proteins.

Electrotransformation of E.coli XL1-Blue

Electrotransformation of bacteria with DNA was alternatively carried out by mixing 2.0-4.0 µl of the ligation reaction with 50 µl of electrocompetent *E. coli XL1-Blue* and pipetting the cells into a 0.1 cm gene pulser cuvette. Electrotransformation was performed with the Ec1 program with 1.8 kV in the MicroPulser Electroporator. Immediately afterwards, transformed bacteria were mixed with 500 µl of SOC medium and incubated for 1 h at 37°C and 250 rpm. Cell suspension was streaked on LB agar plates, containing either 100 µg/ml ampicillin or 50 µg/ml kanamycin. Plates were incubated at 37°C overnight.

2.2.4. Preparation of plasmid DNA by alkaline lysis with SDS

Minipreparation

- P1 buffer: 50 mM Tris-HCl, 1 mM EDTA, 10 µg/ml RNaseA, pH8.0
- P2 buffer: 200 mM NaOH, 1% (w/v) SDS
- P3 buffer: 3 M potassium acetate, pH5.5

For the preparation of plasmid DNA, 3 ml of LB medium containing 100 µg/ml ampicillin or 50 µg/ml kanamycin were inoculated with transformed bacteria colonies from LB plates (see 2.2.3.) and incubated overnight at 37 °C and 250 rpm. 2 ml of the overnight culture were spun

down for 10 min at 13,000 g and 4 °C for sedimentation of the cells. Bacteria pellets were resuspended in 200 µl of buffer P1, supplemented with 100µg/ml RNaseA. For alkaline lysis of bacteria, 200 µl of buffer P2 were added and the reaction tube was inverted several times. The solution was neutralized by adding 200 µl of buffer P3, vigorous mixing and incubation for 5 min at RT. Centrifugation at 13,000 g and 4°C for 10 min was performed, and 500 µl of the supernatant were transferred into a new reaction tube. DNA was precipitated by adding 350 µl of 2-Propanol and centrifugation for 20 min at 13,000 g and 4°C. DNA pellets were washed with 1 ml of ice-cold 70% (v/v) ethanol and centrifuged for 10 min at 13,000 g and 4°C, then dried at RT, dissolved in 30 µl of nuclease- free water and stored at -20 °C.

Maxipreparation

To yield a high content of DNA, maxi preparations were performed. The maxi preparation of plasmid DNA from a 200 ml bacteria culture was carried out using the Nucleobond Xtra Maxi kit according to the manufacturer's protocol.

2.2.5. Cleavage of DNA using restriction endonucleases

Both analytical and preparative restriction digestions were carried out using suitable restriction endonucleases and recommended buffers according to manufacturer's instructions (New England Biolabs Inc., table 5). For analytical digestions 0.5-1.0µg DNA, 10% 10xbuffer, and 0.5 U of restriction enzyme were mixed and adjusted to a final volume of 20µl with water before incubation at 37°C for 1 h. Preparative digestions were carried out in a total volume of 50µl, containing 2µg DNA, 10% 10xbuffer, and 1.0-2.0 U of restriction enzyme. Final volume was also adjusted to 50µl with water, and samples were incubated at 37°C for 2-3 h. In both digestions 10% 10xBSA were added when needed, according to the manufacturer's protocol. The cleaved DNA was analyzed by agarose gel electrophoresis.

2.2.6. Ligation of DNA fragments

Ligation was carried out by mixing linearized insert DNA and the vector in a ratio of 3:1, respectively. Ligation buffer (1 µl) and 1 U T4-DNA-ligase (1 µl) were added, and after adjusting the final volume to 10µl with water, the ligation reaction was incubated at 14°C overnight.

2.2.7. DNA sequence analysis

Sequencing of plasmids was performed by the company Eurofins MWG Operon in Ebersberg, Germany, according to the Sanger sequencing method.

2.2.8. DNA gel electrophoresis

- TAE buffer: 40 mM Tris-HCl, 1 mM EDTA, pH8.4
- DNA loading buffer: 40% (w/v) sucrose, 0.5% (w/v) SDS and 0.25% (w/v) bromophenol blue

For the analysis of PCR products and DNA fragments resulting from restriction by endonucleases, DNA fragments were separated electrophoretically according to their size in horizontal agarose gels. Depending on the size of the DNA fragment of interest, the appropriate amount of agarose was dissolved in TAE buffer by heating at a concentration of 1.0-2.0% (w/v). For visualization of bands on the gel, ethidium bromide was added at a final concentration of 0.5µg/ml after cooling. Bromophenol blue was used as loading buffer and TAE buffer was used as running buffer. DNA fragments were visualized via the intercalated ethidium bromide using a UV transluminator. The size of the fragments was estimated by standard size markers such as the 100bp or 1KB DNA ladders, run on the same gel.

2.2.9. Extraction of DNA fragments from agarose-gels

DNA extraction was carried out using NucleoSpin® Gel and PCR Clean-up Kit and following manufacturer's instructions. DNA bands were visualized using a UV transilluminator and desired bands isolated by excising the respective piece of agarose. Gel slices were transferred into 2ml tubes and their weight was determined before NT buffer was added in a 200µl/100mg ratio (for PCR products 200 µl NT buffer/100 µl PCR-product). Gel fragments were incubated at 50°C and 1200rpm in a thermo-mixer, until they melted completely. Samples were loaded onto NucleoSpin Extract columns, which were placed into 1.5 ml collection tubes, and centrifuged at 11,000 g for 1 min. The flow-through was discarded and columns were placed back into the collecting tubes. For washing the silica membranes 700µl NT3 washing buffer were added, followed by 1 min centrifugation at 11,000 g. For drying the silica membranes, columns were centrifuged at 11,000 g for additional 2 min. Columns were placed into new 1.5 ml reaction tubes, and DNA was eluted with 20 µl pre-heated water, which were pipetted in the middle of the silica membrane. After incubation for 1 min at RT, columns were centrifuged for 1 min at 11,000 g. Eluted DNA occurred in the flow-through.

2.2.10. RNA isolation from cells and tissues

For the analysis of mRNA expression, total RNA was isolated from cells or tissues using TRIzol® Reagent. Cells in 6 well plates were lysed by adding 1 ml of TRIzol® Reagent per well. Lysed cells were transferred to 1.5 ml tubes. In the case of tissue samples, a small piece of tissue was homogenized in 1 ml TRIzol® Reagent in the FastPrep®-24 Instrument in 3 cycles for 20 sec and 4 m/s each and using lysis matrix tubes with a matrix of six 2.8 mm ceramic spheres. After centrifugation at 12,000 g for 10 min at 4 °C, homogenized cells were transferred to new 1.5 ml tubes. For phase separation, homogenized samples were incubated for 5 min at RT, and 200 µl of chloroform was added. Tubes were shaken vigorously by hand for 15 sec and incubated for 3 min at RT. After centrifugation at 12,000 g and 4°C for 15 min, the RNA containing aqueous phase was transferred to a new tube and 500 µl of 100% 2-Propanol were added, mixed and incubated on ice for 10 min for RNA precipitation. Samples were centrifuged at 12,000 g and 4°C for 10 min. The supernatant was removed and RNA pellet was washed with 1 ml of 75 % (v/v) ethanol. Samples were vortexed briefly then centrifuged at 7,500 g and 4°C for 5 min. Ethanol was discarded and RNA pellets were air-dried for 10-15 min then dissolved in 30-50 µl of RNase-free water. Before measuring the concentration, RNA samples were incubated in a heat block at 55°C for 10 min. RNA concentration was determined using the NanoDrop1000. RNA samples were stored at -80 °C.

2.2.11. cDNA synthesis

The enzyme Superscript II Reverse Transcriptase was used for the reverse transcription of RNA to cDNA. Transcription was started by mixing 1 µl of 50-250 ng random primers and 1 µl of dNTP Mix (10 mM each) with 1 µg of total RNA and adding RNase-free water to a final volume of 12 µl. Solution was incubated at 65°C for 5 min, then placed on ice. 4 µl of 5xFirst Strand buffer, 2 µl of 0.1 M DTT, 1 µl of RNaseOUT (40 units/µl) and 1 µl of SuperScriptII (200U) were added and mixed. Solution was incubated at 25°C for 10 min, then at 42°C for 50 min and finally at 70°C for 15 min for deactivation of the SuperScriptII enzyme. The reaction was performed in the peqSTAR 96 Universal Gradient PCR machine. The cDNA was stored at 4°C for short term or at -20°C for long term storage.

2.2.12. Quantitative real - time polymerase chain reaction (qRT-PCR)

For the analysis of gene expression by quantitative real-time polymerase chain reaction (qRT-PCR), the SYBR Green-based approach was used in a StepOnePlus™ Real-Time PCR

System and by using MicroAmp® Fast Optical 96-well reaction plates. In a qRT-PCR reaction, 10 ng of cDNA were combined with the components shown in table 11.

Table 11: Components for one quantitative RT-PCR reaction

Components	Volume for one reaction [µl]
5µM forward primer	1
5µM reverse primer	1
Power SYBR Green Master Mix	10
5ng/ µl cDNA in nuclease-free H_2O	2
Nuclease-free H_2O	6

The PCR program used for qRT-PCR is shown in table 12. To ensure specificity of the PCR reaction, a melting curve was generated after each run. DNA amount was calculated by a cDNA dilution curve ("standard curve"). To generate a standard curve, 5 µl of each cDNA sample were collected and pooled, and a serial 1:2 dilution of the cDNA-pool was carried out. This standard curve was used as a reference for every reaction performed. The expression of the specific mRNAs was normalized to the expression level of *Gapdh*.

Table 12: Program used for quantitative RT-PCR reaction

PCR reaction step	Temperature [°C]	Time [min]
1 Initial Denaturation	95	10 min
2 Denaturation	95	15 sec
3 Annealing, elongation	60	1 min
4 Cycling	41x step 2 and 3	
5 Melting curve	0.3°C increment until 95°C	

2.3. Protein biochemical methods

2.3.1. Immunocytochemistry (ICC) of mammalian cells

Cells were seeded on glass coverslips in 6 well plates. 24 h after transfection, cells were washed twice with 1xPBS and fixed using 4% Paraformaldehyde in PBS (pH 7.0) for 20 min at 4°C. Permeabilization of cells was carried out by using 0.2% Triton-x-100 in 1xPBS for 30 min at RT. Cells were then incubated in blocking solution containing 5% FBS in 1xPBS for 1 h at RT. Subsequently, cells were incubated with a specific primary antibody, which was diluted in PBS/5% FBS (blocking solution) in a humid environment for 1-2 h at RT. Alternatively, this step was carried out overnight at 4°C. After washing the cells 3 times with 1xPBS, they were incubated with the corresponding secondary antibody, which was diluted in

1xPBS, in a dark and humid environment for 1 h at RT. Cells were briefly washed with 1xPBS and coverslips were mounted cell-side down on glass microscope slides using DAPI-containing ProLong® Gold Antifade mounting solution. Slides were stored at 4°C in a dark environment.

To determine co-localization of proteins, double- and triple-immunofluorescence staining experiments were performed, whereas two or three specific primary antibodies and their corresponding secondary antibodies (with different fluorescence labels) were used and incubated as described in the single staining procedure.

2.3.2. Isolation of proteins from cells and tissues

Protein sample preparation for western blot analyses

- RIPA-buffer: 50 mM Tris-HCl, 150 mM NaCl, 0.5% (w/v) Sodium-deoxycholate, 1% (v/v) Nonidet P-40, 1 mM Na_2EDTA, 0.2% (w/v) SDS, 1x cOmplete EDTA-free Protease Inhibitors, 1 mM Na_3VO_4, 1 mM PMSF

Cells grown in a 6-well plate were washed once with 1xPBS and lysed with 200 µl of RIPA buffer containing protease inhibitors for 20-30 min at 4°C. The lysed cells were harvested with a cell scraper, transferred into a pre-cooled 1.5 ml reaction tube and the cell lysate was centrifuged at 15,000 rpm for 15 min. The supernatant was collected, transferred to a new 1.5 ml tube and either subjected to SDS-PAGE and western blot or stored at -80 °C for later use.

For the isolation of proteins from tissue samples, a FastPrep®-24 Instrument was used for tissue homogenization. A small piece of tissue was transferred into a 2 ml lysis matrix tube with a matrix of six 2.8 mm ceramic spheres and 500-1000 µl (depending on the size and origin of the tissue) of RIPA buffer containing protease inhibitors were added. Tissue samples were lysed in three homogenization rounds of 20 s and 4 m/s each. The lysis tubes were centrifuged at 15,000 rpm and the clear supernatant was collected and transferred into a new 1.5 ml tube. Samples were stored at -80°C.

Protein sample preparation for MS analysis of SILAC labeling efficiency

For preparing the samples for the labeling efficiency test, cells were seeded in a 6 well plate and incubated at 37°C and 5% CO_2 for 24 h. The next day cells were washed with 1xPBS, harvested with a cell scraper and collected using 8M Urea/ 2M Thiourea in 10 mM HEPES buffer (pH 8.0). Cell lysates were frozen at -80°C for at least an hour then thawed on ice. Cell membranes were destroyed using a syringe (needle size Ø 0.40 x 20 mm), and cell lysates

were centrifuged for 10 minutes at 15000 rpm. The supernatant was collected in a separate tube and analyzed by mass spectrometry (MS) for labeling efficiency.

Protein sample preparation for Nickel-NTA and MS analysis

Cells were lysed with a cell scraper from 6 well plates or T75 cell culture flasks using TRIS (10 mM)/ NaCl (150 mM) - buffer with protease inhibitors. Cell lysates were frozen at -80°C for at least an hour then thawed on ice (in case of myotubes, several freeze-thaw cycles were carried out). Cell membranes were destroyed using a syringe with needle size Ø 0.40 x 20 mm. cell lysates were sedimented with low speed centrifuge at 300 g for 10 min. Supernatants were collected and centrifuged again in an ultracentrifuge at 50000 rpm for 15-20 min. The clear middle phase was collected for Nickel-pull-down assays and subsequent MS analysis.

2.3.3. Affinity purification- and co-immunoprecipitation-assays

Nickel-Pull down assays

Affinity purification of His-tagged proteins for subsequent MS-analysis was carried out in Nickel-pull down assays using Ni-Sepharose-6 Fast Flow. Proteins were isolated from T75 cell culture flasks or 6 well-plates of transiently- or stably- transfected cells (see 2.3.2. and 2.4.5.). Ni-Sepharose (50 µl) was washed 3 times with cold 1xPBS and centrifuged after each washing step for 1 min at 15000 rpm and 4°C. After the third washing step, PBS was removed entirely and cell lysates were added to the beads in a 2 ml tube. Cold 1xPBS was added to a total volume of 1.5 ml. Reaction tubes were rotated in an overhead shaker for 2-3 h at 4°C and 15 rpm. Alternatively, this step was carried out overnight at 4°C. Cell lysates and slurry were transferred to 1.5 ml tubes, and beads were washed 3 times with cold 1xPBS. After each washing step samples were centrifuged for 1 min at 15000 rpm and 4°C. After the third washing step, PBS was removed entirely by using a syringe (needle size Ø 0.40 x 20 mm). Affinity purified proteins were eluted by careful resuspension with 100 µl of 120 mM EDTA (pH 7.4) at RT, followed by a short centrifugation step and collecting the supernatants (eluates). Elution was repeated 4 times. Samples were combined, mixed and stored at -80°C or analyzed by MS.

Co-immunoprecipitation assays

- Potassium-phosphate-buffer (pH 7.4): 50mM [KH_2PO_4 (pH 4.0)/K_2HPO_4 (pH 9.3)], 150 mM NaCl
- Lysis-buffer: Potassium-phosphate-buffer (pH 7.4), 0.2% Triton-x-100, 1x cOmplete EDTA-free Protease Inhibitors

HEK293 cells were seeded in 6 well plates and transfected using PEI-reagent as described below (2.4.4.). Cells were lysed using pre-cooled lysis buffer (200 µl/ well) and a cell scraper, and cell lysates were transferred into 2 ml tubes and frozen at -80°C for at least 30 min. Cell lysates were thawed on ice and rotated in an overhead shaker for 30 min at 4°C, then centrifuged at 10,000 g and 4°C. Supernatant was transferred into a new pre-cooled 2 ml tube, and 10% of the lysate were used as input control. FLAG-M2-Agarose (30 µl) was washed twice using pre-cooled potassium-phosphate-buffer and centrifuged after each washing step at 800 g and 4°C. Agarose was brought to a final volume of 100 µl slurry using lysis buffer and cell lysates were added. Pre-cooled potassium-phosphate-buffer was added to a total volume of 1.5 ml and reaction tubes were rotated in an overhead shaker for 3 h at 4°C and 15 rpm. Cell lysates and slurry were transferred to 1.5 ml tubes, and beads were washed with potassium-phosphate-buffer 3 times, each followed by a 3 min centrifugation at 800 g and 4°C. After the third washing step, washing buffer was removed entirely by using a syringe with needle size of Ø 0.40 x 20 mm. Elution was carried out with 30 µl 2xLaemmli-buffer without β-mercaptoethanol, which were added to and carefully mixed with the beads. Samples were heated for 3 min at 95°C and 500 rpm. After a short centrifugation the supernatant was transferred into a new tube, 3 µl of 100% β-mercaptoethanol were added and the precipitates were heated for additional 7 min at 95°C and 500 rpm. Input- and eluate-samples were subjected to SDS-PAGE and western blot analyses.

2.3.4. Sodium Dodecyle Sulfate Polyacrylamide Gel Electrophoresis (SDS-PAGE)

- Electrophoresis running buffer: 25 mM Tris, 200 mM glycine, 0.1% (w/v) SDS
- Resolving gel 10%: 4 ml H2O, 3.3 ml 30 % acrylamide, 2.5 ml 1.5 M Tris (pH8.8), 100 µl 10 % (w/v) SDS, 100 µl 10 % (w/v) APS, 4 µl TEMED
- Stacking gel 5%: 2.75 ml H2O, 0.65 ml 30 % acrylamide, 0.5 ml 1 M Tris (pH6.8), 40 µl 10 % (w/v) SDS, 40 µl 10 % (w/v) APS, 4 µl TEMED
- 6x Laemmli buffer: 300 mM Tris-HCl pH6.8, 12 % (w/v) SDS, 0.1 % (w/v), bromophenol blue, 50 % (v/v) glycerol

For the separation of proteins under denaturing conditions and according to their molecular weight, sodium dodecylsulphate polyacrylamide gel electrophoresis (SDS-PAGE) was performed using a discontinuous gel buffer system (Laemmli U.K., 1970). Protein samples were mixed at a ratio of 6:1 (v/v) with 6x Laemmli-buffer containing 15% (v/v) β-mercaptoethanol and heated at 95 °C for 5 min. Samples were shortly centrifuged and loaded into the pockets of a 10 % (v/v) acrylamide gel. Separation of proteins was performed in the

Mini-PROTEAN® Tetra Electrophoresis System at 100-200 V for 1-2 h and by using Electrophoresis running buffer. The molecular weight of the separated proteins was estimated by comparison with a pre-stained standard size marker (protein ladder), which was separated on the same gel.

2.3.5. Western blot analysis

- Transfer buffer: 25 mM Tris, 192 mM glycine, 10 % (v/v) methanol
- TBS-T: 20 mM Tris, 150 mM NaCl (pH 7.6), 0.1 % (v/v) Tween20
- Blocking buffer: TBS-T, 5 % (w/v) milk powder
- Stripping buffer: 50 mM Tris (pH6.8), 2% (w/v) SDS, 100 mM β-mercaptoethanol

Transfer of proteins from an SDS gel onto a nitrocellulose membrane was performed by the tank blot procedure (Towbin, H. *et al.* 1979), in which the equilibrated Hybond ECL Nitrocellulose membrane was placed on the gel with layers of wet Whatman filter paper and sponges on both sides. This so-called "sandwich" was set into the Mini-PROTEAN Tetra Electrophoresis System and the transfer was performed in transfer buffer for 1-1.5 h at 100 V. Subsequently, the nitrocellulose membrane was incubated in blocking buffer for 1 h, followed by incubation with the primary antibody, which was diluted in blocking buffer, over night at 4 °C. The next day, the membrane was washed for 10 min with TBS-T. This washing step was repeated two more times before the membrane was incubated with a suitable horseradish peroxidase-labeled secondary antibody in blocking buffer for 1 h at RT. Another three washing steps in TBS-T were performed for 10 min each. For detection of protein bands, the membrane was incubated with WEST-ZOL plus Western Blot Detection Reagent according to manufacturer's instructions for 5 min. The chemiluminescent signal was detected on a high performance chemiluminescence film which was developed in a Curix-60 developing machine. To reuse the nitrocellulose membrane, antibodies and remaining WEST-ZOL plus Western Blot Detection Reagent were removed by incubating the membrane for 10 min at 55 °C in stripping buffer. After three washing steps in TBS-T, the membrane was blocked again and the detection reaction was performed as described before.

2.3.6. Ubiquitination assays

In vitro ubiquitination assays

In a cell-free system, the ubiquitination of a substrate protein and auto-ubiquitination of ubiquitin E3 ligase proteins was initiated under optimal conditions. The following components were mixed together on ice: 50 mM Tris-HCl, 5 mM $MgCl_2$, 8mM ATP (pH

7.4), 0.5 mM DTT, 20 µg Ubiquitin, 1xcOmplete EDTA-free Protease Inhibitors. Recombinant ubiquitin-activating enzyme GST-E1, ubiquitin-conjugating enzyme GST-UbcH5a (E2) and the recombinant ubiquitin E3 ligases MBP-MuRF1, MBP-MuRF2, MBP-MuRF3, as well as the putative substrate SNX5 recombinant protein, were added to the reaction accordingly. For negative controls the different components were respectively left out of the reaction. Reaction tubes were incubated at 30°C and 350 rpm for 1.5 h. Samples were mixed at a ratio of 6:1 (v/v) with 6x Laemmli-buffer containing 15% (v/v) β-mercaptoethanol and heated at 95 °C for 5 min and subsequently subjected to SDS-PAGE and western blot analysis.

In vivo ubiquitination assays

In vivo ubiquitination assays were carried out like the previously described FLAG-co-immunoprecipitation assays (2.3.3.) while additionally applying the proteasome inhibitor MG132 and the de-ubiquitinase inhibitor *N*-Ethylmaleimide (NEM). 24 h after transient transfection, cells were incubated in 10 µl MG132 for 6 h before cell lysis, whereas NEM (20 mM) was added to lysis buffer. Further steps were performed as described before (2.3.3.).

2.3.7. Establishing MBP-MuRF recombinant proteins

Expression of proteins in E. coli

- Column buffer: 20 mM Tris-HCl (pH 7.4), 200 mM NaCl

Maltose binding protein (MBP) - tagged recombinant fusion proteins were expressed in the BL-21 chemically competent *E.coli* strain. Therefore the bacteria were transformed with the pMAL-MuRF expression plasmids and streaked on LB-amp agar plates, which were incubated overnight at 37°C. A single colony was picked and seeded in 10 ml liquid LB-amp medium and shaken over night at 37°C. The next day, 250 ml LB medium with 10mM glucose and ampicillin were inoculated with the 10 ml overnight-culture and grown at 37°C until an OD_{600} of 0.5 was reached. Then 0.3 mM Isopropyl β-D-1-Thiogalactopyranoside (IPTG) were added to the culture to induce protein expression. Incubation was continued at 32°C for 2-4 h followed by cell sedimentation for 20 min at 4000 g and 4°C. Aliquots were taken before and after IPTG induction to analyze the protein expression via SDS-PAGE and Coomassie staining. Cells were resuspended in 30 ml Column buffer and frozen at -80°C.

Purification of recombinant proteins

- Elution buffer: Column buffer and 10 mM Maltose

Cells were thawed and frozen at -80°C in three freeze/thaw cycles before being sonicated 8 times in short pulses of 15 seconds, and sedimented at 9000 g and 4°C for 20 min. Supernatant was transferred to a new pre-cooled tube. Amylose resin (4 ml slurry) was prepared for the binding of expressed proteins by washing with column buffer and a short centrifugation at 4°C. Supernatant was added to the amylose resin and tubes were incubated in an overhead shaker overnight at 4°C. Beads were washed 3 times with 10 ml column buffer, and after the third time a syringe with needle size Ø 0.40 x 20 mm was used to remove the rest of the buffer entirely. Elution was carried out by adding 2 ml Elution buffer to the beads and allowing the mixture to shake gently for 15 min at RT. After a short centrifugation, the supernatant with the precipitated recombinant protein was collected and stored at -80°C.

2.3.8. Mass spectrometric analysis

Mass spectrometric analyses and processing of data were carried out by Dr. Rick Scavetta (AG-Gunnar Dittmar) at the mass spectrometry core facility of Max-Delbrück-Center in Berlin, Buch.

Preparation of samples

Samples were resuspended in 100 µl of denaturation buffer [6M urea, 2M thiourea, 10mM HEPES (pH=8)]. They were reduced by incubating with 2µl of 10mM *tris*(2-carboxyethyl) phosphine (TCEP) for 45 min at RT, followed by an alkylation step using 2 µl of 55mM chloroacetamide for 60 min at RT. The samples were first digested using 0.25 mg/ml endopeptidase LysC for 3 hours. The samples were diluted by adding 100 µl of 50mM ammonium bicarbonate (pH=8.5). The digestion was stopped by acidifying each sample to pH<2.5 by adding 10% trifluoroacetic acid solution. The peptide extracts were purified and stored on stage tips according to Rappsilber J.*et al*. (2003).

High through-put LC-MS/MS analysis

After Stage-Tip extraction, the eluted peptides were lyophilized and resuspended in 3% trifluoro- acetic acid/5% acetonitrile buffer. Peptides were separated on a Proxeon nLC-II system (Thermo Scientific), resolved with a reversed-phase column (15 cm in length, 75 mm ID [inner diameter of the fused silica capillary tubing used to make the column], 3 mm Dr. Maisch GmbH C18) by a gradient from 4 to 42% B in 240 min. MS and MS/MS spectra were analyzed coupled to a QExactive mass spectrometer (Thermo Scientific). The mass

spectrometer was operated in a data-dependent acquisition mode with dynamic exclusion enabled (30 s). Survey scans (mass range 300-1700 Th) were acquired at a resolution of 70,000 with the twenty most abundant multiply charged ($z \geq 2$) ions selected with a 3-Th isolation window for HCD fragmentation. MS/MS scans were acquired at a resolution of 35000 and injection time of 120 ms.

Processing of mass spectrometry data

Protein and peptide quantitation information were extracted from MaxQuant 1.2.2.5 (Cox J. *et al*, 2008). Results were filtered to 1% false discovery rate at peptide level by MaxQuant.

2.4. Cell culture methods

2.4.1. Cell lines and culturing of cells

- High-glucose growth medium: DMEM high glucose (4.5 g/l), 10 % (v/v) FBS, 2mM L-glutamine, 100 U/ml penicillin, 100 µg/ml streptomycin.
- Low-glucose growth medium: DMEM low glucose (1 g/l), 10 % (v/v) FBS, 2mM L-glutamine, 100 U/ml penicillin, 100 µg/ml streptomycin.

C2C12, COS7 and HEK293 cells were grown in sterile T75 cell culture flasks, C2C12 and COS7 cells in low glucose, and HEK293 cells in high glucose growth medium. After reaching an approx. 80% (C2C12) or 90-100% (COS-7 and HEK293) confluence, cells were subcultured by removing the growth medium, briefly washing the cells with 1xPBS and incubating the cells in 2.5 ml 1x trypsin/EDTA solution for 2-4 min at 37°C and 5% CO_2. After detachment from the flask surface, cells were collected using serum containing growth medium for inactivation of trypsin. Cell suspension was then transferred into a sterile 15 ml tube, and cells were sedimented by centrifugation at 1000 g for 4 min. Cell pellet was resuspended in fresh medium and 10-20% of cells were plated into a new T75 flask. All cells were incubated at 37°C and 5% CO_2 in a sterile and humid atmosphere.

2.4.2. Differentiation and atrophy of mouse skeletal muscle cells

- Differentiation medium: DMEM low glucose (1 g/l), 2 % FBS, 100 U/ml penicillin, 100 µg/ml streptomycin.

Mouse skeletal muscle C2C12 myoblasts were differentiated into myotubes by using low glucose growth medium supplemented with 2% FBS. Cells were plated in 6 well plates (approx. 150,000 cells per well) and grown in growth medium and for 24 h before briefly washing the cells with 1xPBS and replacing the medium with differentiation medium. Cells

were differentiated for 5-8 days and differentiation medium was exchanged daily. Skeletal muscle atrophy was induced by 10µM Dexamethasone in differentiation medium for 24 h or 48 h.

2.4.3. Cryoconservation and thawing of cells

- Freezing medium: 20% FBS, 10% (v/v) sterile Di-Methyl-Sulfoxide (DMSO) in DMEM low glucose (1 g/l) or DMEM high glucose (4.5 g/l)

In order to freeze cells they were trypsinized and harvested from the cell culture flask surface (large flask, 75 cm^2 surface) as described above. After cells were sedimented the cell pellet was resuspended in 4 ml freezing medium. Cell suspension was then quickly aliquoted into 4 cryoconservation tubes (1 ml each). Tubes were placed immediately in a cryoconservation box, which was filled with pre-cooled 2-Propanol. The box was frozen at -80°C for a few days, before the cell-containing vials were transferred into liquid nitrogen container for long term storage at approx. -196°C.

Thawing of cells was done quickly in a 37°C water bath immediately after taking the vials out of the nitrogen tank. Vial content was transferred into a 15 ml tube containing 10 ml of pre-warmed complete medium. Cell suspension was sedimented at 1000 g for 5 min. The supernatant was removed and the cell pellet was resuspended in 10ml complete growth medium. Cell suspension was transferred into a sterile T75 cell culture flask, which was incubated at 37°C and 5% CO_2.

2.4.4. Transfection of mammalian cells

- Serum-free medium: DMEM high glucose (4.5 g/l) or DMEM low glucose (1 g/l)

C2C12 cells

Transfection of C2C12 cells was performed using Lipofectamine transfection reagent and PLUS reagent according to the manufacturer's protocol. C2C12 cells were seeded in 6-well plates ($5x10^4$-10^5 cells per well) and incubated at 37°C and 5% CO_2 for 24 h before transfection. Transfection was prepared in two separate vials. In the first vial, 12 µl of PLUS reagent were diluted in 100 µl of low glucose serum free medium (SFM) and 2 µg of plasmid DNA were added. Contents were mixed and incubated for 15 min at RT. In the second vial, 8 µl of Lipofectamine transfection reagent were diluted in 800 µl of serum free medium. The contents of the two vials were then combined, mixed and incubated for 15 min at RT. Cells were washed with 1xPBS and the transfection mix was pipetted dropwise onto the cells. Cells

were incubated for 3.5 h at 37°C and 5% CO_2 before the transfection reaction was stopped by adding 2 ml of complete growth medium per well. Cells were incubated for 24 h at 37 °C and 5% CO_2.

COS7 and HEK293 cells

COS7 and HEK293 cells were transfected using either Fugene6® or Polyethylenimine (PEI)-transfection reagent according to the manufacturer's protocol. Cells were seeded in 6-well plates ($5x10^4$ COS7 cells/well or $3x10^5$ HEK293 cells/well) and incubated at 37°C and 5% CO_2 for 24 h before transfection. For a transfection using Fugene6®, 6 µl of Fugene6® reagent were diluted in 100 µl of SFM and 2 µg of plasmid DNA were added. The transfection mix was incubated for 20-30 min at RT. For transfection using PEI-reagent, transfection was prepared in two separate vials. In the first vial, 6 µl of PEI-reagent (1 µg/ µl) were diluted in 100 µl of SFM, and in the second vial 2 µg of plasmid DNA were also diluted in 100 µl of SFM. Both vials were incubated for 5 min at RT, then contents were mixed and the transfection mix was incubated for 20-30 min at RT. In both methods, cells were washed briefly with 1xPBS and culture growth medium was exchanged before the transfection mix was pipetted dropwise onto the cells. Cells were incubated for 24 h at 37 °C and 5% CO_2.

2.4.5. Establishing stably transfected cell lines

- Selection growth medium: DMEM low glucose (1 g/l), 10 % (v/v) FBS, 2mM L-glutamine, 100 U/ml penicillin, 100 µg/ml streptomycin, 2 mg/ml Neomycin

C2C12 cells were plated in 6 well plates at a concentration of $5x10^4$ cells per well and incubated in growth medium for 24 h at 37°C and 5% CO_2. Cells were then transfected with one of pcDNA3.1(-)A-MuRF-Myc(His)$_6$ constructs as discussed above (2.4.4.). 24 h after transfection growth medium was exchanged with selection medium containing the antibiotic neomycin. Because the transfected DNA plasmid contains an aminoglycoside phosphotransferase gene (*neo* gene) as a selectable marker, which confers a neomycin resistance, cells expressing the MuRF-protein would exhibit neomycin resistance and therefore were expected to survive, whereas those which were not transfected with the *neo* carrying DNA plasmid were expected to die off when the culture was treated with neomycin. Selection was maintained for 4-10 days and cells which survived were trypsinized, harvested, counted and seeded in 96 well plates in selection medium and at an average of 2-3 cells per well. Plates were screened for single cell colonies and those wells were marked. When cells reached an 80% confluence, they were harvested and transferred to 24 well plates, then to 6

well plates and subsequently to cell culture flasks while maintaining selection the whole time. To test the stable transfection, DNA and proteins were isolated from the cells and subjected to PCR- and western blot analyses, respectively.

2.4.6. Stable Isotope Labeling by Amino acids in Cell culture (SILAC)

- SILAC growth medium: SILAC DMEM high glucose (w/o glutamine, lysine and arginine), 10% (v/v) dialyzed FBS, 100 U/ml penicillin, 100 µg/ml streptomycin, 2mM L-glutamine, 20 µg/ml arginine, 40 µg/ml normal lysine (lysine0) or 50 µg/ml non-radioactive lysine4- or lysine8- isotope.

At a concentration of $5x10^4$ cells per well, C2C12 cells were plated in 6 well plates in complete growth medium for 24 h. Growth medium was then exchanged with SILAC growth medium, supplemented with a non-radioactive isotopically labeled form of lysine, lysine4 (Lys4) or lysine8 (Lys8). Cells were passaged in a 1:4 ratio once every two days as described above. In every cell passage, cell pellets were washed and resuspended twice with 1xPBS, before they were collected with fresh SILAC medium. After five rounds of cell passaging, the incorporation efficiency of lysine4 and lysine8 was tested in MS-analysis as described above. After reaching a labeling efficiency of approx. 100%, cells were transferred into sterile T75 cell culture flasks and grown in SILAC growth medium at 37°C and 5% CO_2.

2.4.7. Cycloheximide chase assays

For analysis of protein stability, C2C12 cells expressing the respective protein were seeded in 6 well plates and incubated at 37°C for 24 h. Cells were then incubated in complete medium with cycloheximide (dissolved in DMSO) at a final concentration of 100 µg/ml for 0, 1, 2, 4, and 6 hours. Cells were harvested at the different time points of cycloheximide-treatment. Proteins were isolated and subjected to SDS PAGE and western blot analysis.

2.5. Animal experiments

The following experiments were performed by colleagues at the lab of AG-Fielitz who kindly provided RNA and protein samples for respective RT-PCR and western blot analyses shown in this study. All animals were kept and treated according to the German animal protection law.

2.5.1. Denervation-induced skeletal muscle atrophy

Skeletal muscle atrophy was induced by ligation and dissection of the left sciatic nerve of adult male C57BL/6N mice at 12 weeks of age, resulting in the disuse of the lower hindlimb muscles. The muscle tissue of the contra-lateral leg and muscle tissue from unaffected mice were used as controls. 6 operated mice and 6 sham mice were sacrificed after 7, 14 and 21 days of denervation. Skeletal muscles *M. gastrocnemius/plantaris* (GP), *M. tibialis anterior* (TA), *M. Extensor digitorum longus* (EDL), and *M. soleus* (Sol) were obtained. Body weight and the weight of skeletal muscles were determined. Tibia length was measured and used as a reference. A loss of skeletal muscle weights and an up-regulated gene expression of the atrophy-related genes *Trim63* and *Fbxo32* in GP and TA muscles were determined, confirming muscular atrophy. RNA and protein samples isolated from GP muscles of denervated and sham mice were used in this study.

2.5.2. Starvation-induced skeletal muscle atrophy

Male C57BL/6N mice at the age of 6-8 weeks were food deprived for 24 h and 48 h but given free access to drinking water. For each time period 6 food deprived mice were sacrificed. Male littermate control mice were treated accordingly except that they were not exposed to starvation, and they were sacrificed after 0 h, 24 h and 48 h. Skeletal muscles (GP, TA, EDL, and Sol), left and right atria, left and right ventricles, and the interventricular septum were obtained. Body weight and the weight of skeletal muscles were determined. Tibia length was measured and used as a reference. A loss of skeletal muscle weights and an up-regulated gene expression of the atrophy-related genes *Trim63* and *Fbxo32* in GP and TA were determined, confirming muscular atrophy. RNA and protein samples isolated from GP muscles of food-deprived and control mice were used in this study.

2.6. Fluorescence and confocal microscopy

Fluorescence microscopy was performed with Leica CTR 6500HS fluorescence microscope, using a black-white camera. Confocal microscopy was performed at a Leica SPE confocal microscope. Fluorescence and confocal images were analyzed with Leica software LASAF 2.3.5 build 5379 Version 2010.

3 Results

3.1. Detection of novel interaction partners for MuRF1, 2 and 3 using SILAC-AP-MS

3.1.1. Cloning and over-expression of MuRF1, MuRF2, and MuRF3 and SILAC labeling of cells

The coding sequences of MuRF1, 2, and 3 - proteins were amplified from mouse muscle cDNA using polymerase chain reactions (PCRs) and cloned into the expression plasmid pcDNA3.1(-)A-Myc(His)$_6$, which carries sequences encoding C-terminal hexahistidine- and Myc-tags resulting in MuRF1-Myc(His)$_6$, MuRF2-Myc(His)$_6$, and MuRF3-Myc(His)$_6$ cDNA expression plasmids. To test the expression of these cDNA expression plasmids, COS7 cells were transfected with either one of these constructs, proteins were isolated from cell-lysates and a western blot analysis was carried out. Lysates from cells transfected with pcDNA3.1(-) A-Myc(His)$_6$ were used as control. Specific antibodies against the His- and Myc-tag were used for detection of the fusion proteins (Fig. 5). MuRF1 and MuRF3 were both detected at 43kDa, whereas full length MuRF2 was detected at 80kDa. While the band size of MuRF1 and MuRF3 corresponded with the predicted size of the proteins, the detected band of MuRF2 was larger than the predicted size of the protein which is 60kDa. This could be due to posttranslational modifications or the relative charge of the protein. Furthermore, another smaller yet to be described MuRF2 isoform was also discovered and was detected at 60kDa in western blot analyses. The sequence of this MuRF2-isoform showed that it lacked exon 9, compared with the sequence encoding the full length MuRF2-protein. It was therefore called MuRF2Δex9 (Fig. 5).

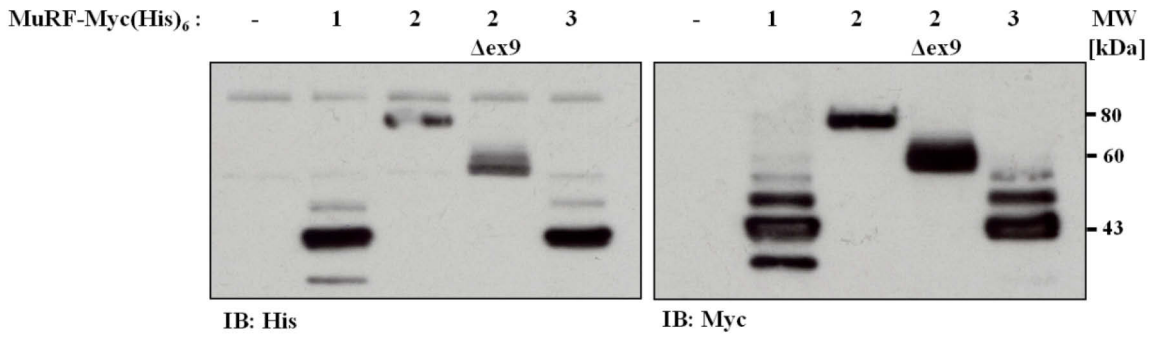

Figure 5: Testing the expression of MuRF-myc(His)$_6$ in COS7 cells. COS7 cells were transfected with MuRF1-Myc(His)$_6$, MuRF2-Myc(His)$_6$, MuRF2Δex9-Myc(His)$_6$ or MuRF3-Myc(His)$_6$. Western blot analysis was carried out to detect the overexpressed proteins. Anti-His- (left) or anti-myc- antibodies (right) were used for detection. MuRF1 and MuRF3 were detected as predicted at 43kDa. Full length MuRF2 was detected at 80kDa and MuRF2Δex9, a novel MuRF2 isoform, was detected at 60kDa.

3.1.2. SILAC- labeling of mouse skeletal muscle cells

This study was carried out in two screens to identify novel interaction partners of MuRF1, MuRF2 and MuRF3. These experiments were based on the method of stable isotope labeling of amino acids in cell culture (SILAC), coupled with affinity purification assays and mass spectrometric analyses (SILAC-AP-MS). Cells used for these assays were mouse skeletal muscle cells (C2C12). These cells were used for establishing cell lines stably expressing MuRF2-Myc(His)$_6$ as well as the transient transfection of MuRF1-Myc(His)$_6$, MuRF2-Myc(His)$_6$, and MuRF3-Myc(His)$_6$.

For SILAC labeling, three different C2C12 cell lines, carrying different isotope-labeling, were established. While Lysine0-cells carried the normal (so-called light, Lys0) lysine, two other cell lines were grown in media lacking this standard essential amino acid but supplemented with a non-radioactive, isotopically labeled form of lysine, in this case the medium Lysine4 (Lys4) or the heavy Lysine8 (Lys8), respectively. To ensure sufficient isotope labeling, C2C12 cells were cultivated in isotope-containing medium for at least 5 passages before their labeling efficiency was tested in mass spectrometric analysis. All labeling tests showed at least 97% labeling efficiency, which means that at least 97% of lysines in these cells have been replaced by either Lysine4 or Lysine8 (Fig. 6).

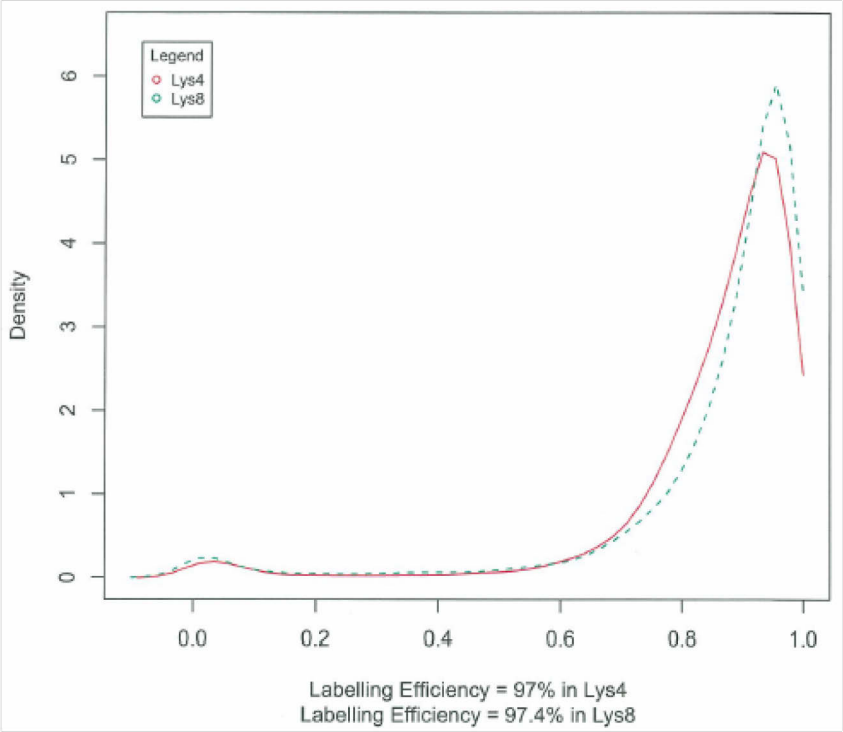

Figure 6: Labeling-efficiency test of Lys4- and Lys8- cell lines. In mass spectrometric analysis the incorporation rate of Lysine4 and lysine8 in C2C12 cells was tested. In both cell lines at least 97% of normal lysines were replaced by the medium or heavy isotopes.

To test the stability of overexpressed MuRF-proteins in C2C12 cells, their expression was detected in western blot analysis 24 h, 48 h and 72 h after transfection. All MuRF-proteins were detectable after 24 h and 48 h but not 72 h after transfection. MuRF2 was also not detectable in stably transfected C2C12 cells, although it could be shown in PCR- and RT-PCR-analyses that MuRF2-DNA was integrated in the cell genome. It was therefore assumed, that MuRF1, MuRF2 and MuRF3 get degraded if they are continuously and/or increasingly overexpressed. Therefore, the proteasome inhibitor MG132 was used to prevent degradation of MuRF-proteins. When C2C12 cells stably expressing MuRF2-Myc(His)$_6$ were treated with 10µM MG132 for different time points, MuRF2 was detectable after 6 h of treatment (Fig. 7).

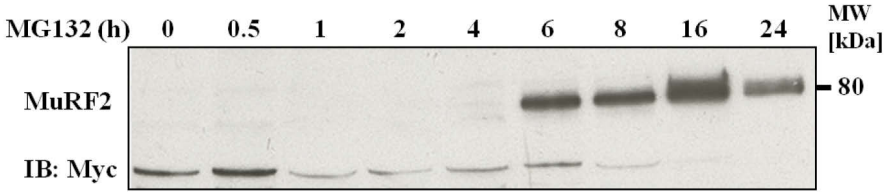

Figure 7: Stabilizing MuRF2-expression using the proteasome inhibitor MG132. MuRF2-stably transfected C2C12 cell line was treated with the proteasome inhibitor MG132 (10µM) for different time points as indicated. Cell lysates were subjected to western blot analysis using anti-Myc antibody for the detection of MuRF2. Expression of MuRF2 was recovered after at least 6 hours of MG132 incubation.

3.1.3. Detection of MuRF1, 2, or 3- interaction partners in C2C12 myoblasts

For identification of MuRF interaction partners in C2C12 myoblasts, the first screen was performed, in which up- or down-regulation of proteins in relation to MuRF-protein overexpression was investigated (Fig. 8). In this assay Lys0-C2C12 cells were transiently transfected with MuRF1-Myc(His)$_6$, MuRF2-Myc(His)$_6$, or MuRF3-Myc(His)$_6$, whereas Lys4-C2C12 cells were mock-transfected with control pcDNA3.1(-)A-Myc(His)$_6$. A Lys4-labeled stable cell line containing pcDNA3.1(-)A-Myc(His)$_6$ served as a control for the Lys0-labeled MuRF2-Myc(His)$_6$ stable cell line. Transiently transfected cells were lysed 24 h after transfection and cell lysates were subjected to protein affinity purification (Nickel pull down assays). Stably transfected cells were treated with 10µM MG132 for 8 h before cell lysis. Nickel sepharose was used for purification of His-tagged proteins. Elution was performed with EDTA and eluates of Lys0 and Lys4 labeled cells were mixed and analyzed by MS. The abundance ratio of the same protein in Lys0 and Lys4 (Lys0/Lys4) labeled cells for an overexpressed MuRF-protein led to the identification of putative interaction partners of this MuRF-protein. Presumably, a protein which was enriched in Lys0-MuRF-overexpressing

cells compared to Lys4-mock-transfected cells was considered a putative interaction partner of this particular MuRF-protein (Fig. 8).

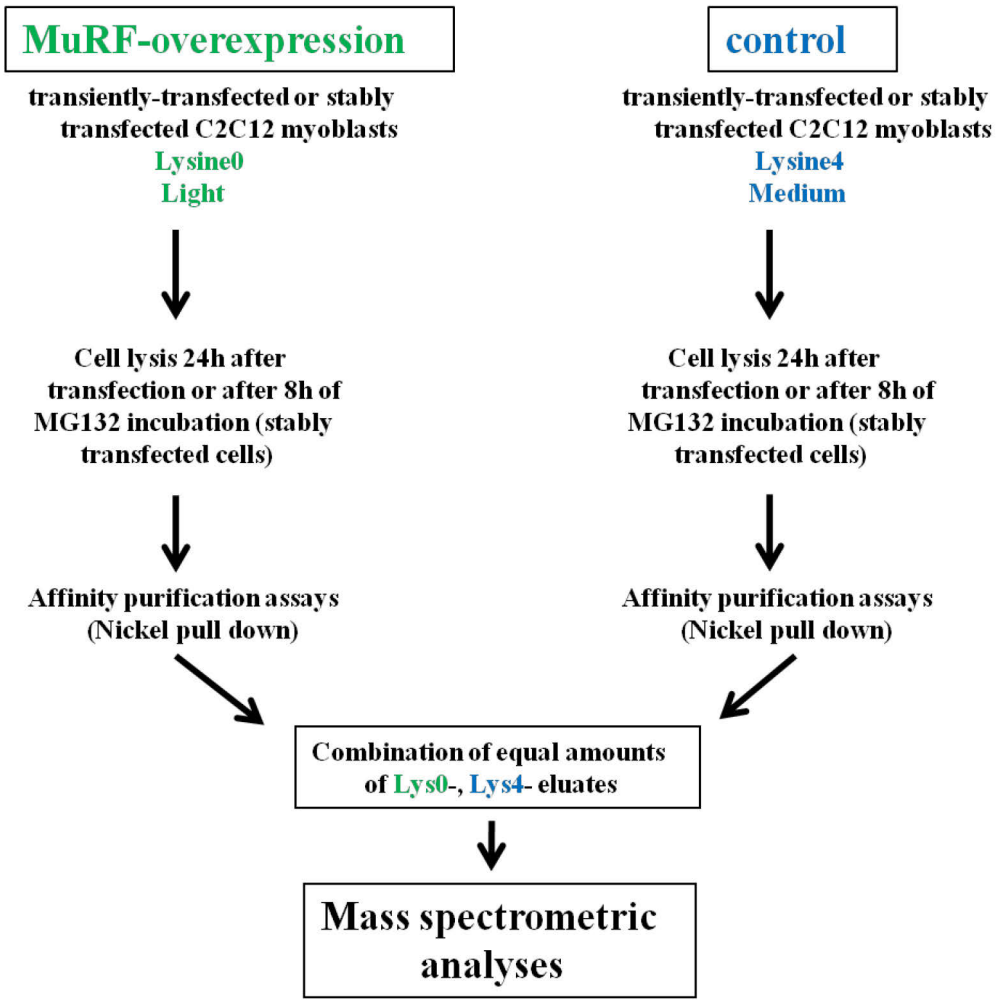

Figure 8: Scheme of experiment for identifying MuRF- interaction partners in C2C12 myoblasts. C2C12 myoblasts were SILAC-labeled, using the isotopes Lys0 (light) or Lys4 (medium). Lys4 myoblasts were stably or transiently mock-transfected with an empty expression plasmid and served as control, whereas Lys0 myoblasts were stably or transiently transfected with one of the MuRF-Myc(His)$_6$ - constructs. 24 hours after transfection, cells were either lysed (transient transfection), or incubated for 8 hours in MG132 before lysis (stable transfection). Cell lysates were subjected to affinity purification assays using His-Sepharose (Nickel pull downs). Eluates were analyzed in mass spectrometric analyses.

Analysis of mass spectrometric data revealed over 6% of proteins which were significantly either up- or down-regulated in myoblasts overexpressing a MuRF-protein in comparison with the control. Several of these proteins detected in myoblasts overexpressing MuRF1, MuRF2 or MuRF3 are shown in tables 13, 14 and 15, respectively. One of the interesting proteins detected was the mammalian retromer component sorting nexin 5 (SNX5). SNX5 exhibited a 1.9 fold up-regulation in MuRF3-overexpressing myoblasts, and was particularly interesting because of the diversity of its roles in different cellular processes and pathways.

Table 13: Mass spectrometric data of proteins with a significant abundance difference in myoblasts overexpressing MuRF1 compared with the control. A total of 1865 proteins were detected in this screen, of which 123 were proteins whose abundance has significantly changed as a result of MuRF1-overexpression, which make approx. 6.6%. 70 proteins were significantly up-regulated and 53 proteins were significantly down-regulated. Significance was set to p-value < 0.05 (according to Benjamini-Hochberg False Discovery Rate).

Protein	Log2 (fold change)	Significance pvalue<0.05	Biological process	Molecular function	Cellular component
	Up-regulated				
Trim 54 (MuRF3)	5.3	3,9378E-18	Microtubule-regulation, cell differentiation	Microtubule-binding	Microtubule, z- disc
Chaperonin 10 Heat shock protein	3.0	9,856E-08	Protein folding	Protein binding	Mitochondria
Transferrin receptor Protein 1	2.0	7,455E-05	Proteolysis	Transferrin receptor, peptidase	Endosome
Spectrin alpha	1.5	0,00323284	Actin filament capping	Actin binding	Cytosol, cytoskeleton
Plectin-1	1.4	0,00173397	Apoptosis, cell junction assembly	Actin binding	Cytoplasm, cytoskeleton
Annexin A3	1.3	0,00840633	Phagocytosis	Phospholipase inhibition	Cytoplasm, membrane
Ahnak	1.0	0,02568389	Neuronal differentiation	S100 protein binding	Nucleus, cytoplasm
Ring finger protein 213	1.0	0,03394145	Protein ubiquitination	Ubiquitin ligase activity	Cytoplasm
Filamin alpha	0.9	0,04597676	Actin-cytoskeleton organization	Actin binding	Nucleus, TGN, cytoplasm
	Down-regulated				
AP3 complex, subunit mu-1	-2.4	4,515E-05	Protein targeting to lysosome, intracellular protein transport	Protein binding	Lysosome, Golgi apparatus
subunit beta1	-2.2	0,00023653			
subunit delta1	-1.4	0,02161786			
Ankyrin-2	-1.7	0,00383246	Signal transduction	Structural component of cytoskeleton	Cytoplasm, cytoskeleton
Actin	-1.3	0,00343137	Muscle contraction	ATP binding	Cytoskeleton, cytoplasm
Importin-7	-1.2	0,01113961	Protein import into nucleus	Ran GTPase binding	Cytoplasm, Golgi, nucleus

Vimentin	-1.1	0,01418154	Immune response	Cytoskeleton component	Cytoskeleton

Table 14: Mass spectrometric data of proteins with a significant abundance difference in myoblasts overexpressing MuRF2 compared with the control. A total of 2030 proteins were detected in this screen, of which 124 were proteins whose abundance has significantly changed as a result of MuRF2-overexpression, which make approx. 6.1%. 65 proteins were significantly up-regulated and 59 proteins were significantly down-regulated. Significance was set to p-value < 0.05 (according to Benjamini-Hochberg False Discovery Rate).

Protein	Log2 (fold change)	Significance p-value<0.05	Biological process	Molecular function	Cellular component
	Up-regulated				
Trim 54 (MuRF3)	4.4	3,4504E-20	Microtubule-regulation, cell differentiation	Microtubule-binding	Microtubule, Z- disc
Clathrin light chain B	2.0	0,00489275	Intracellular protein transport	Protein binding	Plasma membrane, TGN
Sorting nexin 8	1.9	0,00721413	EE to Golgi transport	PtdIns-binding	EE membrane, retromer
Dynamin like protein	1.8	0,01130669	Mitochondrial fission, endocytosis	Ubiquitin E3 ligase binding	Cytoplasm, Golgi, mitochondria
Ahnak	1.4	0,01702681	Neuronal differentiation	S100 protein binding	Nucleus, cytoplasm
EEA1	1.1	0,0463232	Endocytosis, EE to LE transport	Protein binding	Cytoplasm, EEs
Filamin alpha	1.1	0,02843639	Actin-cytoskeleton organization	Actin binding	Nucleus, TGN, cytoplasm
	Down-regulated				
AP3 complex, subunit mu-1	-5.2	1,3344E-17	Protein targeting to lysosome, intracellular protein transport	Protein binding	Lysosome, Golgi apparatus
subunit beta1	-3.0	6,703E-07			
subunit delta1	-2.3	0,00021728			
Ankyrin-2	-2.3	0,00015154	Signal transduction	Cytoskeleton component	Cytoplasm, cytoskeleton
Myosin light chain 9	-1.7	0,00096395	Muscle contraction	Muscle structural component	Cytosol, Z- disc
Importin-7	-1.3	0,00425637	Protein import into nucleus	Ran GTPase binding	Cytoplasm, Golgi, nucleus

Importin-8	-1.3	0,03767737	Intracellular protein transport	Ran GTPase binding	Cytoplasm, nucleus
ESCRT-I complex subunit TSG101	-1.2	0,04911709	Protein transport	UbiquitinE3 ligase binding	EEs, LEs, cytoplasm, nucleus

Table 15: Mass spectrometric data of proteins with a significant abundance difference in myoblasts overexpressing MuRF3 compared with the control. A total of 2177 proteins were detected in this screen, of which 135 were proteins whose abundance has significantly changed as a result of MuRF3-overexpression, which make 6.2%. 85 proteins were significantly up-regulated and 50 proteins were significantly down-regulated. Significance was set to p-value < 0.05 (according to Benjamini-Hochberg False Discovery Rate).

Protein	Log2 (fold change)	Significance p-value<0.05	Biological process	Molecular function	Cellular component
	Up-regulated				
Tropomyosin alpha1	4.5	3,0057E-09	Muscle contraction	Actin-binding, cytoskeleton component	Cytoplasm, cytoskeleton
Tumor suppressor p53	3.6	8,6962E-05	Apoptosis induction	Protease binding	Nucleus
Heme oxygenase 1	2.5	0,00054209	Angiogenesis, cell prolifiration	Signal transduction	Nucleus, ER
Sorting nexin 4	2.0	0,01111567	Intracellular protein transport	PtdIns-binding	Cytoplasm, dynein complex, EEs
Dynamin like protein	2.0	0,00207498	Mitochondrial fission, endocytosis	Ubiquitin E3 ligase binding	Cytoplasm, Golgi, mitochondria
Sorting nexin 5	1.9	0,02061741	Intracellular protein transport	PtdIns-binding	EEs, TGN
Trim55 (MuRF2)	1.8	0,02601982	Microtubule regulation, signal transduction	Protein binding, signal transduction	Cytoplasm, microtubule, nucleus
Annexin A1	1.4	0,0487735	Inflammatory response	Calcium ion binding	Nucleus, cytoplasm
	Down-regulated				
Ankyrin-2	-2.4	5,457E-05	Signal transduction	Cytoskeleton component	Cytoplasm, cytoskeleton
Importin alpha S2	-1.3	0,01976295	Protein transport into nucleus	Protein transporter	Cytoplasm, nucleus
Exportin (tRNA)	-1.3	0,01033502	tRNA export from nucleus	tRNA and Ran GTPase binding	Cytoplasm, nucleus
Ataxin-10	-1.0	0,03967533	Apoptosis, neuronal development	Protein binding	Cytoplasm, plasma membrane

Ubiquitin E3 ligase RNF25	**-1.0**	**0,02999157**	**Protein ubiquitination**	**Ubiquitin ligase activity**	**Nucleus, cytosol**
ESCRT-II complex subunit VPS36	**-1.0**	**0,04605794**	**Endosomal transport, membrane organization**	**PtdIns3-P and ubiquitin binding**	**EEs, LEs, lysosomes, cytosol, nucleus**

3.1.4. Detection of MuRF1, 2, or 3- interaction partners during skeletal muscle differentiation and atrophy

To identify putative interaction partners and targets for MuRF1, MuRF2 or MuRF3 during myocyte differentiation or atrophy of myotubes, an assay specifically addressing these processes was performed. Figure 9 shows a schematic illustration and timeline of this experiment. Three C2C12 cell lines with different isotope labeling were used. Lys0-cells were left as myoblasts (MBs). Lys4-labeled cells were differentiated for 5 days (MTs), and Lys8-labeled cells were differentiated and subjected to atrophy for 24 h using dexamethasone. All three differently labeled cell lines were transfected with MuRF1-Myc(His)$_6$, MuRF2-Myc(His)$_6$, and MuRF3-Myc(His)$_6$, respectively, at the blast stage. Lys0-cells were lysed 24 h after transfection. Lys4-labeled cells were treated with MG132 for 8 h after differentiation and then lysed. Lys8-labeled cells were treated with MG132 for 8 h after they were differentiated and subjected to atrophy and afterwards lysed. After treatment with MG132 and cell lysis, overexpressed MuRF-proteins were affinity purified in Nickel-pull down assays. Elution was carried out several times using EDTA and eluates were analyzed by western blot to identify the precipitated MuRF-protein (Fig. 10). Same procedure was carried out with labeled MuRF2-stably transfected cell lines (Fig. 11). Elution-samples from cell lines with three different labels (MBs, MTs and MTAs), but overexpressing the same MuRF-protein, were then collected, mixed and analyzed by MS (Fig. 9). Three biological replicates of each of these assays were carried out and separately analyzed. In a mass spectrometric analysis, the abundance difference of the same protein in the different cell populations (with different isotope labeling) was measured, which provided important information about the probable enrichment or down-regulation of this protein in two different cell conditions, in this case during myocyte differentiation (Lys4/Lys0) or atrophy of myotubes (Lys8/Lys4).

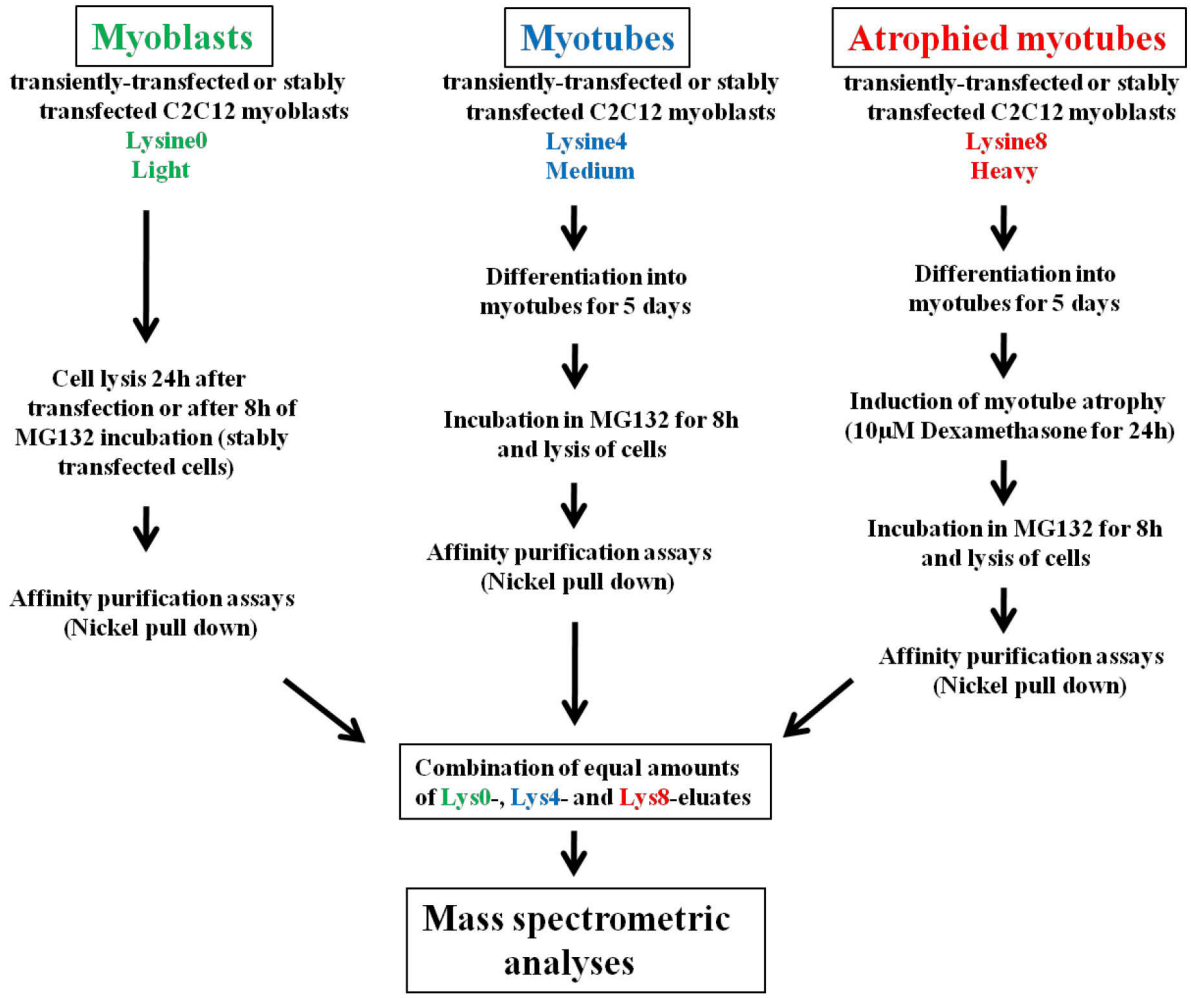

Figure 9: Scheme of the experiment for the detection of MuRF- interaction partners during skeletal muscle - differentiation and - atrophy. C2C12 cells were SILAC-labeled using the isotopes Lys0 (light), Lys4 (medium) or Lys8 (heavy). Cells were either stably or transiently transfected with one of the MuRF-Myc(His)$_6$ - constructs. Lys0 cells were lysed 24 hours after transfection as myoblasts and served as a control and starting condition for differentiation and/or atrophy. Lys4 cells were differentiated for 5 days using DMEM containing 2% dFBS. Cells were then incubated in MG132 (10µM) for 8 hours before they were lysed. Lys8 cells were also differentiated for 5 days and atrophied for 24 hours using 10 µM Dexamethasone before lysis. All cell lysates were subjected to affinity purification assays using Ni-Sepharose (Nickel pull downs). Eluates were analyzed in mass spectrometric analyses.

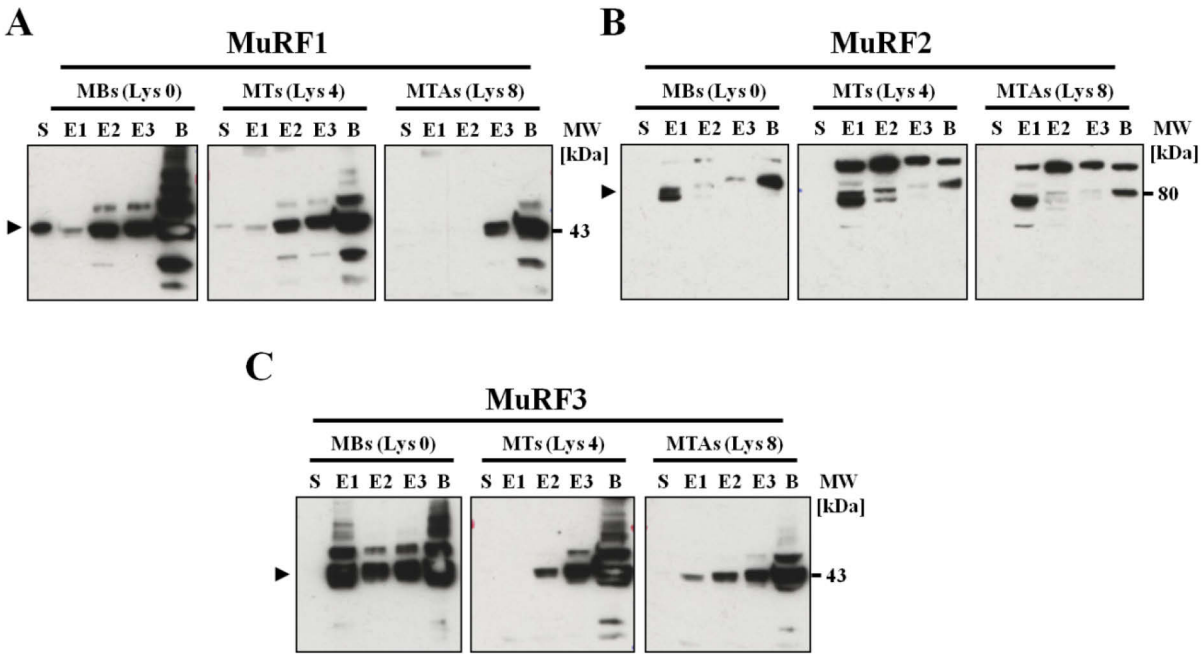

Figure 10: Western blot analysis of MuRF-protein affinity purification assays. MuRF1-Myc(His)$_6$, MuRF2-Myc(His)$_6$ or MuRF3-Myc(His)$_6$ were transiently expressed in C2C12 cells. Cell lysates were subjected to Ni - Sepharose in affinity purification assays and the bound proteins were eluted in three elution steps using EDTA. Purified, overexpressed MuRF1 **(A)**, MuRF2 **(B)**, and MuRF3 **(C)** were detected in western blot analyses using anti-His antibody. MB= myoblasts, MT= myotubes, MTA= atrophied myotubes, S= supernatant, E1, E2, E3= Elution steps 1, 2 and 3, respectively. B= beads.

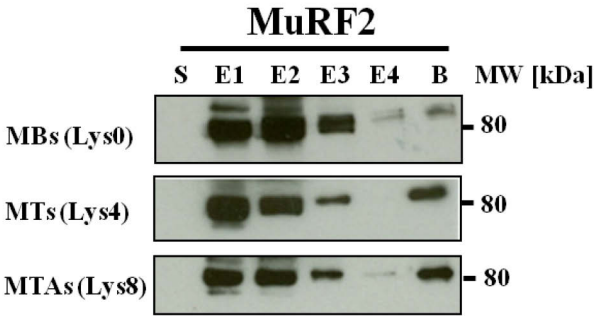

Figure 11: Western blot analysis of protein affinity purification assays for stably expressed MuRF2. MuRF2-Myc(His)$_6$ was stably expressed in C2C12 cells. Cell lysates were subjected to Ni - Sepharose in an affinity purification assay and the bound proteins were eluted in four elution steps using EDTA. Purified, overexpressed MuRF2 was detected in western blot analysis using anti His antibody. MB= myoblasts, MT= myotubes, MTA= atrophied myotubes, S= supernatant, E1, E2, E3, E4= Elution steps 1, 2, 3 and 4, respectively. B= beads.

A summary of most interesting proteins showing a significant abundance change in cells overexpressing MuRF1, MuRF2 or MuRF3 during differentiation and atrophy can be found in Tables 1-6 (Appendix). The distribution of these proteins was schematically illustrated in figures 1-3 (Appendix).

3.2. Endogenous expression of SNX5

3.2.1. Endogenous expression of SNX5 in mouse tissues

SNX5 expression in skeletal and heart muscle tissues was investigated in qRT-PCRs and western blot analyses. For this purpose, RNA and proteins were isolated from four different mouse skeletal muscle tissues; *M. gastrocnemius plantaris* (GP), *M. tibialis anterior* (TA), *M. extensor digitorum longus* (EDL) and *M. soleus* (Sol), as well as the left and right atrium and left and right ventricle. Results of qRT-PCR showed *Snx5* mRNA expression in all four skeletal muscles and both atria and ventricles of the heart. *Snx5* expression was much higher in the heart compared to skeletal muscle tissues (Fig. 12, A). Western blot analyses using specific antibodies against MuRF2, MuRF3 and SNX5 were carried out. Glyceraldehyde 3-phosphate dehydrogenase (GAPDH) was used as loading control. SNX5 was expressed in all four skeletal muscles, and the left and right ventricles. No significant difference in *Snx5* mRNA expression or SNX5 protein content among the different skeletal muscle types was observed (Fig. 12, A).

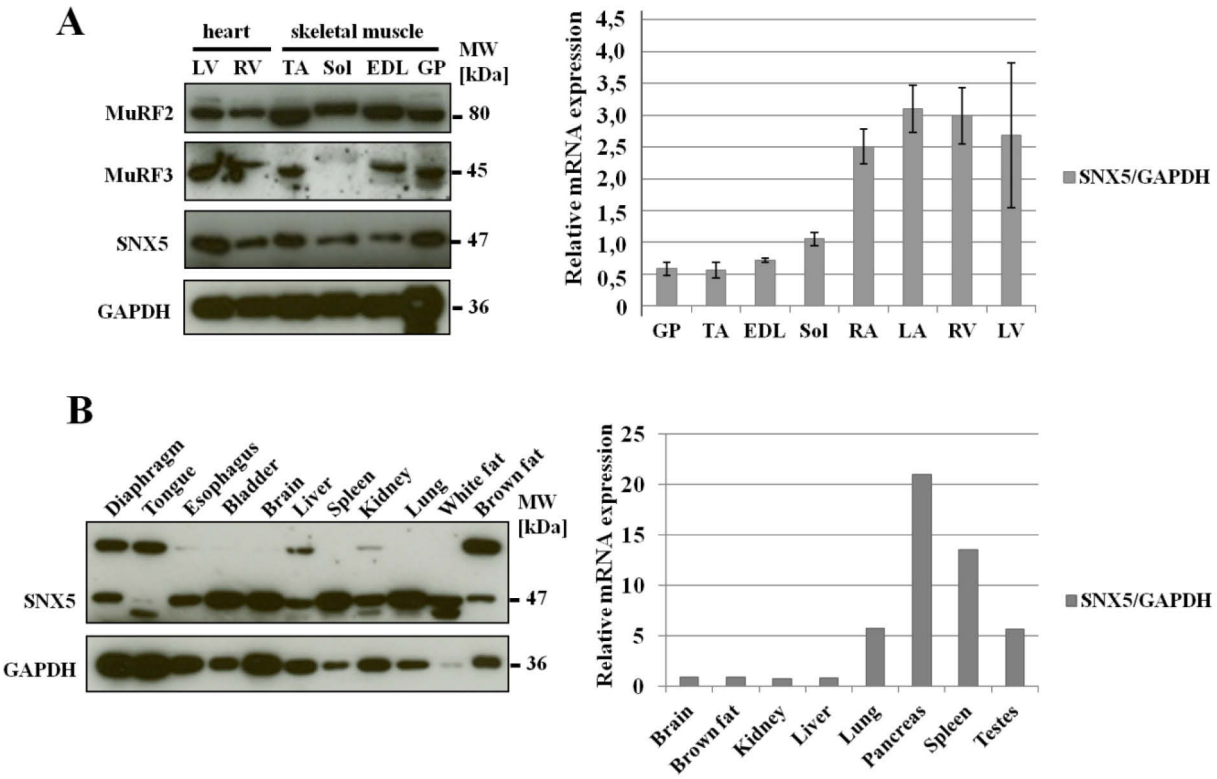

Figure 12: SNX5 endogenous expression pattern in mouse tissues. Western blot analyses were carried out using protein samples isolated from different skeletal- and heart- muscle tissues **(A, left)**, and from different mouse organs **(B, left)**. SNX5 was detected using a specific anti SNX5 antibody. GAPDH was used as loading control. Quantitative real-time-PCR-analyses of *Snx5* expression in skeletal- and heart- muscle tissues **(A, right)**,

and in different mouse organs **(B, right)**, were also carried out. Data are presented as mean ± SEM. GP=Gastrocnemius-plantaris, TA=Tibialis-anterior, EDL=Extensor digitorum longus, Sol=Soleus, RA=right atrium, LA=left atrium, RV=right ventricle, LV=left ventricle.

RNA and proteins were also isolated from different mouse organs. *Snx5* mRNA expression and protein content were detected in qRT-PCR and western blot analysis, respectively. Interestingly, qRT-PCR data showed an especially high expression in the pancreas, lung and spleen, while western blot results showed a ubiquitous SNX5 protein expression (Fig. 12, B).

3.2.2. SNX5 expression during myocyte differentiation and atrophy of myotubes

SNX5 expression during C2C12 myocyte differentiation and atrophy of myotubes was examined. C2C12 cells were differentiated for 1 to 8 days (Fig. 13, A and B). Myotubes were subjected to atrophy for 1 or 2 days by using dexamethasone (Fig. 13, A and C). Western blot analysis using specific antibodies against SNX5, myogenin (differentiation marker) and MHC-slow was performed, and showed that neither differentiation nor atrophy of C2C12 cells had an effect on SNX5 expression (Fig. 13, A).

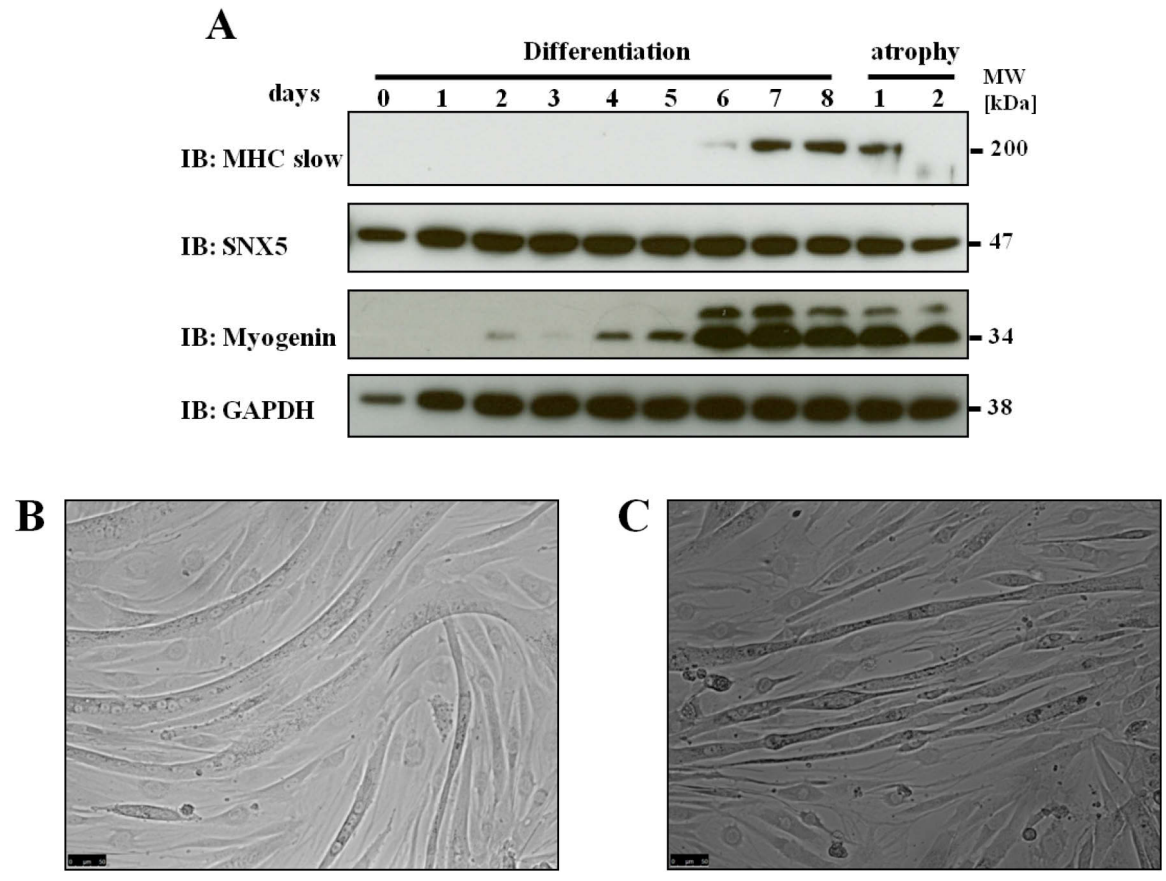

Figure 13: Differentiation and atrophy of skeletal muscle cells does not affect the endogenous expression of SNX5. C2C12 cells were differentiated with DMEM-medium containing 2%FBS. Atrophy was induced using 10µM Dexamethasone for 24 or 48 hours. Cell samples were collected every day and analyzed in western blot.

Specific antibodies against SNX5, slow-twitch MHC (NOQ7) and myogenin were used for detection. GAPDH was used as loading control **(A).** Light microscopy images show differentiated C2C12 cells (7 days) **(B)** and atrophied C2C12 myotubes (48 h) **(C)**. Scale bar, 50µm.

3.2.3. Subcellular localization of SNX5 in myoblasts

Immunocytochemistry was used to examine the subcellular expression of endogenous SNX5 in C2C12 myocytes. Cells were fixed and stained with a specific anti-SNX5 antibody. A perinuclear and cytosolic staining pattern was observed for SNX5, which has not been described in muscle cells, thus far (Fig. 14).

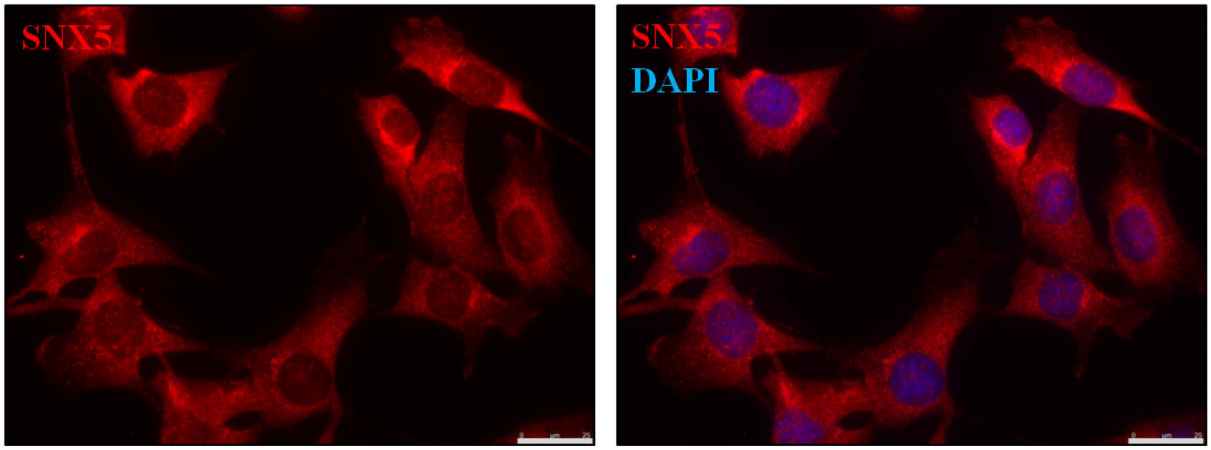

Figure 14: SNX5 endogenous expression pattern in C2C12 myoblasts. C2C12 cells were plated onto glass coverslips for 24 hours, then fixed and stained with a specific anti-SNX5 antibody, and an Alexa555 coupled secondary antibody. Nuclei were stained with DAPI. Scale bar, 25 µm.

Immunofluorescence staining was performed to investigate the subcellular localization of SNX5 to early and late endosomes and lysosomes. Early endosome antigen 1 marker (EEA1) was used for EE staining, and lysosomal-asssociated membrane protein 1 marker (LAMP1) was used for the staining of LEs and lysosomes. COS7 cells were fixed and stained with anti-SNX5 and EEA1 marker (Fig. 15, A), or anti-SNX5 and LAMP1 marker (Fig. 15, B). SNX5 co-localized with EEA1 but not LAMP1, indicative to its localization to EEs and not to LEs and lysosomes (Fig. 15).

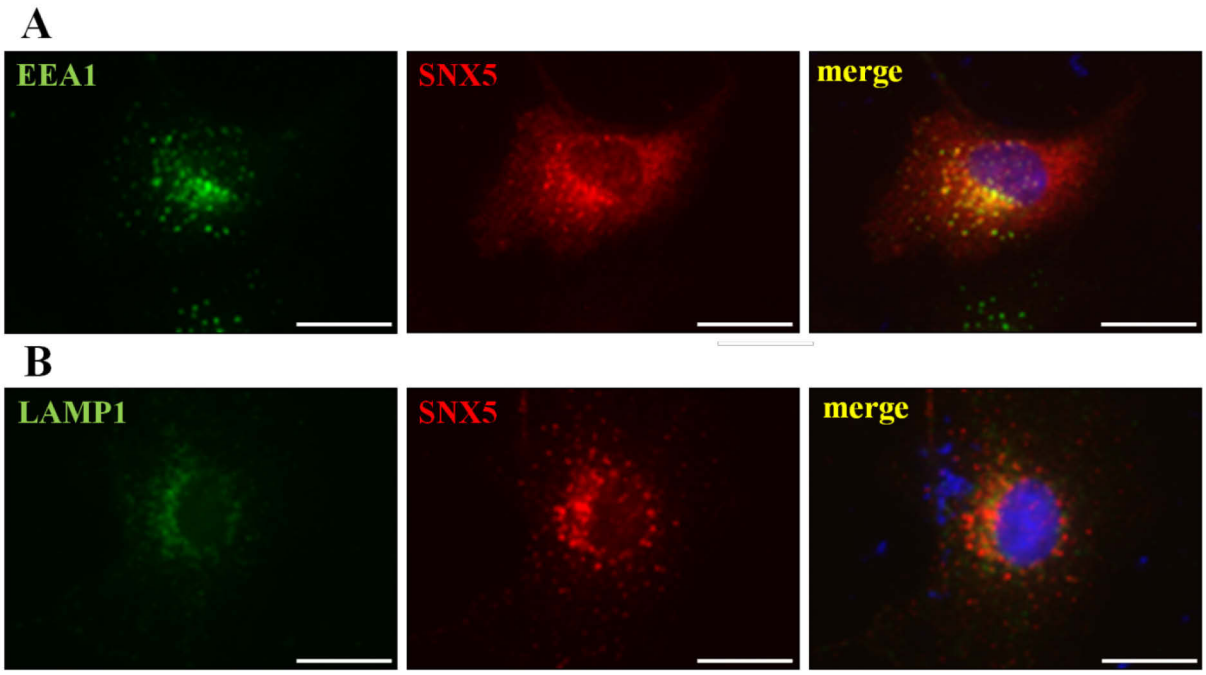

Figure 15: SNX5 localizes to early endosomes and does not localize to late endosomes and lysosomes. COS7 cells were plated onto glass coverslips for 24 h before they were fixed and stained using specific antibodies against SNX5 and EEA1 **(A)** or SNX5 and LAMP1 **(B)**, and fluorophore – conjugated secondary antibodies Alexa488 (green) and Alexa555 (red). Nuclei were stained with DAPI. Scale bar, 25 µm.

3.3. Identification of SNX5 as a MuRF3 interaction partner

3.3.1. SNX5 interacts physically with MuRF3

To investigate a possible physical interaction between SNX5 and MuRF-proteins, co-immunoprecipitation assays were carried out after co-expressing SNX5-FLAG with one of the three MuRF-Myc(His)$_6$ in HEK293 cells. Anti-FLAG-coupled agarose was used for immunoprecipitation of SNX5, and anti-Myc antibody was used for detection of MuRF-Myc(His)$_6$ proteins in the precipitates (Fig. 16). As positive controls for the co-immunoprecipitation, the known interactions between MuRF2-Myc(His)$_6$ and MuRF1-FLAG and between Histone Deacetylase 5 (HDAC5-Myc) and protein kinase D2 (PKD2-FLAG) were used. MuRF3 co-immunoprecipitated with SNX5 verifying their physical interaction. Because MuRF1 was also detected in the SNX5-precipitate, it might also interact with SNX5. An interaction between SNX5 and MuRF2 was not detectable (Fig. 16).

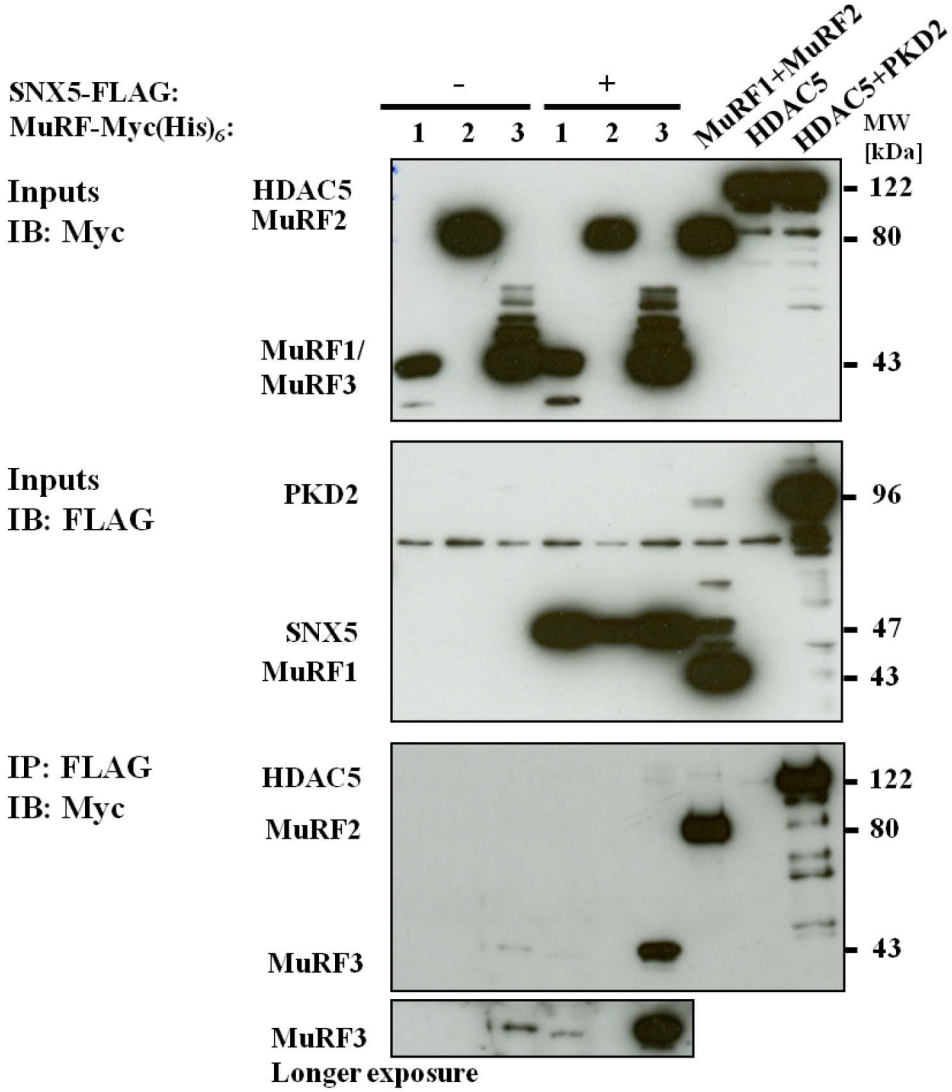

Figure 16: SNX5 physically interacts with MuRF3 in Co-Immunoprecipitation-assays. HEK293 cells were co-transfected with expression plasmids encoding either one of the MuRF-Myc(His)$_6$ - proteins and SNX5-FLAG or empty FLAG-vector. As positive control HEK293 cells were co-transfected with MuRF1-FLAG and MuRF2-Myc(His)$_6$, or HDAC5-Myc and PKD2-FLAG. Inputs (make up 5% of total cell lysates) were analyzed by Immunoblotting (IB), using anti-Myc and anti-FLAG antibodies, and are shown in the upper and middle panels, respectively. Immunoprecipitates (IP) were analyzed using anti-Myc antibody and are shown in the lower panel.

3.3.2. SNX5 co-localizes with MuRF3 in myocytes

To provide further evidence for the interaction between SNX5 and MuRF3, immunofluorescence staining was performed to show possible co-localization. MuRF3-Myc(His)$_6$ and SNX5-FLAG were overexpressed in C2C12 cells. Cells were fixed and stained with either anti-Myc antibody or anti-FLAG antibody. SNX5 showed a perinuclear and cytosolic staining, whereas MuRF3 showed its typical microtubule-like staining pattern,

where fine threads or filament-like structures radiate from the perinuclear region into the cytoplasm (Fig. 17; Spencer J.A. *et al*., 2000).

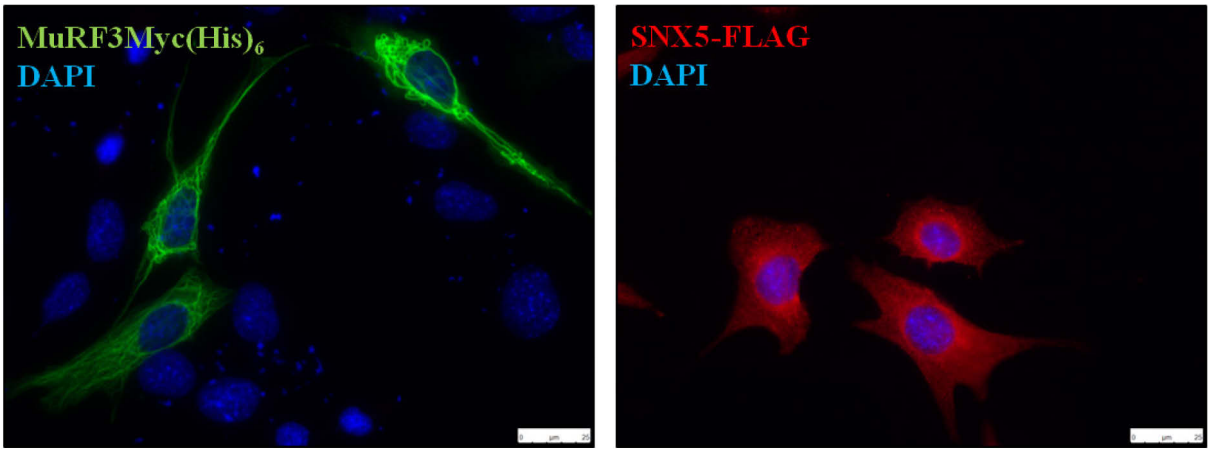

Figure 17: Immunostaining of overexpressed MuRF3 and SNX5 in C2C12 myoblasts. C2C12 cells were plated onto glass coverslips for 24 h before they were transfected either with SNX5-FLAG (right image) or MuRF3-Myc(His)$_6$ (left image). Cells were fixed and stained using specific primary antibodies (anti-FLAG and anti-Myc), and fluorophore - conjugated secondary antibodies (Alexa555, red and Alexa488, green). Nuclei were stained with DAPI. Scale bar, 25 µm.

MuRF3-Myc(His)$_6$ and SNX5-FLAG were co-expressed in C2C12 cells for 24 h and stained using anti-Myc and anti-FLAG antibodies. Images showed a co-localization of MuRF3 and SNX5 (Fig. 18). While MuRF3 showed its typical microtubule-like staining pattern, SNX5 changed its subcellular localization and was co-localized with MuRF3, and therefore exhibited the same staining pattern as MuRF3 (Fig. 18).

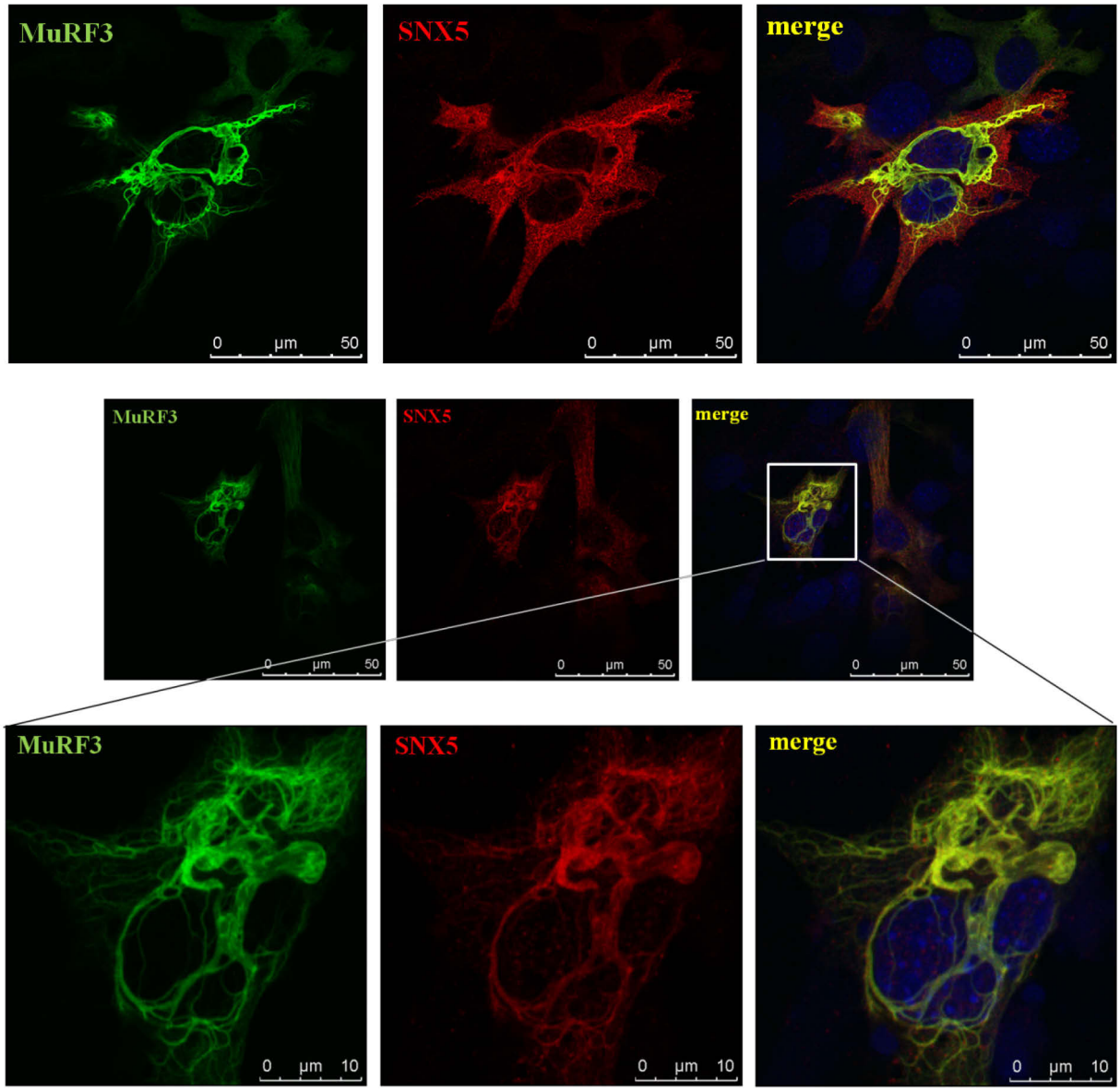

Figure 18: SNX5 co-localizes with MuRF3 in C2C12 myoblasts. C2C12 cells were plated onto glass coverslips for 24 h before they were co-transfected with SNX5-FLAG and MuRF3-Myc(His)$_6$. Cells were fixed and stained using specific primary antibodies (anti-FLAG and anti-Myc), and fluorophore - conjugated secondary antibodies (Alexa555, red and Alexa488, green). Nuclei were stained with DAPI. Immunofluorescence microscopy was performed using 63X objective on a Leica SPE confocal microscope.

Immunofluorescence staining was also performed to investigate the effect of MuRF3-overexpression on the subcellular localization of endogenous SNX5. MuRF3-Myc(His)$_6$ was overexpressed in C2C12 cells which were stained with anti-Myc and anti-SNX5 antibody. Endogenous SNX5 co-localized with MuRF3 (Fig. 19).

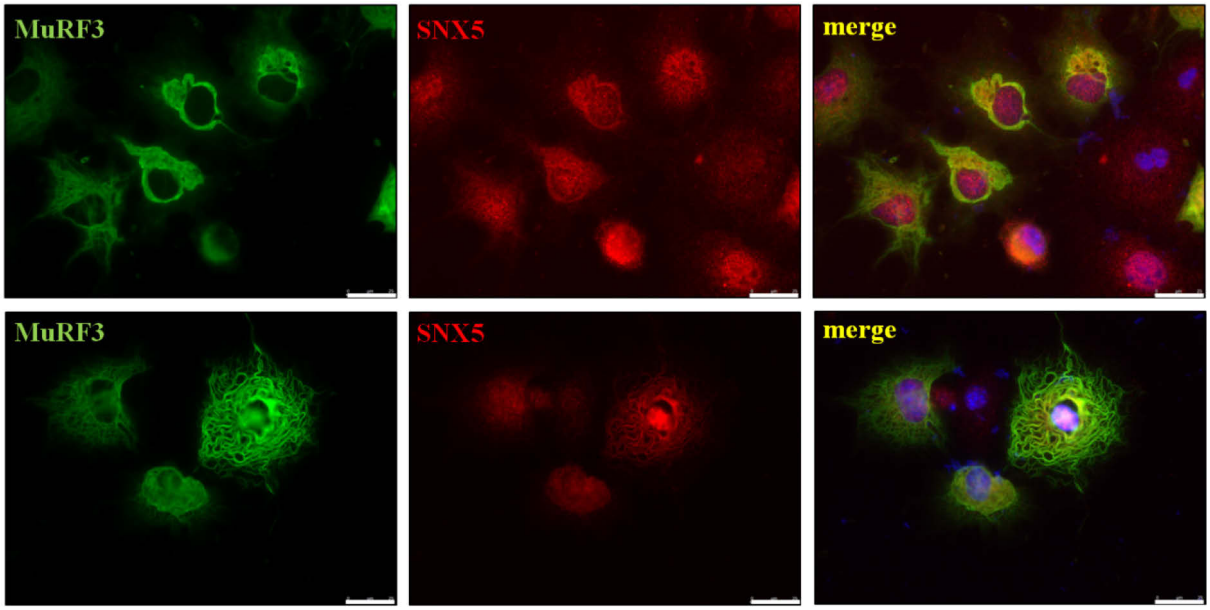

Figure 19: MuRF3 co-localizes with endogenous SNX5. C2C12 cells were transfected with MuRF3-Myc(His)$_6$. Cells were fixed and stained using specific primary antibodies (anti-SNX5 and anti-Myc), and fluorophore - conjugated secondary antibodies (Alexa555, red and Alexa488, green). Nuclei were stained with DAPI. Scale bar, 25 µm.

3.3.3. MuRF3 and SNX5 co-localize and associate with early endosomes

SNX5 predominantly localizes to the membrane of early endosomes (Teasdale R.D. *et al*., 2001; Merino-Trigo A. *et al*., 2004; Sun Y. *et al*., 2013). This could also be shown in this study for endogenous SNX5 (Fig. 15). To show if this was also the case for overexpressed SNX5, SNX5-FLAG was overexpressed in COS7 cells, which were stained with anti-FLAG and anti-EEA1 or with anti-FLAG and anti-LAMP1. Overexpressed SNX5 co-localized with EEA1 (Fig. 20 A, upper panel) but not with LAMP1 (Fig. 20 A, lower panel), indicative to its localization to early endosomes and not to late endosomes or lysosomes.

To investigate the association of MuRF3 with early and late endosomes and lysosomes, MuRF3-cherry (MuRF3 was expressed in pmCherry-N1 expression plasmid, also expressing a red fluorescence protein) was overexpressed in COS7 cells. Cells were stained with either anti-EEA1 or anti-LAMP1. MuRF3 showed its typical microtubule-like structure, where microtubules radiate out of a perinuclear region, the microtubule organizing center (MTOC), where LAMP1, thus most late endosomes and lysosomes are located (Fig. 20 B, lower panel). EEA1 co-localized partially with MuRF3, indicating that early endosomes, which are predominantly located in the cell periphery, are localized to microtubules and thus to MuRF3 (Fig. 20 B, upper panel).

Having shown that SNX5 and MuRF3 co-localize, the logical next step was to analyze their association with early endosomes in a triple immunostaining experiment of MuRF3, SNX5 and EEA1. SNX5-FLAG and MuRF3-cherry were co-expressed in COS7 cells, which were stained with anti-FLAG and anti-EEA1. While MuRF3-cherry carried the red-colored fluorescence marker, a green and a blue fluorophore conjugated secondary antibodies were used for the detection of SNX5 and EEA1, respectively (Fig. 20, C). MuRF3 and SNX5 co-localized and showed the microtubule-like staining pattern. EEA1 staining showed cytosolic, mostly peripheral distribution, partially along the microtubule-like structures, indicative of a partial localization of early endosomes to MuRF3 and SNX5 (Fig. 20, C).

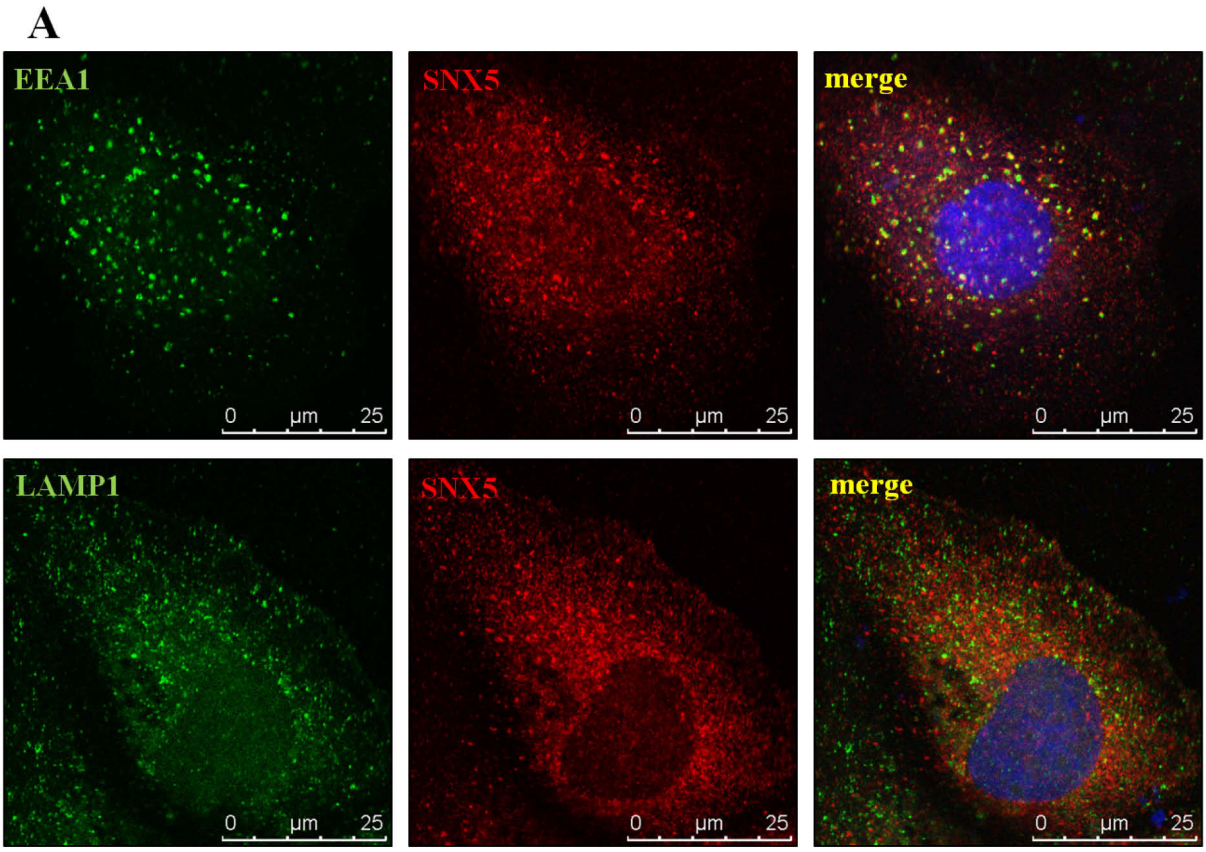

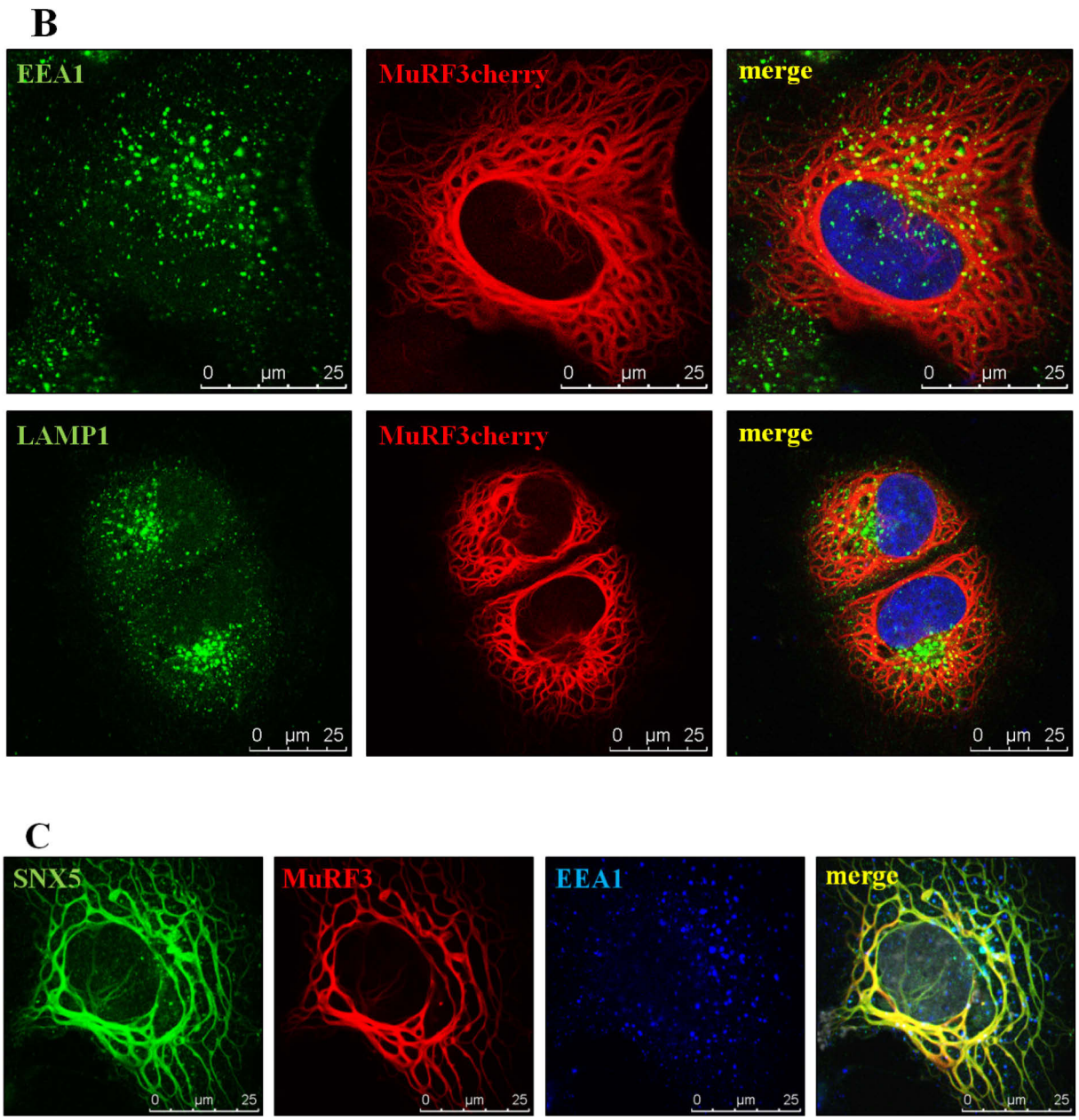

Figure 20: MuRF3 and SNX5 interaction and association with early endosomes. (A) SNX5-FLAG was overexpressed in COS7 for 24 h before they were fixed and stained with anti-FLAG and anti-EEA1 or anti-FLAG and anti-LAMP1. Fluorophore conjugated secondary antibodies Alexa488 (green) and Alexa555 (red) were used. Nuclei were stained with DAPI. **(B)** MuRF3cherry was overexpressed in COS7 cells for 24 h before they were fixed and stained with anti-EEA1 or anti-LAMP1. Fluorophore conjugated secondary antibody Alexa488 (green) was used. Nuclei were stained with DAPI. **(C)** Triple staining of COS7 cells, in which SNX5-FLAG and MuRF3cherry were co-expressed for 24 h before they were fixed and stained with anti-FLAG and anti-EEA1. Fluorophore conjugated secondary antibodies Alexa488 (green) and Alexa647 (blue) were used. Nuclei were stained with DAPI (grey). Images were obtained at a Leica SPE confocal microscope. Scale bar, 25 µm.

3.3.4. Mapping the interaction domains of SNX5 and MuRF3

For the characterization of the interaction between MuRF3 and SNX5, mapping analyses of the interaction domains of both proteins were carried out. In order to determine the interaction domain of MuRF3, its cDNA was cloned into pcDNA3.1(+)-FLAG expression plasmid and deletion mutants, which spanned the full length of MuRF3, were generated. In these deletion mutants the different functionally important domains of MuRF3 were partially or completely deleted (Fig. 21 A). While the deletion mutant MuRF3aa1-81 included only the RING-finger domain and part of the MuRF-family conserved domain, MuRF3aa1-277 deletion mutant lacked the C-terminal acidic rich region and MuRF3aa203-277 only contained the second coiled coil domain (Fig. 21 A). Co-immunoprecipitation assays were carried out after overexpressing wild type SNX5 with either wild type MuRF3 or one of the MuRF3 deletion mutants in HEK293 cells. The expression of the deletion mutants lacking MuRF3 C-terminus was not detectable in western blot. The expression of MuRF3aa1-81, MuRF3aa82-117, MuRF3aa118-159, MuRF3aa160-202, MuRF3aa203-277, as well as MuRF3aa278-267 could not be detected due to their small size (Fig. 21, B). Deletion mutants including either one of the two MuRF3 coiled coil domains; MuRF3aa1-202, MuRF3aa1-277, MuRF3aa118-367, MuRF3aa160-367, MuRF3aa203-367, as well as MuRF3aa160-202, which only included the first coiled coil domain and none of the other domains, were all found to interact with SNX5, indicating that MuRF3-coiled coil domains mediated the interaction. In addition, deletion mutant MuRF3aa1-159 interacted with SNX5 as well although it only contained an 18 aa residue of the first coiled coil domain in addition to the RING-finger domain, the MuRF-family conserved (MFC)-domain and the B-Box. Deletion mutant MuRF3aa82-367 which contained both coiled coil domains did not interact with SNX5 (Fig. 21 B).

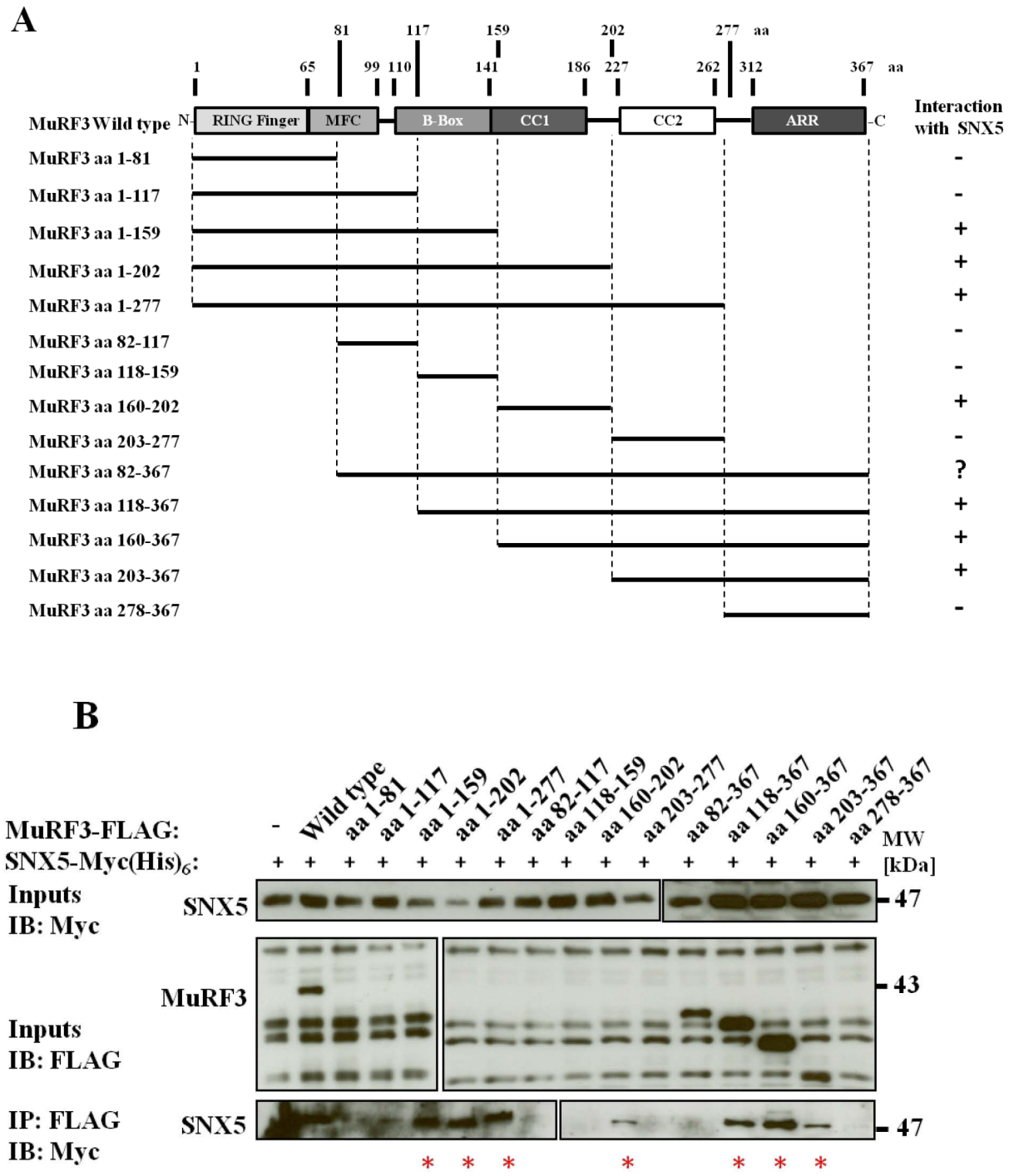

Figure 21: Mapping the interaction between MuRF3-deletion mutants and wild type SNX5. (A) A schematic diagram of MuRF3-domain organization and the different deletion mutants used in co-immunoprecipitation assays for determining the MuRF3-interaction domain. **(B)** HEK293 cells were co-transfected with expression plasmids encoding wild type SNX5-Myc(His)$_6$ and either one of the MuRF3-FLAG deletion mutants or empty FLAG-vector. Wild type MuRF3 was used as positive control. Inputs (make up 5% of total cell lysates) were analyzed by Immunoblotting (IB), using anti-Myc and anti-FLAG antibodies, and are shown in the upper and middle panels, respectively. Immunoprecipitates (IP) were analyzed using anti-Myc antibody and are shown in the lower panel. Red asterisks show the precipitates in which SNX5 was co-immunoprecipitated with the MuRF3-deletion mutant. MFC=MuRF-family conserved domain, CC1=coiled coil domain 1, CC2=coiled coil domain 2, ARR=acidic rich region.

For a more accurate characterization of the MuRF3-interaction domain, three additional deletion mutants of MuRF3 were generated in which either the first (MuRF3Δaa141-186), the second (MuRF3Δaa227-262), or both coiled coil domains (MuRF3Δaa141-262), were deleted. A schematic diagram of these deletion mutants is shown in Fig. 22 A. Co-immunoprecipitation assays were carried out to examine the interaction of these deletion mutants with wild type SNX5. Results showed a very weak interaction compared to the interaction between SNX5 and wild type MuRF3, confirming that the MuRF3 coiled coil domains are responsible for the interaction (Fig. 22, B).

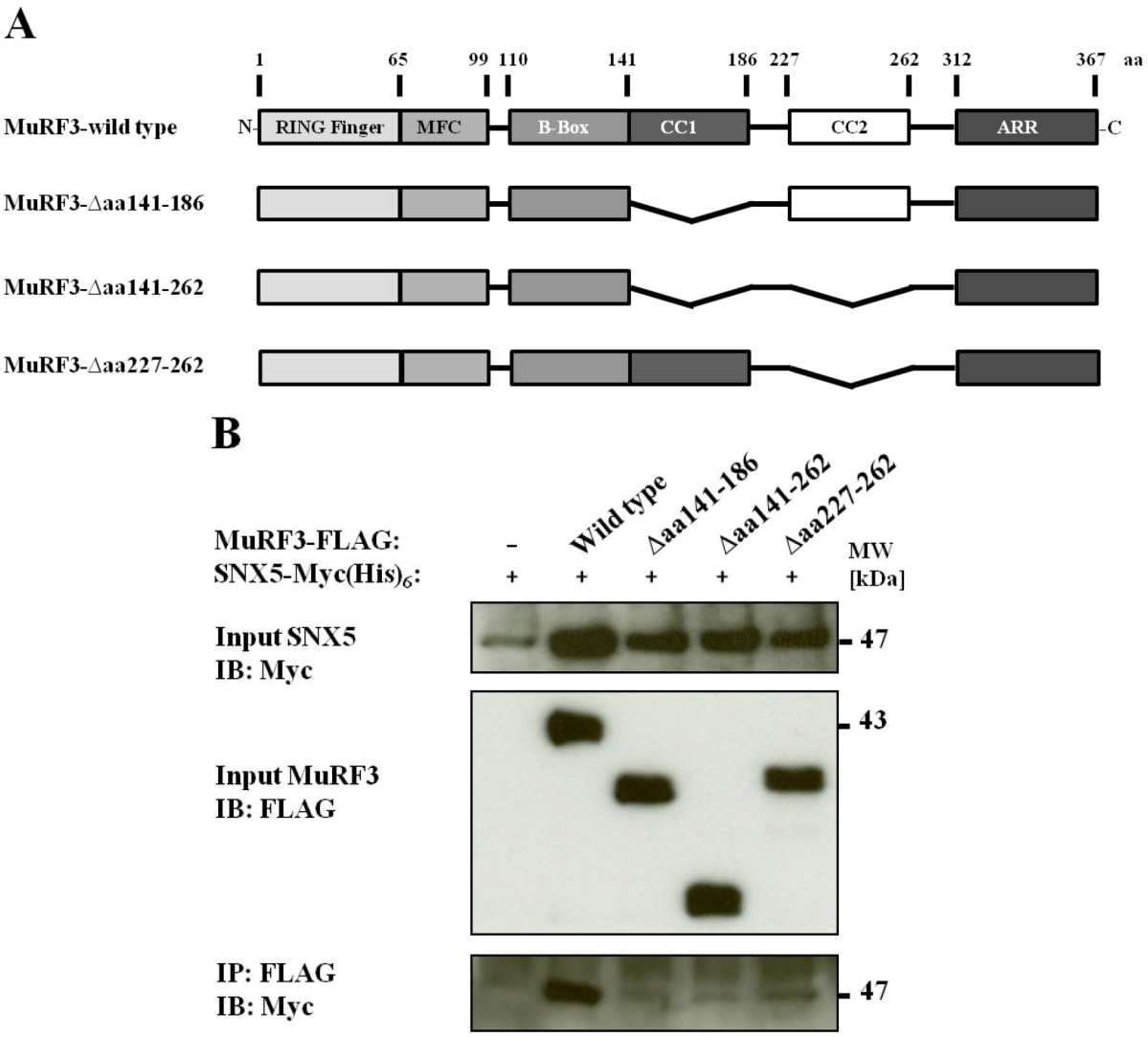

Figure 22: Mapping of the interaction between MuRF3-coiled-coil domain-deletion mutants and wild type SNX5. (A) A schematic diagram of MuRF3 coiled coil-domain deletion mutants. **(B)** HEK293 cells were co-transfected with expression plasmids encoding wild type SNX5-Myc(His)$_6$ and one of the three MuRF3-FLAG coiled coil domain deletion mutants or empty Flag-vector. Wild type MuRF3 was used as positive control. Inputs (make up 5% of total cell lysates) were analyzed by Immunoblotting (IB), using anti-Myc and anti-FLAG

antibodies, and are shown in the upper and middle panels, respectively. Immunoprecipitates (IP) were analyzed using anti-Myc antibody and are shown in the lower panel. SNX5 was co-immunoprecipitated with all three MuRF3-deletion mutants. MFC=MuRF-family conserved domain, CC1=coiled coil domain 1, CC2=coiled coil domain 2, ARR=acidic rich region.

To determine which domain of SNX5 is responsible for its interaction with MuRF3, five different deletion mutants were generated (Fig. 23, A). SNX5-PX deletion mutant lacked the BAR domain, SNX5-BAR lacked the Phox domain and SNX5Δaa206-256, SNX5Δaa262-327 and SNX5Δaa344-397 had deletions in the first, second or third coiled coil domain (CCD) of the BAR-domain, respectively (Fig. 23, A). SNX5-FLAG deletion mutants were overexpressed with wild type MuRF3-Myc$(His)_6$ in HEK293 cells and co-immunoprecipitation assays were carried out. Results showed that the BAR domain of SNX5 mediated its interaction with MuRF3. Also, deleting one of the three CCDs composing the BAR domain did not affect the interaction, although the first and the third CCDs might be more essential for the interaction, since it was weaker when either one was deleted. SNX5-Phox-domain did not mediate MuRF3- interaction (Fig. 23, B).

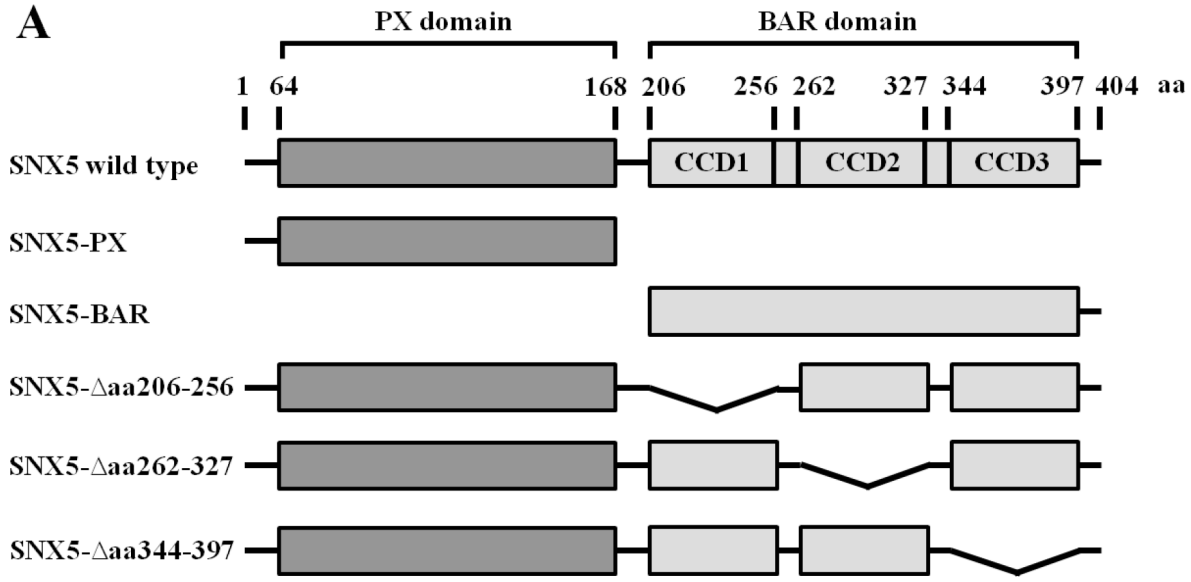

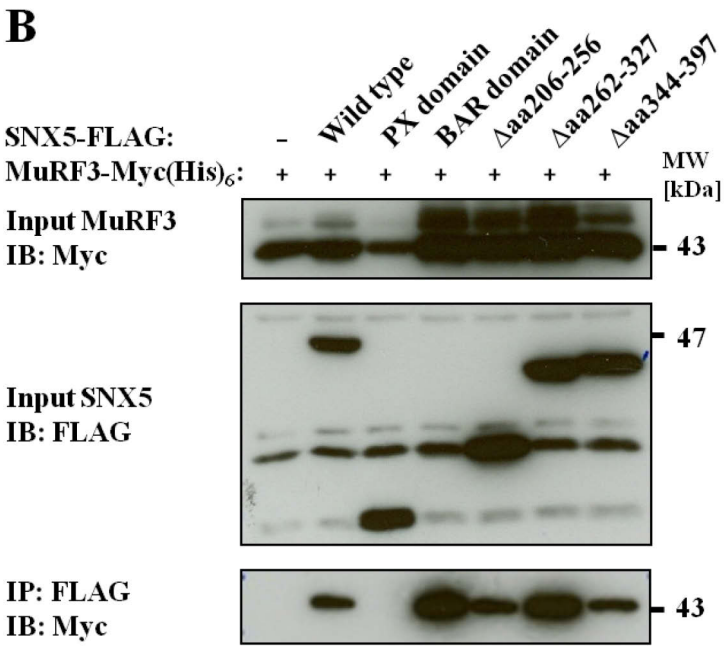

Figure 23: Mapping of the interaction between SNX5-deletion mutants and wild type MuRF3. (A) Schematic diagram of five SNX5 deletion mutants which were generated to determine the accurate interaction domain of SNX5. **(B)** Co-immunoprecipitation assays were performed after co-transfection of HEK293 with expression plasmids encoding wild type MuRF3-Myc(His)$_6$ and either one of the five SNX5-FLAG deletion mutants or the empty Flag-vector. Wild type SNX5 was used as positive control. Inputs (make up 5% of total cell lysates) were analyzed by Immunoblotting (IB), using anti-Myc and anti-FLAG antibodies, and are shown in the upper and middle panels, respectively. Immunoprecipitates (IP) were analyzed using anti-Myc antibody and are shown in the lower panel. MuRF3 was only co-immunoprecipitated with SNX5-BAR domain, or SNX5-BAR domain lacking one of its CCDs, but not with SNX5-PX-domain. SNX5-PX=SNX5-Phox homology domain. CCD=coiled coil domain.

These results were confirmed in immunofluorescence assays. Wild type MuRF3-Myc(His)$_6$ and either wild type SNX5-FLAG or one of its deletion mutants were co-expressed in C2C12 cells, which were stained with anti-Myc and anti-FLAG. SNX5-BAR domain co-localized with MuRF3, whereas no co-localization was observed between SNX5-PX and MuRF3 (Fig. 24). The BAR-domain deletion mutants, with each lacking one of the three CCDs, also co-localized with MuRF3, confirming results of co-immunoprecipitation assays (Fig. 25).

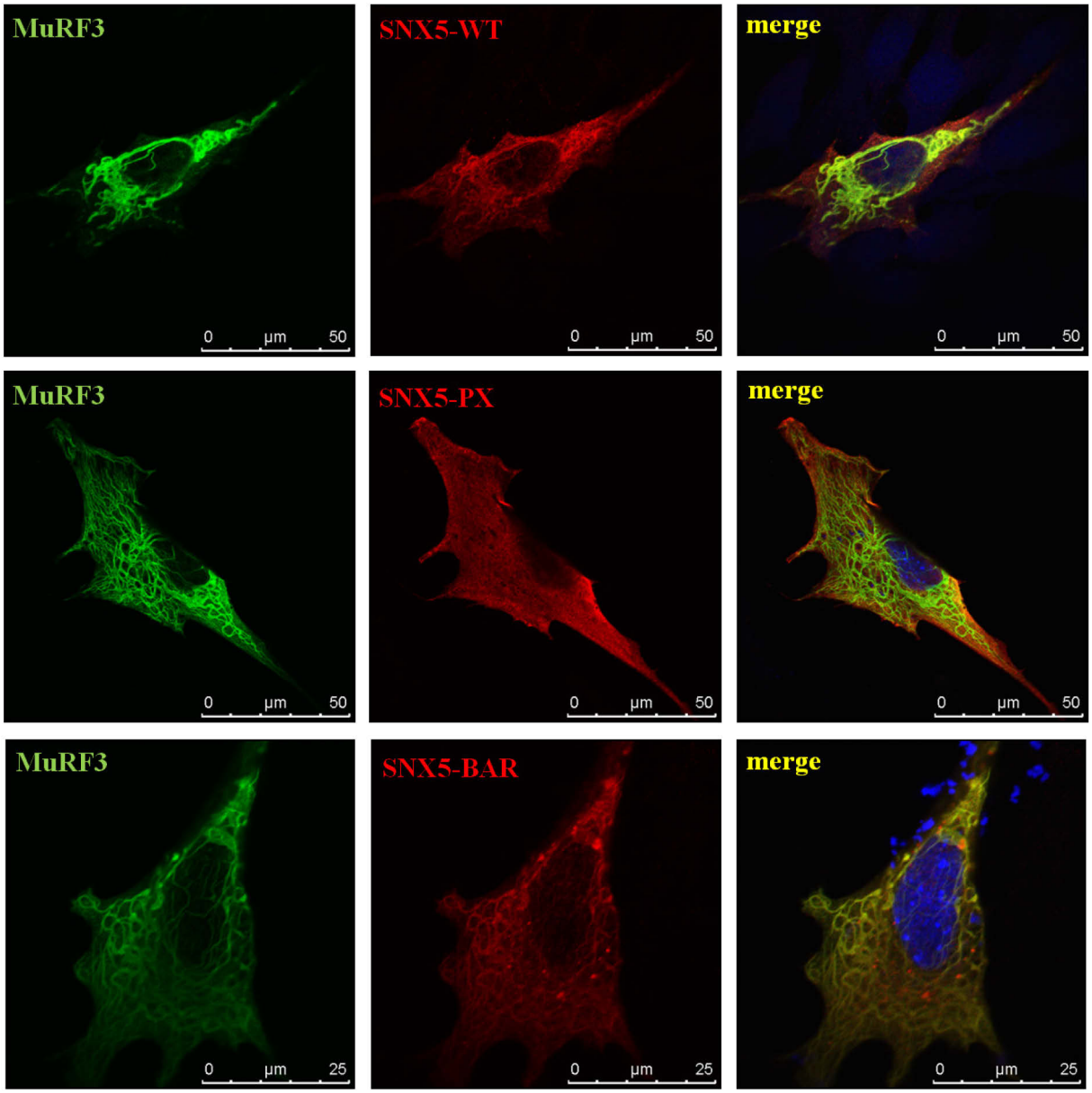

Figure 24: MuRF3 co-localized with SNX5-BAR-domain and not SNX5-PX-domain. C2C12 cells were plated onto glass coverslips for 24 h before they were co-transfected with either SNX5-BAR-FLAG or SNX5-PX-FLAG (red) and MuRF3-Myc(His)$_6$ (green). Cells were fixed and stained using specific primary antibodies (anti-FLAG and anti-Myc), and fluorophore - conjugated secondary antibodies (Alexa555, red and Alexa488, green). Nuclei were stained with DAPI. Immunofluorescence microscopy was performed using 63X objective on a Leica SPE confocal microscope.

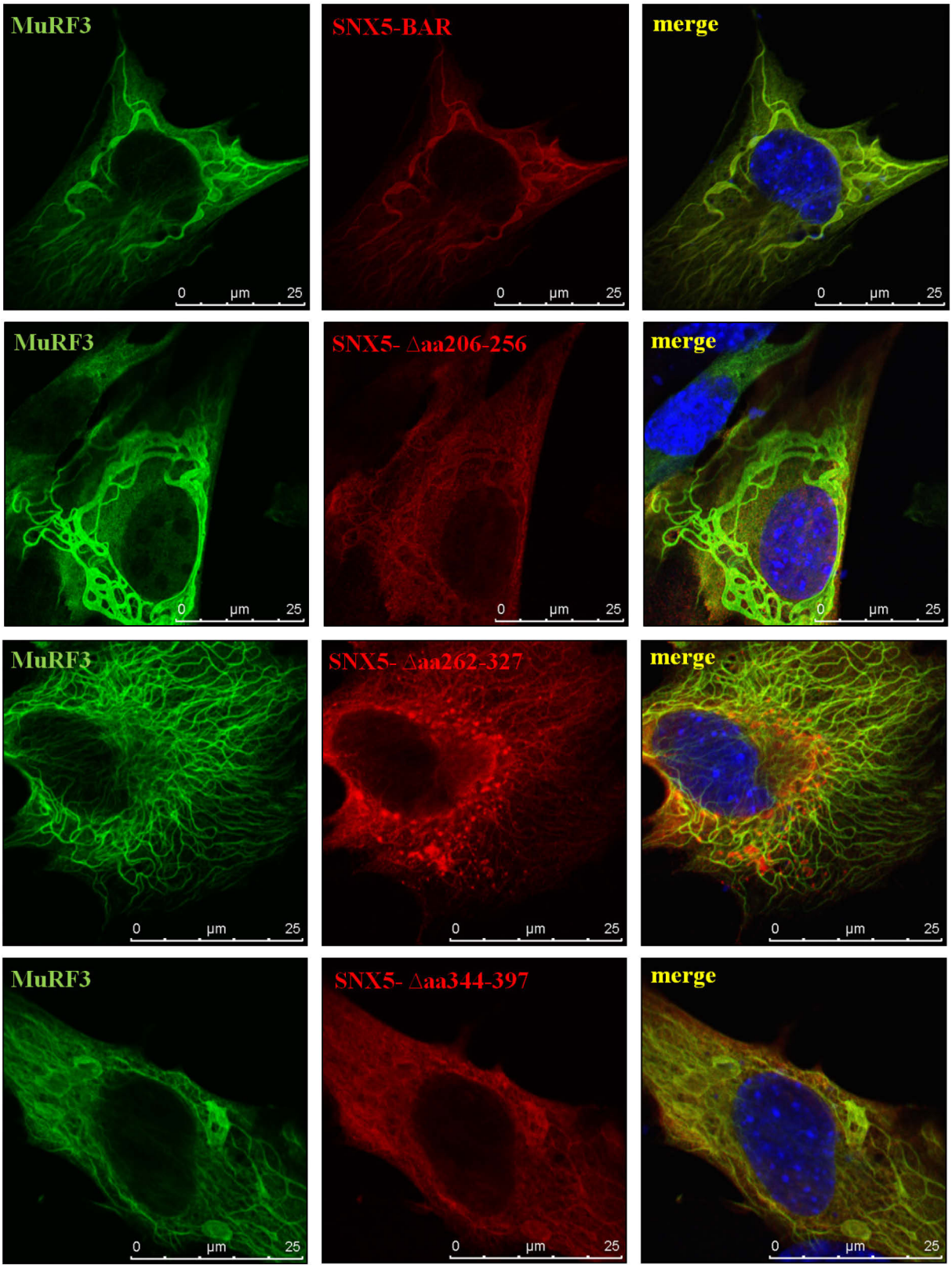

Figure 25: MuRF3 co-localized with all three SNX5-BAR-domain deletion mutants. C2C12 cells were co-transfected with either one of the three SNX5-BAR-FLAG deletion mutants (red), each lacking one of the three CCDs of the BAR domain, and MuRF3-Myc(His)$_6$ (green). Cells were fixed and stained using specific primary antibodies (anti-FLAG and anti-Myc), and fluorophore - conjugated secondary antibodies (Alexa555, red and Alexa488, green). Nuclei were stained with DAPI. Immunofluorescence microscopy was performed using 63X objective on a Leica SPE confocal microscope.

3.4. SNX5 is a target protein of MuRF2

3.4.1. MuRF2-overexpression causes SNX5 depletion in C2C12 cells

Once co-expressed with MuRF2, SNX5 expression decreased. This observation was made repeatedly in several expression tests, leading to the assumption that SNX5 was a putative MuRF2 substrate. To further investigate this, expression assays were carried out, in which C2C12 cells were co-transfected with increasing amounts of MuRF2-Myc(His)$_6$ or MuRF3-Myc(His)$_6$ and a constant amount of SNX5-FLAG. Western blot analysis, using anti-Myc and anti-FLAG antibodies showed a decrease in SNX5 expression the more MuRF2-Myc(His)$_6$ was expressed. On the other hand, increasing amounts of MuRF3 had no effect on SNX5 (Fig. 26, A). Because the RING finger domain of MuRF-proteins mediates their E3 ligase activity (Lorick K.L. *et al*., 1999; Joazeiro C.A. and Weissman A.M., 2000; Spencer J.A. *et al*., 2000), two of the four functionally essential cysteine residues in the MuRF2 RING-finger domain (cysteines 42 and 50) were mutated to serine residues through site directed mutagenesis, generating the E3 ligase deficient MuRF2-[(C42S; C50S)]. In another expression assay, increasing amounts of MuRF2-[(C42S; C50S)]-Myc(His)$_6$ and a constant amount of SNX5-FLAG were co-transfected in C2C12 cells. Western blot analysis, using anti-Myc and anti-FLAG antibodies showed that increasing expression of E3 ligase deficient MuRF2 did not affect SNX5 expression, indicating that SNX5 was subjected to MuRF2-mediated degradation (Fig. 26, B).

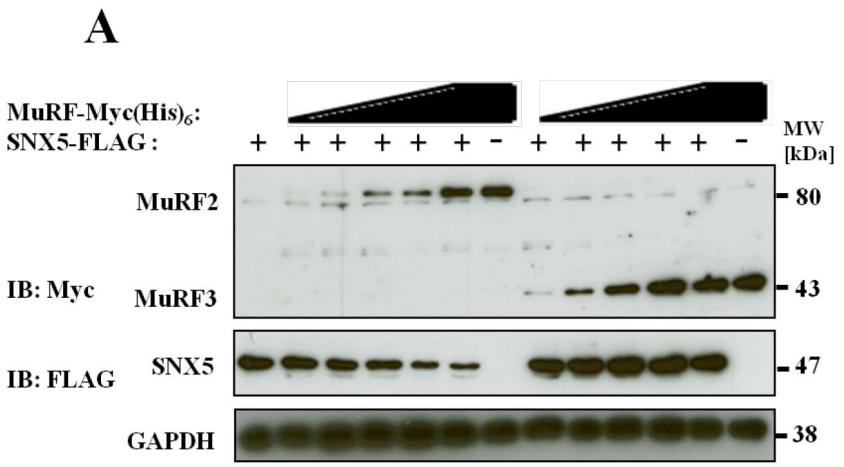

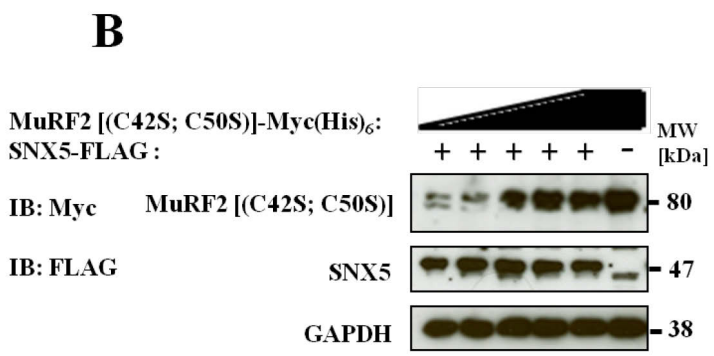

Figure 26: SNX5 is a target of MuRF2 and not MuRF3. (A) C2C12 cells were co-transfected with increasing amounts of MuRF2-Myc(His)$_6$ or MuRF3-Myc(His)$_6$ and a constant amount of SNX5-FLAG. Cells were lysed 24 h later and overexpressed proteins were analyzed in a western blot using anti-Myc and anti-FLAG antibodies for detection. **(B)** The same analysis was carried out with the E3 ligase deficient MuRF2-[(C42S; C50S)]-Myc(His)$_6$, in which two functionally essential cysteine residues (42 and 50) of its RING finger domain were mutated to serines, thus inactivating its E3 ligase function. In this case, as in the case of overexpressing MuRF3, no decrease in SNX5 was observed.

For further investigation of SNX5 degradation by MuRF2, Cycloheximide (CHX) chase experiments were performed. First, SNX5-FLAG, MuRF2-Myc(His)$_6$ and MuRF3-Myc(His)$_6$ were overexpressed separately in C2C12 cells for 24 h. Cells were then treated with CHX for different time points. Western blot analysis showed that overexpressed SNX5 had a half-life of 2 hours. MuRF2 was stable even after 6 hours of CHX treatment, and MuRF3 was stable after 4 hours but showed a decrease in protein content after 6 hours of CHX treatment (Fig. 27, A). SNX5 and MuRF2 were also co-expressed in C2C12 cells for 24 hours, which were then treated with CHX. Western blot results showed that even without CHX treatment (time point 0 h), a decrease in SNX5 expression was observed when co-expressed with MuRF2. In comparison with CHX-chase of SNX5 alone, an enhanced SNX5 degradation was observed when co-expressed with MuRF2, indicating that MuRF2 increases the degradation of SNX5 (Fig. 27, B). The densitometrical analysis of SNX5 expression showed 0% remaining SNX5 after 6 hours of CHX treatment when co-expressed with MuRF2 compared with over 10% remaining SNX5 when expressed alone (Fig. 27, D). The same experimental approach was used to investigate the effect of MuRF3 on SNX5. Interestingly, MuRF3 not only did not increase SNX5 degradation, but it rather stabilized SNX5 protein content throughout the course of the experiment, with over 30% of SNX5 remaining after 6 hours of CHX treatment, when it was co-expressed with MuRF3 (Fig. 27, C and D).

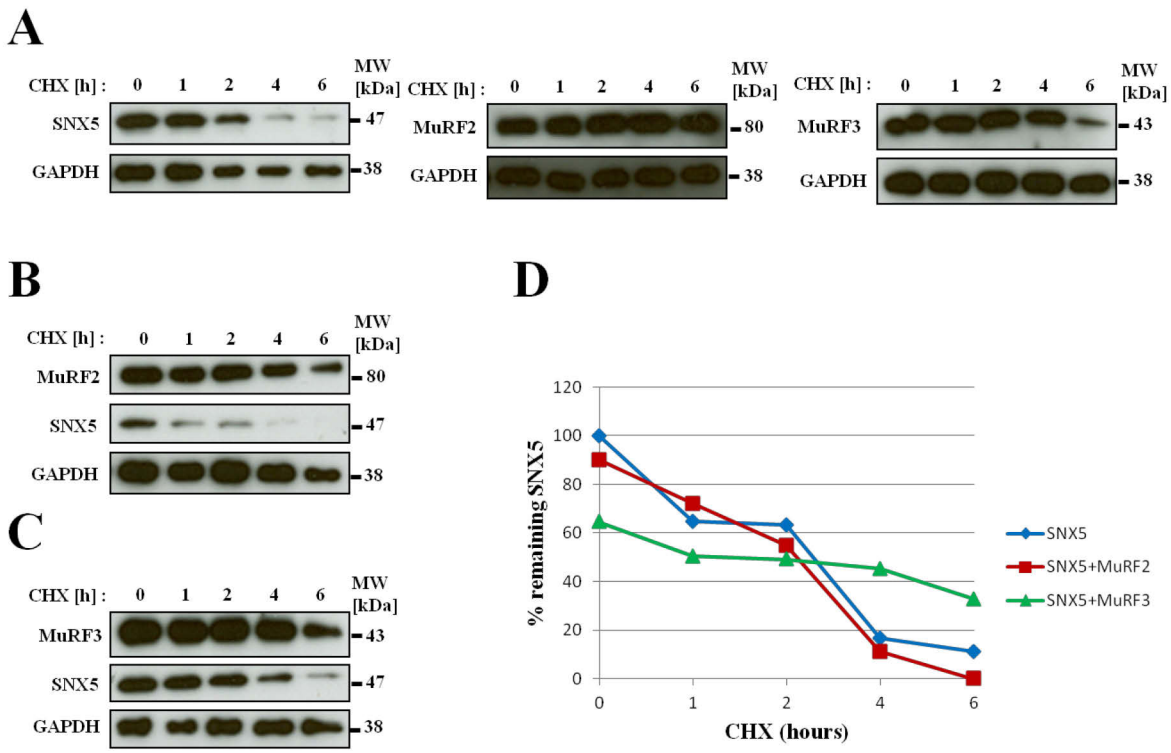

Figure 27: MuRF2 enhanced SNX5 degradation in Cycloheximide chase experiments. (A) SNX5-FLAG, MuRF2-Myc(His)$_6$ and MuRF3-Myc(His)$_6$ were overexpressed separately for 24 h in C2C12 cells which were then treated with Cycloheximide for 0, 1, 2, 4, or 6 h. Anti-Myc and anti-FLAG antibodies were used for detection of protein expression. **(B)** SNX5-FLAG was co-expressed with MuRF2-Myc(His)$_6$ or with MuRF3-Myc(His)$_6$ **(C)** in C2C12 cells for 24 hours, which were then treated with Cycloheximide. GAPDH was used as loading control. **(D)** Densitometrical analysis of **(B)** and **(C)**. For evaluation of protein degradation, the signal intensities of SNX5 bands were normalized against the accordant GAPDH signals and SNX5 signal in **(A)** of the '0 h' sample was set as 100%. Densitometrical analysis was carried out in ImageJ processing program. CHX=Cycloheximide

3.4.2. SNX5 inhibits MuRF2-auto-ubiquitination in *in vitro* ubiquitination assays

In vitro ubiquitination assays were performed to investigate if MuRF2 ubiquitinates its putative target protein SNX5. For these experiments, MBP-MuRF1, -2 and -3, and SNX5-recombinant proteins were expressed and purified, and the assays were performed in a cell free system. As negative controls either E1, E2 (UbcH5a), E3 (MuRF), or ubiquitin were not added to the reaction. SNX5 was used as a potential substrate to be ubiquitinated, but was left out of the reaction as a control and to test auto-ubiquitination of MuRF E3 ligases (Fig. 28, left blot). Samples were subjected to SDS-PAGE and analyzed by western blot using anti-ubiquitin antibody (Fig. 28). Ubiquitination of SNX5 could not be detected. However, MuRF2 was found to auto-ubiquitinate. Auto-ubiquitination of MuRF2 was inhibited when SNX5 was added to the reaction, providing further evidence that MuRF2 interacts with SNX5

and mediates its degradation (Fig. 28, red arrows). Auto-ubiquitination of MuRF1 and MuRF3 was not detected.

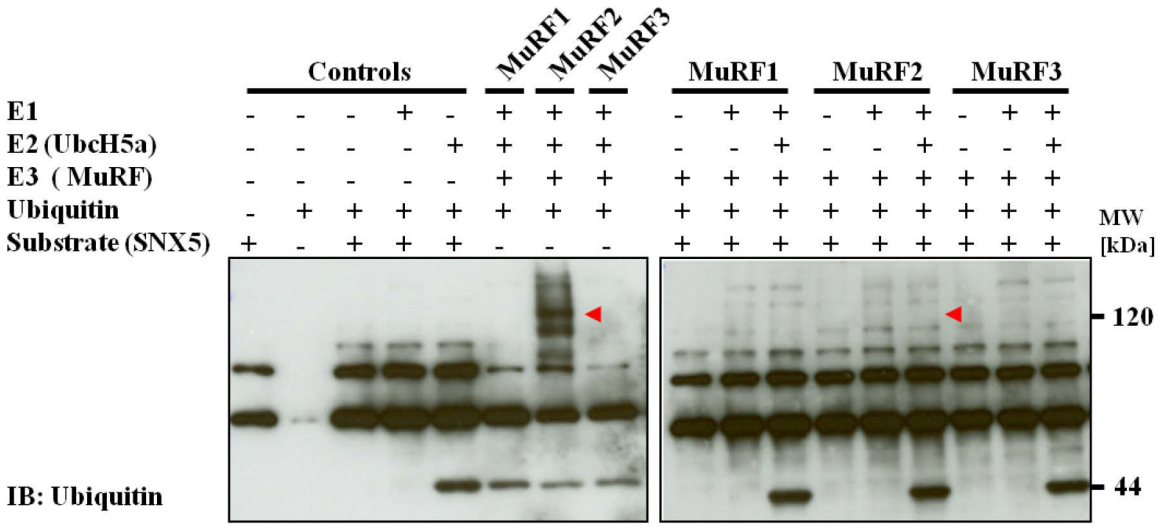

Figure 28: SNX5 inhibition of MuRF2 auto-ubiquitination in *in vitro* ubiquitination assay. *In vitro* ubiquitination assays were performed with recombinant GST-E1, GST-UbcH5a (E2), MBP-MuRF1, MBP-MuRF2, or MBP-MuRF3, ubiquitin, and either with (right) or without (left) recombinant SNX5 as substrate. Western blot analysis was performed and anti-ubiquitin antibody was used for detection. The high molecular weight multiubiquitin chains detected on the left blot (red arrow) represent the auto-ubiquitination of MuRF2, which was inhibited after adding the substrate SNX5 to the reaction (right blot, red arrow).

3.4.3. MuRF2 degrades SNX5 in a UPS-dependent manner

To investigate whether MuRF2-mediated SNX5 degradation is UPS-dependent, expression assays in the presence or absence of MG132 were carried out. First, MuRF2, MuRF3 and SNX5 were expressed separately in C2C12 cells for 24 hours. Cells were then treated with MG132 or vehicle for 6 hours before lysis. Protein expression was examined in western blot analysis. MG132 led to an increased MuRF2, MuRF3 and SNX5 protein content compared to controls (Fig. 29). Consistent with previous results (Fig. 26 and 27), co-expression of SNX5 and MuRF2 resulted in a decrease in SNX5 protein, compared to its separate expression, indicative of its MuRF2-mediated degradation. This effect was reversed through proteasome inhibition by MG132, indicating that MuRF2-mediated SNX5-degradation occurs via the proteasome. When MuRF2, MuRF3 and SNX5 were overexpressed together, the MuRF2-mediated SNX5-degradation was abolished, confirming the stabilizing effect of MuRF3 on SNX5 (Fig. 29).

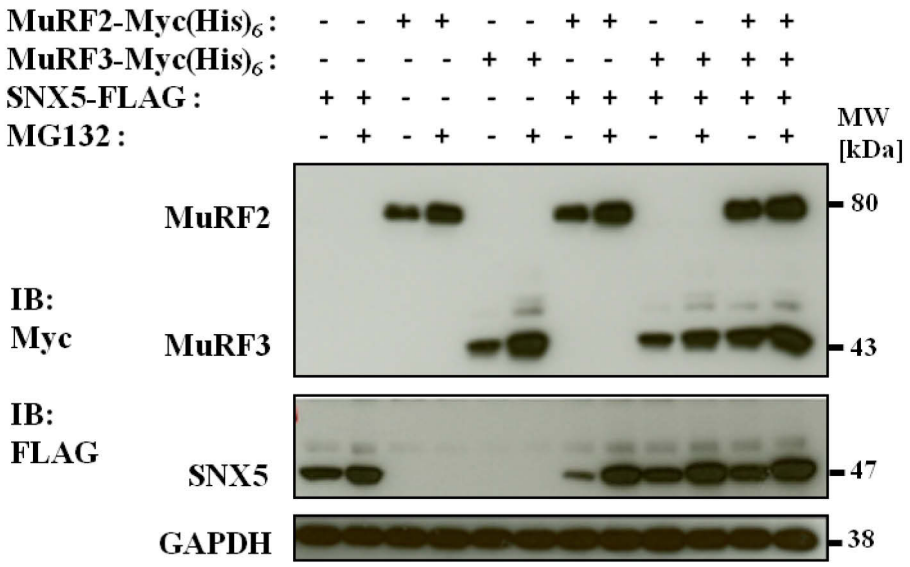

Figure 29: SNX5 is degraded by MuRF2 in a UPS-dependent manner. MuRF2-Myc(His)$_6$ or MuRF3-Myc(His)$_6$ and SNX5-FLAG were overexpressed in C2C12 cells for 24 h either separately or in a co- or triple-transfection. Cells were then incubated for another 6 h in MG132 (10µM) for proteasome inhibition or vehicle before they were lysed. Western blot analysis was carried out to detect overexpressed proteins. Specific antibodies against Myc-tag and FLAG-tag were used. GAPDH was used as loading control.

Immunofluorescence staining was used to examine the effects of MG132 treatment on MuRF2 and SNX5 expression. SNX5-FLAG and MuRF2-Myc(His)$_6$ were co-expressed in C2C12 cells. Cells were either fixed or treated with MG132 for 6 hours before they were also fixed and stained. As expected, cells which were not treated with MG132 showed almost no SNX5 expression, indicative of its rapid degradation by MuRF2 (Fig. 30, A). After MG132 treatment, SNX5-expression was detectable, as its MuRF2-mediated UPS-dependent degradation was prevented (Fig. 30, B).

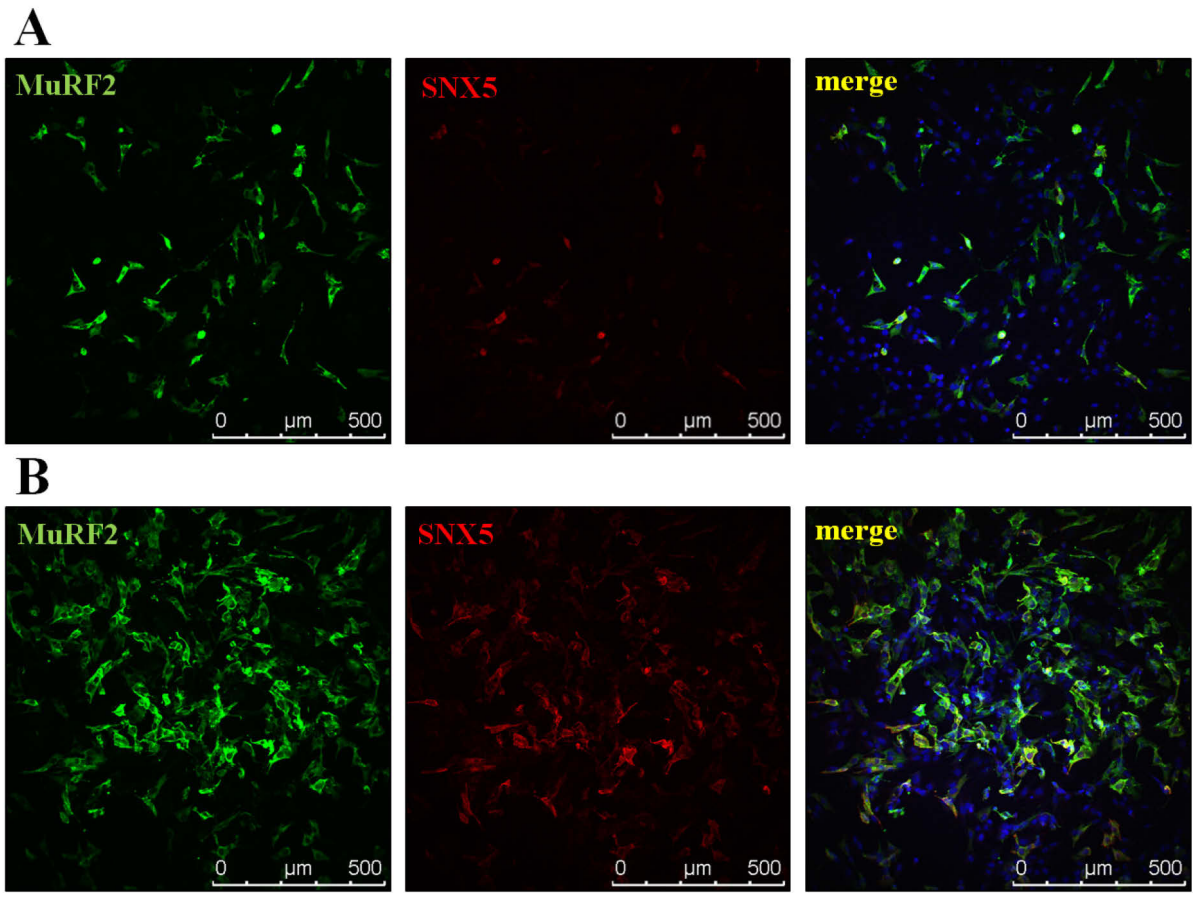

Figure 30: MG132 rescues the depletion effect of MuRF2 overexpression on SNX5 in C2C12 cells. C2C12 cells were co-transfected with SNX5-FLAG and MuRF2-Myc(His)$_6$. Cells were fixed 24 h after transfection **(A)**, or were incubated for another 6 h in MG132 before they were fixed **(B)**. Cells were stained using specific primary antibodies against FLAG-tag and Myc-tag, and fluorophore - conjugated secondary antibodies (Alexa555, red and Alexa488, green). Nuclei were stained with DAPI. Immunofluorescence microscopy was performed using 63X objective on a Leica SPE confocal microscope.

3.4.4. MuRF2 interacts with and ubiquitinates SNX5 in *in vivo* ubiquitination assays

A physical interaction between MuRF2 and its substrate SNX5 in co-immunoprecipitation assays could not be shown thus far, presumably due to its rapid degradation. To stabilize ubiquitinated SNX5 and inhibit its UPS-mediated degradation, *in vivo* ubiquitination assays were carried out, in which MG132 was used. In addition, the deubiquitinase-inhibitor *N*-Ethylmaleimide (NEM) was applied during cell lysis to prevent the cleavage of ubiquitin bound to SNX5 by deubiquitinating enzymes (DUBs). SNX5-FLAG was co-expressed with MuRF2-Myc(His)$_6$ or MuRF3-Myc(His)$_6$ in C2C12 cells for 24 h. Co-immunoprecipitation assays were performed after incubation with MG132 and application of NEM. As control cells were incubated in vehicle and NEM-free lysis buffer was used. Immunoprecipitates were

subjected to SDS-PAGE and western blot analysis using anti-Myc antibody for the detection of MuRF2-Myc(His)$_6$ and MuRF3-Myc(His)$_6$. While MuRF3 interacted with SNX5, regardless of whether MG132 and NEM were used or not, MuRF2 only co-precipitated with SNX5 after MG132 treatment and NEM application. This indicates a physical interaction between MuRF2 and SNX5, which is detectable only when the degradation is inhibited. Also, auto-ubiquitination of MuRF2 was detected in the precipitate (Fig. 31).

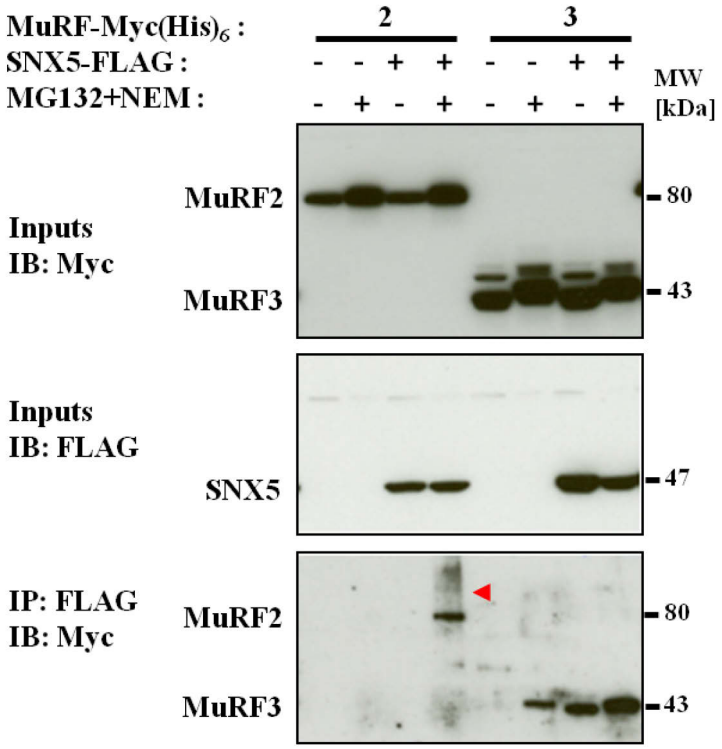

Figure 31: MuRF2 is co-precipitated with SNX5 in *in vivo* ubiquitination assay. C2C12 cells were co-transfected with MuRF2-Myc(His)$_6$ or MuRF3-Myc(His)$_6$ and SNX5-FLAG or empty FLAG-vector. Co-immunoprecipitation assays were performed with or without MG132-incubation and application of NEM. Inputs (make up 5% of total cell lysates) were analyzed by Immunoblotting (IB), using anti-Myc and anti-FLAG antibodies, and are shown in the upper and middle panels, respectively. Immunoprecipitates (IP) were analyzed using anti-Myc antibody and are shown in the lower panel. MuRF3 was detected in SNX5 immunoprecipitates both with and without MG132 and NEM. MuRF2 was only co-precipitated with SNX5 after MG132 treatment and NEM application, and showed auto-ubiquitination (red arrow). NEM= *N*-Ethylmaleimide.

Another *in vivo* ubiquitination assay was performed to investigate the interaction between MuRF2 and SNX5 in more detail. In addition to the previous assay, MG132 and NEM were also applied separately, and detection of co-precipitates was also carried out with specific anti-SNX5 antibody. SNX5-FLAG was co-expressed with MuRF2-Myc(His)$_6$ in C2C12 cells for 24 h. Co-immunoprecipitation assays were performed after incubation with MG132 and

application of NEM. As control cells were incubated in vehicle and NEM-free lysis buffer was used. Immunoprecipitates were subjected to SDS-PAGE and western blot analysis using anti-Myc or anti-SNX5 antibodies. When anti-Myc antibody was used for detection, the interaction between SNX5 and MuRF2 was detectable when only MG132 was used. However, more MuRF2 was co-precipitated with SNX5 when both MG132 and NEM were used. In contrast, MuRF2 was not detected in SNX5-precipitates when only NEM was applied. When detection of co-precipitates was carried out with specific anti-SNX5 antibody, and after longer exposure of western blots, ubiquitination of SNX5 was detectable, but only in co-immunoprecipitations where either MG132 or both MG132 and NEM were applied. These results provided further evidence that MuRF2 interacts with and ubiquitinates SNX5, mediating its UPS-dependent degradation (Fig. 32).

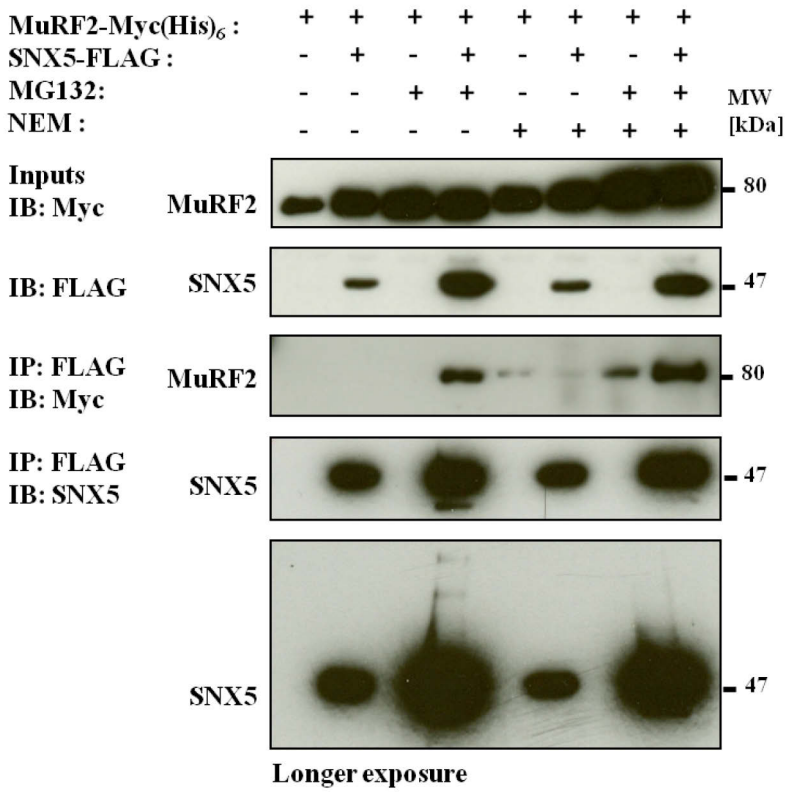

Figure 32: MuRF2 interacts with and ubiquitinates SNX5 in *in vivo* ubiquitination assay. C2C12 cells were co-transfected with MuRF2-Myc(His)$_6$ and SNX5-FLAG or empty FLAG-vector. Co-immunoprecipitation assays were performed with or without MG132-incubation and application of NEM in cell lysis. Inputs (make up 5% of total cell lysates) were analyzed by Immunoblotting (IB), using anti-Myc and anti-FLAG antibodies, and are shown in the two upper panels. Immunoprecipitates (IP) were analyzed using anti-Myc and anti-SNX5 antibodies and are shown in the three lower panels. MuRF2 was co-precipitated with SNX5 after MG132 treatment, regardless of NEM application. Ubiquitination of SNX5 was detectable after longer exposure. NEM= *N*-Ethylmaleimide.

3.4.5. MuRF3 stabilizes SNX5 and prevents its MuRF2-mediated degradation

This study showed that MuRF3 stabilized SNX5. To investigate this in more detail, an expression assay was performed, in which MuRF2-Myc(His)$_6$ or MuRF3-Myc(His)$_6$ and SNX5-FLAG were overexpressed in C2C12 cells for 24 h either separately or in co- or triple-transfections. In triple-transfections, constant amounts of MuRF2 and SNX5 were overexpressed with three increasing amounts of MuRF3 expression plasmid. Cell lysates were subjected to SDS-PAGE and western blot analysis. Co-expression of MuRF2 with SNX5 led to a decrease in SNX5 expression. This effect was inhibited by increasing amounts of MuRF3, indicating that MuRF3 stabilizes SNX5 and prevents its MuRF2-mediated degradation. Interestingly, MuRF3 appeared to stabilize MuRF2 as well (Fig. 33).

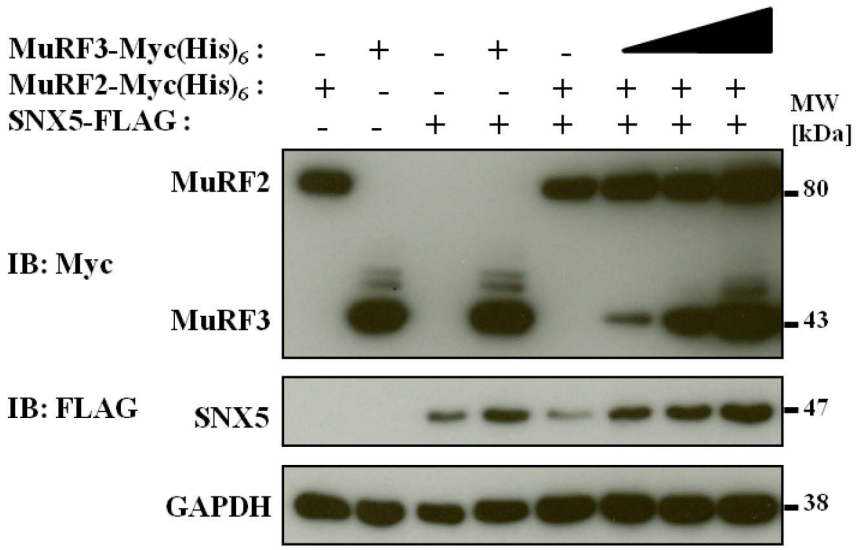

Figure 33: MuRF3 stabilizes SNX5 and prevents its MuRF2-dependent degradation. MuRF2-Myc(His)$_6$ or MuRF3-Myc(His)$_6$ and SNX5-FLAG were overexpressed in C2C12 cells for 24 h either separately or in a co- or triple-transfection. Three different amounts of expression plasmid encoding for MuRF3-Myc(His)$_6$ were transfected to examine its effect on SNX5 expression. Western blot analysis was carried out to detect overexpressed proteins, using specific antibodies against Myc-tag and FLAG-tag. GAPDH was used as loading control.

3.5. SNX5 expression during skeletal muscle atrophy

3.5.1. SNX5 expression in the denervation atrophy mouse model

Because endogenous expression tests showed especially high SNX5 expression in muscle, a possible change in *Snx5* mRNA expression and SNX5 protein content during skeletal muscle atrophy was investigated. Therefor, two different mouse atrophy models were used. In the first mouse model denervation-induced muscle atrophy was induced in adult male wild type mice by ligation of the left sciatic nerve, resulting in neurogenic atrophy of the lower hindlimb muscles. Mice were sacrificed 7, 14 and 21 days after surgery and muscle tissues were obtained. In addition, muscle tissues from non-treated mice were used as control. For further analyses of SNX5 expression only gastrocnemius-plantaris (GP) muscle was used. Deneravtion resulted in a significant loss of muscle weight, a reduction of myocyte cross sectional area, and increased *Trim63* and *Fbxo32* expression (these results were recently published on the same mice used in this study, Schmidt F. *et al*., 2014; Langhans C. *et al*., 2014). Denervation resulted in a significant upregulation of *Snx5* mRNA expression in the GP muscle 7 (5 fold, $p<0.05$), 14 (4.7 fold, n.s.) and 21 (4.5 fold, $p<0.05$) days after denervation. These results were consistent with western blot analysis, where an increase in SNX5 protein expression 7, 14 and 21 days after denervation was observed. SNX5 expression was increased during denervation-induced atrophy (Fig. 34).

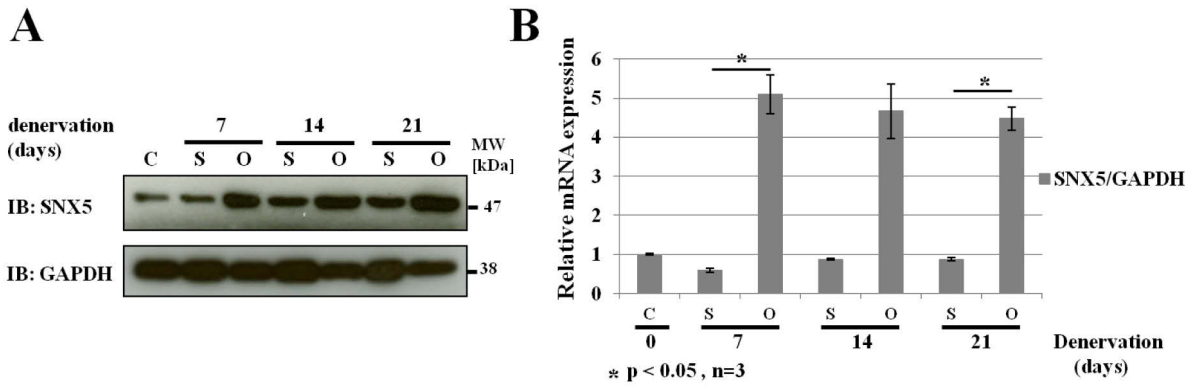

Figure 34: SNX5 expression in denervation-induced skeletal muscle atrophy. Skeletal muscle atrophy was induced in adult male mice by ligation of the left sciatic nerve. Operated (O) and sham (S) mice were sacrificed 7, 14 and 21 days after surgery and muscle tissues were obtained. Muscle tissues from non-treated mice were used as controls (C). Western blot analysis **(A)** and qRT-PCR for *Snx5* expression **(B)** were performed with only *M. gastrocnemius-plantaris* (GP). SNX5 expression was detected in western blots using specific anti-SNX5 antibody. GAPDH was used as control. Data are presented as mean ± SEM. n=3.

3.5.2. SNX5 expression in the starvation atrophy mouse model

The second atrophy mouse model used was starvation. In starvation-induced muscle atrophy, adult male mice were food-deprived for 24 h and 48 h to induce muscle atrophy before they were sacrificed. Control mice were not exposed to starvation and were sacrificed after 0 h, 24 h and 48 h. Muscle tissues were obtained for analyses. Only GP muscle was used for further analysis of SNX5 expression. Starvation resulted in a significant loss of muscle weight, a reduction of myocyte cross sectional area, and increased *Trim63* and *Fbxo32* expression (these results were recently published on the same mice used in this study, Schmidt F. *et al*., 2014; Langhans C. *et al*., 2014). A small increase in *Snx5* mRNA expression was observed after 24 h of starvation. However, no significant change in SNX5 protein content was observed (Fig. 35).

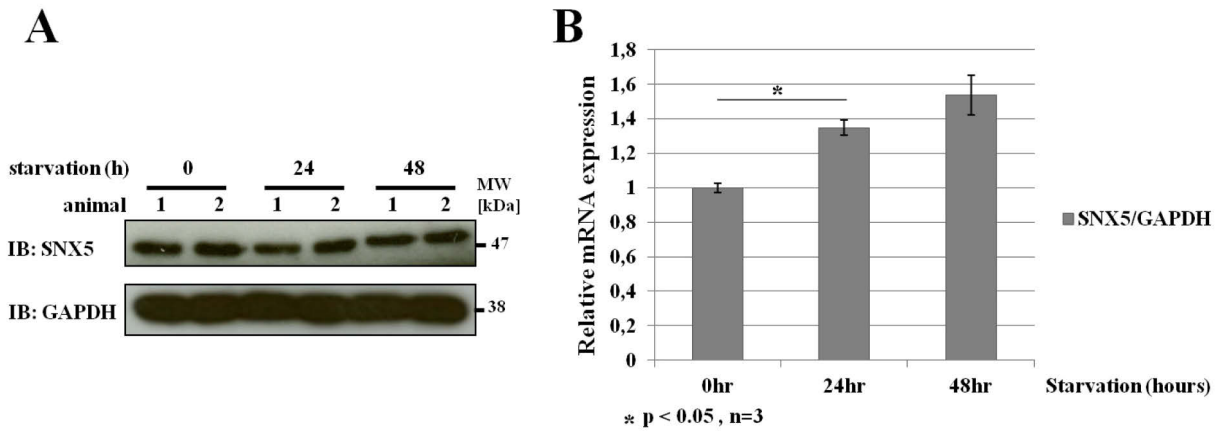

Figure 35: SNX5 expression in starvation-induced skeletal muscle atrophy. Adult male mice were food-deprived for 24 h and 48 h to induce muscle atrophy before they were sacrificed. Control mice were not exposed to starvation and were sacrificed after 0 h, 24 h and 48 h. Muscle tissues were obtained for analyses. Western blot analysis **(A)** and qRT-PCR for *Snx5* expression **(B)** were performed with only *M. gastrocnemius-plantaris* (GP). SNX5 expression was detected in western blots using specific anti-SNX5 antibody. GAPDH was used as control. Quantitative real-time-PCR-analyses of *Snx5* expression were carried out. Data are presented as mean ± SEM. n=3.

4 Discussion

Muscle specific E3 ligases, MuRF1, MuRF2 and MuRF3 have been implicated in several cellular functions such as the degradation of sarcomeric proteins (MuRF1 and MuRF3), indicating their importance in maintenance of skeletal and cardiac muscle structure and function (Fielitz J. *et al.,* 2007 b), stabilization of microtubules (MuRF2 and MuRF3; Spencer J.A. *et al*., 2000, Pizon V. *et al*. 2002), and myocyte differentiation (MuRF2 and MuRF3; Spencer J.A. *et al*., 2000; Centner T. *et al*., 2001; Pizon V. *et al*. 2002). Nevertheless, the precise mode of action of these enzymes is still uncertain. In addition, very little is known about the E3 ligase function of MuRF2, for which no substrate proteins have been identified thus far.

In this study, the aim was to identify and characterize interaction partners and target proteins of MuRF1, MuRF2 and MuRF3 for a better understanding of their functions. For the first time, MuRF2 and MuRF3 were linked to subcellular trafficking through interaction with and regulation of SNX5, which as a retromer subunit is a key player in the retrograde transport from endosomes to TGN (Wassmer T. *et al*., 2007). Also, SNX5 interacts with the muscle specific CHC22 and mediates an intermediate microtubule-dependent retrograde transport step, which is crucial for GLUT4 trafficking in human muscle. Disruption of GLUT4 pathways has been indicated in patients of type 2 diabetes (Vassilopoulos S. *et al.,* 2009; Esk C. *et al*., 2010).

4.1. Using the SILAC-AP-MS approach for the identification of novel substrates and interaction partners for MuRF1, MuRF2, and MuRF3

The quantitative mass spectrometry (MS)-based approach offers the unique potential to place proteins into a functional context while improving the understanding of the molecular processes in which they are involved. For an accurate quantification of proteins, SILAC labeling was combined with conventional protein affinity purification (AP) and MS-analysis (SILAC-AP-MS). This technique allowed the comparison between different cellular states, such as proliferating myoblasts with differentiated myotubes, and differentiated myotubes with atrophic myotubes. This approach also allowed an accurate detection of proteins with a significant change in abundance as a result of MuRF-overexpression, in myoblasts as well as during differentiation and atrophy. An increase in protein abundance indicated that the protein was likely to interact with MuRF or with another up-regulated protein in the same cell population. Conversely, the most likely explanation for decreased protein abundance was that

this protein was a possible substrate of the overexpressed MuRF or it binded another downregulated protein.

An analysis of MS data from the different assays showed that, as expected, a large number of muscle structural and cytoskeleton associated proteins were detected. In addition, many components of the UPS, such as proteasome subunits were also detected in the different screens. MuRF3 was detected as the most enriched protein in myoblasts overexpressing MuRF1 and MuRF2, and MuRF2 was also enriched in myoblasts overexpressing MuRF3, confirming the heterodimerization of MuRF-proteins. Interestingly, many proteins with a significant abundance difference in myoblasts overexpressing MuRF2 and MuRF3 were detected, which were found to be involved with intracellular transport, especially vesicle-mediated transport. For example, in myoblasts overexpressing MuRF2, EEA1 and clathrin light chain B (CLCB) were detected displaying abundance enrichment. EEA1 participates in endocytosis and transport from EEs to LEs, and CLCB is a regulatory subunit of clathrin, the main structural component of coated pits essential for receptor-mediated endocytosis. Another protein which was detected in myoblasts overexpressing MuRF2 with a 1.9-fold enrichment was SNX8. Interestingly, SNX8 regulates endosome-to-TGN transport through a pathway that is distinct from that of the SNX1/SNX5-containing retromer complex (van Weering J.R. *et al*., 2012a; van Weering J.R. *et al*., 2012b). In myoblasts overexpressing MuRF3, SNX4 and the mammalian retromer subunit SNX5 were detected, both displaying a 2-fold abundance enrichment. SNX4 is involved in the endosomal recycling pathway and is associated with specific tubular elements which are spatially and functionally different from the SNX1/SNX5-retromer complex. SNX4, SNX5 and SNX8 are all linked to microtubule-based motor function, and although they are all targeted to the early endosome, these three SNXs are involved in separate endosomal sorting events and define distinct membrane trafficking pathways (van Weering *et al.,* 2012b; van Weering *et al.,* 2012a; Hunt S.D. *et al*., 2013).

In addition, several downregulated proteins involved in subcellular trafficking were detected, such as subunits of adapter protein 3 (AP3) complex, which plays a role in protein targeting to the lysosome, importin-7, importin-8 and importin alpha S2, which function in nuclear protein transport, and subunits of the endosomal sorting complex required for transport (ESCRT)-I and II, which are required for the sorting of endosomal cargo into multivesicular bodies (MVBs).

4.2. SNX5 was identified as a novel interaction partner of MuRF3

MS-data showed an almost 2-fold enrichment of SNX5 in myoblasts expressing MuRF3 compared to the control, suggesting its putative interaction with MuRF3. SNX5 was of special interest because it mediates retrograde trafficking as a retromer subunit and regulates the degradation of membrane receptors like epidermal growth factor receptor (EGFR), thus regulating different signal transduction pathways (Wassmer T. *et al*., 2007; Sun Y *et al*., 2013). Very little is known about the expression and function of SNX5 in muscle. In addition to its ubiquitous expression in all mouse organs tested in this study, with especially high expression in the pancreas, lung and spleen, SNX5 was strongly expressed in heart and skeletal muscle. Due to its essential role in subcellular trafficking and transport, and therefore in numerous secretion pathways, and its indispensable role in differentiation of alveolar epithelial type I cells in mice, its high expression in pancreas and lung was somewhat expected. It has been reported that disruption of the *Snx5* gene in mice results in 40% perinatal lethality due to cyanosis and respiratory failure (Im S.K. *et al*., 2013).

SNX5 exhibited a perinuclear and homogenous cytosolic staining pattern in C2C12 cells. A comparable subcellular distribution of SNX5 was also described for non-muscle cells (Teasdale R.D. *et al*., 2001; Sun Y. *et al*., 2013). Because subcellular trafficking is a dynamic process that takes place continuously, it was expected to observe retromer-carrying vesicles, and therefore SNX5, in cell periphery as well as in the perinuclear region, where TGN is localized. In addition, SNX5 colocalized with the early endosome marker EEA1 but not with the late endosome and lysosome marker LAMP1. These data indicate that SNX5 localizes to early endosomes but not to late endosomes and lysosomes in muscle cells. This is consistent with previous reports which showed the predominant localization of SNX5 to the membranes of early endosomes in human breast carcinoma and human epitheloid cervix carcinoma cells (Teasdale R.D. *et al*., 2001; Merino-Trigo A. *et al*., 2004; Sun Y. *et al*., 2013).

4.3. SNX5 interacts physically and co-localizes with MuRF3

Co-immunoprecipitation experiments were performed to examine a possible interaction of MuRF1, MuRF2 and MuRF3 with SNX5. MuRF3 co-immunoprecipitated with SNX5 indicating they physically interact with each other. MuRF1 was also detected in the SNX5-precipitate, suggesting a possible interaction between the two proteins. Nevertheless, putative interaction between MuRF1 and SNX5 could not be validated.

Results of co-immunoprecipitation assays were supported by immonostaining experiments, which were carried out to investigate the co-localization of MuRF3 and SNX5. SNX5 was overexpressed in C2C12 cells and immunostaining showed the expected perinuclear and homogenous cytosolic staining pattern. MuRF3 was also overexpressed in C2C12 cells and exhibited its typical filament-like staining pattern. This MuRF3 staining pattern was described by Spencer *et al*. in 2000, when MuRF3 was reported to bind to and stabilize microtubules. In immunostaining experiments, they showed that MuRF3 co-localized with glutamylated microtubules and exhibited filament-like structures which radiated from the perinuclear region, the microtubule organizing center (MTOC), into the cell periphery (Spencer J.A. *et al*., 2000). Interestingly, when SNX5 was co-expressed with MuRF3, it changed its cellular distribution and co-localized with MuRF3, exhibiting the same microtubule-like staining pattern as MuRF3. Likewise, overexpressed MuRF3 also caused endogenous SNX5 to change its cellular localization to co-localize with MuRF3. These results provide further proof for the interaction between SNX5 and MuRF3.

4.4. Identification of the interaction domains of SNX5 and MuRF3

To identify the regions in SNX5 and MuRF3 which are responsible for their interaction, several deletion mutants in both proteins were generated. As a member of the SNX-BAR subfamily of SNXs, SNX5 has one C-terminal BAR domain in addition to its N-terminal PX domain. SNX5-BAR has been shown to be responsible for the interaction of SNX5 with different proteins, such as FANCA, for which the PX domain is not required (Otsuki T. *et al*., 1999), CHC22 (Towler M.C. *et al*., 2004), or DOCK180 (an activator of small GTPases), which interacts with SNX5 through either one of the CCDs of SNX5-BAR (Hara S. *et al*, 2008). In addition, the dimerization of SNX5 with SNX1 or SNX2 is mediated by the BAR domains of both SNXs, where either one of the three CC domains of SNX5-BAR is sufficient for their interaction. On the other hand, the PtdIns(3)P-binding SNX5-PX domain has been shown to associate with PtdIns(3)P-enriched elements of the endosomal pathway (Teasdale R.D. *et al*., 2001; Cullen P.J., 2008), and is the functional domain in regulation of EGFR pathway (Liu H. *et al*., 2006). Here, five different deletion mutant of SNX5 were generated; SNX5-PX lacked the BAR domain, SNX5-BAR lacked the PX domain, and SNX5Δaa206-256, SNX5Δaa262-327 and SNX5Δaa344-397 had deletions in the first, second or third CCDs of the BAR domain, respectively. In co-immunoprecipitation assays and immunostaining experiments SNX5-PX did not co-immunoprecipitate or co-localize with MuRF3, indicating that it is not required for the interaction of SNX5 with MuRF3. SNX5-BAR, on the other

hand, co-immunoprecipitated and co-localized with MuRF3, indicating that the BAR domain of SNX5 was responsible for its interaction with MuRF3. All three CCD deletion mutants of the BAR domain interacted with MuRF3, although SNX5Δaa206-256 and SNX5Δaa344-397 (deletion of CCD1 and CCD3, respectively) showed a weaker interaction, indicating that the first and the third CCDs are more essential for SNX5 interaction with MuRF3.

To determine the MuRF3-domain responsible for its interaction with SNX5, 14 different deletion mutants were generated, in which the different functionally important domains of MuRF3 were partially or completely deleted. Unfortunately, the expression of the small deletion mutants, such as MuRF3aa1-81, MuRF3aa82-117, MuRF3aa118-159, MuRF3aa160-202, MuRF3aa203-277, as well as MuRF3aa278-267, was not possible in western blot analyses. Also, deletion mutants lacking the C-terminus of MuRF3 could not be detected either, suggesting the importance of an intact C-terminus for MuRF3 expression. Nevertheless, in a co-immunoprecipitation assay, deletion mutants including either one of the two MuRF3 coiled coil domains; MuRF3aa1-202, MuRF3aa1-277, MuRF3aa118-367, MuRF3aa160-367, MuRF3aa203-367, as well as MuRF3aa160-202, which only included the first coiled coil domain and none of the other domains, were all found to interact with SNX5. In addition, deletion mutant MuRF3aa1-159 interacted with SNX5 although it only contained an 18 aa residue of the first coiled coil domain, the RING finger domain and the MFC domain. On the other hand, deletion mutant MuRF3aa82-367 which contained both coiled coil domains did not interact with SNX5, which could be due to technical failure in this particular co-immunoprecipitation. These results suggested the coiled coil domains of MuRF3 are responsible for mediating the interaction with SNX5. Previous studies showed that the coiled coil domains of MuRF-proteins mediate protein interactions. In a yeast two-hybrid system, MuRF1, 2 and 3 were shown to interact with each other through their coiled coil domains, which were sufficient for the interaction, to form heterodimers. On the other hand, for the binding of MuRF1 to titin a central 144 aa residue segment of MuRF1 was required, which included part of the conserved MuRF family domain, the B-box and only one coiled coil domain. The N-terminal RING-finger domain and the C-terminal acidic domain were not required for the interaction (Centner T. *et al*., 2001). In another study, the coiled coil domain of MuRF3 was shown to not only be necessary but also sufficient for its interaction with the glutamylated microtubules. However, amino acids 168-211 are required for optimal association, and the RING-finger domain is required for continuous binding along and stabilization of microtubules *in vivo* (Spencer J.A. *et al*., 2000).

Three more deletion mutants of MuRF3 coiled coil domains were generated; MuRF3Δaa141-186 with a deletion in the first CCD, MuRF3Δaa227-262 with a deletion in the second CCD, or MuRF3Δaa141-262 with deletions in both CCDs. Results of co-immunoprecipitation experiments showed a very weak interaction with SNX5 compared to the interaction between wild type MuRF3 and SNX5. Altogether, these results confirm that MuRF3 coiled coil domains mediate its interaction with SNX5.

4.5. SNX5 and MuRF3 co-localize and associate with early endosomes and microtubules

Although there have been conflicting reports about the subcellular localization of SNX5, it has predominantly been shown to localize to the membrane of EEs (Sun Y. *et al*., 2013; Teasdale R.D. *et al*., 2001; Merino-Trigo A. *et al*., 2004). This could also be shown in this study for endogenous and overexpressed SNX5. On the other hand, MuRF3 localized to microtubules and exhibited its typical microtubule-like staining pattern. To investigate the association of MuRF3 with EEs, LEs and lysosomes, its co-localization with EEA1 and LAMP1 was tested. Results showed that LAMP1, thus most LEs and lysosomes, was localized to the microtubule organizing center (MTOC) in the perinuclear region, from which the microtubules, as well as MuRF3, radiate into the cell periphery. On the other hand, EEA1 co-localized with MuRF3, although partially, indicating that early endosomes, which are predominantly located in the cell periphery, were localized to microtubules and thus to MuRF3. This is consistent with previous studies which showed that EEs as well as LEs move along microtubules. EEs patrol the peripheral cytoplasm close to the plasma membrane through saltatory movement along microtubules. On the other hand, LEs are transported on microtubules in a bidirectional manner, with a net movement towards the MTOC in the perinuclear region of the cell, where most of the LEs and lysosomes localize (Huotari J. and Helenius A., 2011). Nevertheless, because subcellular trafficking is a dynamic and adaptable pathway, EEs, LEs, endolysosomes and lysosomes are continuously undergoing maturation and transformation. This makes it difficult and only partially useful for protein components, such as EEA1 and LAMP1, to be used as specific molecular markers, since most of them are only transiently associated with these organelles (Huotari J. and Helenius A., 2011). That's why it was expected to have partial co-localization of MuRF3 with EEs and LEs.

These results are also in line with a very interesting study by Kaisto *et al*., which is one of the very few studies investigating endocytic trafficking pathway in muscle. It showed the localization of the different compartments of the endocytic trafficking pathway in rat

myofibers, which were isolated and exposed to endocytic tracers and labeled with antibodies against markers of the endocytic and exocytic pathways. Results showed that the recycling and the lysosome- directed pathways were distinct. Sarcolemmal coated-pits, which indicate endocytic activity, were concentrated at the I-bands and accordingly, EEs were distributed along the whole length of the myofibers and in a cross-striated fashion. Furthermore, recycling and LEs showed perinuclear and interfibrillar localization with a distribution pattern that followed the course of the microtubule network, indicating that LEs, as well as EEs, travel along microtubule tracks (Kaisto T. *et al*., 1999).

In this study, a triple immunostaining experiment of MuRF3, SNX5 and EEA1 was performed. The localization of MuRF3 and SNX5 to EEs was tested. MuRF3 and SNX5 co-localized and showed the microtubule-like staining pattern. EEA1 staining showed cytosolic, mostly peripheral distribution, partially along the microtubule-like structures. Results suggest that MuRF3 and SNX5 co-localized with each other and partially localized to EEs. This can be explained by the complexity of the spatial organization of the retromer-endosomal network. As a subunit of the retromer, SNX5 is localized to retromer-labeled EEs and recycling endosomal vesicles, which display a spatial organization defined not only by the presence of dispersed peripheral endosomes, but also an enrichment of recycling endosomal vesicles and tubules which cluster in the vicinity of the TGN, localized to the MTOC in the perinuclear region. From previous studies and live cell imaging experiments, it has become apparent that this steady-state is highly dynamic. In retromer-mediated retrograde trafficking pathways the retromer-labeled vesicular and tubular structures undergo a number of fission and fusion events as they move from the cell periphery along microtubules towards TGN in the perinuclear region. This steady-state distribution relies upon the interaction of retromer-subunits SNX5 and SNX6 with $p150^{glued}$ component of dynactin, an activator of the minus-end directed microtubule motor dynein, and the binding of SNX1 to the TGN-localized Rab6-interacting protein 1 (Rab6IP1). By recruiting the dynein/dynactin motor complex, the SNX BAR retromer subcomplex coordinates cargo sorting and tubular-based carrier formation at the donor endosomal membrane with long-range minus-end-directed microtubule-based transport and carrier recognition at the recipient TGN membrane. Suppression of $p150^{glued}$ or Rab6IP1 or disruption of microtubules results in the generation of a new steady-state characterized by the peripheral dispersal of retromer-labeled vesicles and a correlated impairment in retromer-mediated sorting to TGN. Disruption of microtubules also causes the dispersal of LEs and lysosomes throughout the cytoplasm, as well as a delay in the maturation of endosomes and cargo degradation (Cullen P.J., 2008; Wassmer T. *et al*., 2009; Huotari J.

and Helenius A., 2011). These reports as well as the results of this study indicate a functional association between SNX5 and the microtubule cytoskeleton, and suggest a role of MuRF3 in stabilizing this association.

4.6. SNX5 is a target protein of MuRF2

After repeatedly making the observation of a decrease in SNX5 expression once co-expressed with MuRF2, SNX5 was assumed to be a putative MuRF2 substrate. A first proof of this assumption was delivered when a decrease in SNX5 expression was observed when co-expressed with increasing amounts of MuRF2. In contrast, increasing MuRF3 expression had no effect on SNX5, indicating that SNX5 is a target protein of MuRF2 and not MuRF3. Because the RING finger domain of ubiquitin E3 ligases is the functional domain responsible for their E3 ligase activity, the RING finger domain of MuRF2 was inactivated to examine the ability of an E3 ligase deficient MuRF2 to degrade SNX5. The RING finger domain of MuRF-proteins is a C3HC4-type zinc finger domain which contains one histidine and seven cysteine residues which are highly conserved and essential for the coordination of the two zinc cations and for maintaining the structural and functional integrity of the RING finger domain (Lorick K.L. *et al*., 1999; Joazeiro C.A. and Weissman A.M., 2000; Spencer J.A. *et al*., 2000). Two cysteine residues, Cys42 and Cys50, were altered into serines, generating the E3-ligase deficient MuRF2-[(C42S; C50S)]. In a further expression assay, increasing the expression of MuRF2-[(C42S; C50S)] did not cause a decrease in SNX5 expression which remained constant, providing additional evidence that SNX5 is a MuRF2 substrate.

In Cycloheximide chase experiments, the putative MuRF2-mediated degradation of SNX5 was investigated further. Co-expression with MuRF2 enhanced SNX5 degradation even without CHX treatment, as a decrease in SNX5 expression was observed in comparison with SNX5 expression when expressed alone, which is consistent with previous results. SNX5 degradation was enhanced throughout the whole time course of the assay when co-expressed with MuRF2, until it was completely abolished after 6 hours of CHX treatment (0% remaining SNX5 in densitometrical analysis), confirming its MuRF2-mediated degradation. On the other hand, MuRF3 did not enhance SNX5 degradation, but rather stabilized SNX5 expression. Although at time point 0 hours (no CHX treatment), only about 65% SNX5 was expressed in comparison with the control, SNX5 expression remained stable throughout the course of the experiment, with over 30% remaining SNX5 after 6 hours of CHX treatment.

Further evidence of MuRF2-mediated degradation of SNX5 was provided by *in vitro* ubiquitination assays. These assays were performed to test possible MuRF2-mediated SNX5 ubiquitination. As a control reaction and for testing whether MuRF E3 ligases auto-ubiquitinate, the substrate SNX5 was taken out of the reaction. Because the UPS is highly regulated at multiple levels, E3 ligases as well as other components of the system can be regulated by ubiquitination and subsequent degradation, mediated by themselves (a process known as regulatory self- or auto-ubiquitination) or by heterologous ligases. Auto-ubiquitination is a general characteristic of E3 ligases *in vitro*, and is often used to confirm that a certain protein is an active E3 ligase and to assess functionally significant interactions with specific E2 enzymes (Lorick K.L. *et al*., 1999). The result of ligase auto-ubiquitination is auto-regulation or targeting for self-destruction (Weissman A.M. *et al*., 2011).

In these assays, the ubiquitination of SNX5 could not be detected by either one of the MuRF proteins, but MuRF2 was found to auto-ubiquitinate. Interestingly, this auto-ubiquitination of MuRF2 was inhibited when SNX5, the substrate, was added to the reaction. Inhibition of auto-ubiquitination by the substrate has not been described for MuRF E3 ligases thus far, but it has been reported for F-box proteins of the Skp1-Cullin-F-box protein (SCF) complex, which provide substrate specificity to the complex. It was observed that their degradation is mediated via an 'autocatalytic' mechanism within the complex (mediated by the RING finger components), and attenuated by their respective substrates. This regulation mechanism ensures that sufficient levels of F-box proteins are maintained to target high level of substrates when they occur. However, after substrate concentration decreases, the F-box protein becomes abundant, and therefore is targeted for proteasomal destruction, while preserving the other components of the SCF complex, allowing for a quick reassembly of the complex with different F-box proteins to adapt to changes in the desired specificity (Galan J.M. *et al*, 1999; Li Y. *et al*, 2004; de Bie P. and Ciechanover A., 2011). Although this auto-regulatory mechanism has not been reported for MuRF-proteins, the results of these *in vitro* ubiquitination assays strongly suggest that MuRF2 is regulated by auto-ubiquitination *in vitro.* In addition, these results confirm that MuRF2 has an E3 ligase activity, which mediates the degradation of SNX5.

4.7. MuRF2 degrades SNX5 in a UPS-dependent manner

Having shown that SNX5 is a MuRF2 target protein, it was important to clarify, if SNX5 degradation occurs via the 26S-proteasome. In expression and immunostaining assays the proteasome inhibitor MG132 was applied with the assumption that if SNX5 degradation is

MuRF2-mediated, then this degradation would be inhibited by MG132 treatment. Indeed, MG132 prevented MuRF2 mediated degradation of SNX5 indicating that SNX5 is degraded in a UPS-dependent manner and that MuRF2 contributes to this reaction. When MuRF2, MuRF3 and SNX5 were overexpressed together, the MuRF2-mediated SNX5-degradation was prevented by MuRF3, confirming the stabilizing effect of MuRF3 on SNX5. The fact that the amount of expressed MuRF-proteins increased after treatment with MG132 indicated that the degradation of MuRF-proteins is also UPS-dependent. Inhibition of MuRF2-mediated UPS-dependent degradation of SNX5 was also observed in immunostaining assays, in which MG132 was also used. After co-expression with MuRF2, SNX5 could not be detected without MG132 treatment, which confirms its rapid degradation by MuRF2. Nevertheless, after MG132 treatment, MuRF2-mediated UPS-dependent degradation of SNX5 was prevented and it could therefore be detected.

A physical interaction between MuRF2 and its substrate SNX5 could not be shown in conventional co-immunoprecipitation assays. Presumably, the interaction occurs in a very short period of time, in which SNX5 is rapidly ubiquitinated and degraded, making it difficult to be detected. In *in vivo* ubiquitination assays, ubiquitinated SNX5 was stabilized and its UPS-mediated degradation and deubiquitination were inhibited by MG132 and the deubiquitinase-inhibitor *N*-Ethylmaleimide (NEM), respectively. Importantly, when UPS-mediated degradation and deubiquitination were inhibited, a physical interaction between MuRF2 and SNX5 was detected in co-immunoprecipitation experiments. On the other hand, MuRF3 interacted with SNX5 regardless of whether MG132 and NEM were used or not, which is consistent with previous results. In addition, auto-ubiquitination of MuRF2 was detected in the precipitate, probably due to NEM application. These results were verified in a further *in vivo* ubiquitination assay, in which MG132 and NEM were also applied separately. The interaction of MuRF2 with SNX5 was shown when MG132 was used alone or together with NEM. The application of NEM alone was not sufficient for stabilizing SNX5 and for the detection of its interaction with MuRF2, which supports previous results. By using specific antibodies against SNX5 and at longer exposure in western blot analysis, ubiquitination of SNX5 was detectable when MG132 and NEM were applied, but also when only MG132 was used, which indicates that although DUBs in the cell are active, they are not active enough to significantly inhibit the ubiquitination of SNX5 by MuRF2. These results provide strong evidence that MuRF2 interacts with and ubiquitinates SNX5, thus mediating its UPS-dependent degradation *in vivo*.

4.8. MuRF3 stabilizes SNX5 and prevents its MuRF2-mediated degradation

As already observed in expression assays and CHX-chase experiments, MuRF3 had a stabilizing effect on SNX5 expression. This observation was verified in further expression tests, in which increased amounts of MuRF3 were co-expressed with constant amounts of MuRF2 and SNX5. Results showed that MuRF2-mediated degradation of SNX5 was inhibited by MuRF3 in a dose dependent manner. These results confirm the stabilization of SNX5 by MuRF3 and inhibition of MuRF2 mediated degradation. Therefore, MuRF2 and MuRF3 function antagonistically in the regulation of SNX5.

4.9. A possible regulatory role of MuRF2 and MuRF3 in SNX5-mediated trafficking pathways through microtubule stabilization

Microtubules are dynamic structures that have many functions ranging from organelle and cargo transport to mitosis and myogenesis (Pizon V. *et al*., 2002). Over the past years, a growing body of evidence has suggested a role of microtubules and other non-contractile cytoskeletal components in muscle differentiation and maintenance. Furthermore, microtubules are required for proper contractile function of the muscle and their levels increase in cardiac hypertrophy (McElhinny A.S. *et al*., 2004). It has been reported that disruption of microtubule dynamics with depolymerizing or destabilizing agents inhibits skeletal myoblast fusion, differentiation, and normal myofibrillogenesis. Microtubule dynamics is reduced in the early stages of myogenic differentiation by transient formation of the stable glutamylated microtubules, which seem to be involved in the active transport of sarcomeric proteins to the sites of myofibrillogenesis, while the dynamic pool of tyrosinated tubulin is simultaneously reduced (Gundersen G. *et al*., 1989; Pizon V. *et al*., 2002). MuRF2 was shown to be required for the integrity of stable glutamylated and acetylated microtubules, but not the dynamic tyrosinated microtubules. Through its transient association with stable glutamylated microtubules, myosin and titin during early myofibrillogenesis MuRF2 acts as an adaptor between the sarcomeric proteins and the microtubule network (Pizon V. *et al*., 2002). Nevertheless, the molecular mechanisms responsible for regulating the stability of glutamylated microtubules have remained elusive. Because MuRF2 colocalizes with only a portion of cardiac microtubules and appears to be only transiently associated with skeletal myocyte glutamylated microtubules, it has been suggested that it may interact with microtubules via hetero-oligomerization with MuRF3 (McElhinny A.S. *et al*., 2004). Therefore, MuRF3, which associates with glutamylated microtubules throughout development

regulating their dynamics (Centner *et al.*, 2001; Spencer *et al*., 2000), was suggested to act as the primary stabilizer while MuRF2 plays an accessory role in microtubule stabilization (McElhinny A.S. *et al.,* 2004).

Stable microtubule arrays are not only required for normal muscle development and function, but are also essential for maintaining the integrity of intracellular trafficking-pathways. In this respect, their disruption causes a delay in the maturation of endosomes and cargo degradation, the dispersal of late endosomes and lysosomes throughout the cytoplasm, and the impairment of retromer-mediated retrograde transport to the TGN (Cullen P.J., 2008; Wassmer T. *et al*., 2009; Huotari J. and Helenius A., 2011). GLUT4 transport pathway is a specialized trafficking pathway in skeletal muscle. In humans, 70–90% of insulin-stimulated glucose clearance depends on skeletal muscle and the GLUT4 pathway (Towler M.C. *et al*., 2004a). As a response to insulin or exercise, GLUT4 transporter is translocated from intracellular GLUT4 storage compartments (GSCs) to the plasma membrane to clear glucose from the bloodstream (Bryant N.J. *et al*., 2002; Hou J.C. *et al*., 2007; Huang S. *et al*., 2007). Disruption of GLUT4 membrane trafficking has been implicated in some forms of human type 2 diabetes (Garvey W.T. *et al*., 1998; Maianu L. *et al*., 2001). Previous reports regarding the role of an intact microtubule-network in insulin-dependent GLUT4 transport have been conflicting. Several studies have established microtubules as a major determinant for subcellular localization of GLUT4 by showing that GLUT4-containing vesicles associated with microtubules and that inhibition of the microtubule motor proteins dynein and kinesin as well as microtubule-depolymerization dispersed the perinuclear localized GLUT4 and partially inhibited insulin-stimulated glucose uptake and GLUT4 translocation to the cell surface (Emoto M. *et al*., 2001; Fletcher L.M. *et al*., 2000; Guilherme A. *et al.*, 2000; Olson A.L. *et al*., 2000; Patki V. *et al*., 2000). On the other hand, other studies have failed to support a role of microtubules in insulin-induced GLUT4 translocation to the plasma membrane, and showed that microtubule disruption did not alter the initial rate of GLUT4 endocytosis (Shigematsu S. *et al*., 2002). Nevertheless, it remains undisputed, that an intact microtubule-network is essential for the correct retrograde recycling of GLUT4 transporter from early endosomes back to the perinuclear TGN after its initial internalization, an intermediate trafficking step critical for the subsequent transport of GLUT4 to GSCs (Shigematsu S. *et al*., 2002). This particular intermediate stage of GLUT4 transport is mediated by the muscle specific CHC22, which is involved in the biogenesis of insulin-responsive GSCs in human muscle (Vassilopoulus S. *et al*., 2009). It occurs after the retrograde cargo exit from early endosomes, which is mediated by the ubiquitously expressed CHC17. CHC22 function

requires retromer, which it recruits by specific binding to SNX5, facilitating the tubulation of GLUT4-containing recycling vesicles which move along microtubules towards TGN in the perinuclear region. It has also been shown to require dynein/dynactin motor activity on microtubules, thus an intact microtubule-network (Esk C. *et al*., 2010). The defective and expanded GSCs in some patients with type 2 diabetes exhibit high levels of CHC22, raising the possibility that CHC22 modulation of GLUT4 traffic might influence human tendency toward type-2 diabetes (Vassilopoulos S. *et al.,* 2009).

In addition to the GLUT4 trafficking pathway, other SNX5-mediated transport pathways have been shown to require a stable microtubule network. An example for such trafficking pathways is macropinocytosis, a pathway which mediates the endocytosis of solute molecules, nutrients and antigens, and is therefore important in functions associated with immune responses, and in which SNX5 plays an essential role in macropinosome-to-early-endosome trafficking (Lim J.P. *et al*., 2008; Wang J.T. *et al*., 2010; Lim J.P. *et al.,* 2012). Upon EGF stimulation, SNX5 is sequestered to discrete subdomains of the macropinosomes. These subdomains are subsequently incorporated into highly dynamic SNX5-labeled tubular structures that depart from the macropinosome body and traffic to the perinuclear region of the cell, before fusing with early endosomal acceptor membranes. The extension and subsequent fission of these tubular structures is dependent upon intact microtubules. As a result of microtubule-destabilization using the agent nocodazole, SNX5-labeled microdomains were observed to coalesce and emerge from the macropinosome before collapsing back onto the surface of the structure (Kerr M.C. *et al*., 2006).

While the role of MuRF2 and MuRF3 in stabilizing microtubules has been reported only in regard to muscle differentiation and contraction, in this study they have been linked for the first time with a trafficking protein, SNX5, which is directly associated with microtubules through its binding to the dynactin component $p150^{glued}$, and functionally dependent on a stable microtubule network. The interaction between SNX5 and MuRF3, the MuRF2-mediated degradation of SNX5 and the stabilizing effect which MuRF3 has on SNX5 expression suggest a possible regulatory role of MuRF2 and MuRF3 in microtubule-dependent subcellular trafficking pathways.

4.10. SNX5 is up-regulated during denervation but not during starvation or in atrophied myotubes

As already mentioned, SNX5 has been implicated in muscle membrane trafficking through its interaction with the muscle specific CHC22, whereas it does not interact with the ubiquitous CHC17 (Towler M.C. *et al*., 2004b). Moreover, its notably high expression in muscle tissue and the interaction with MuRF3 are further indications for its muscle specificity. Therefore, in this part of the study, SNX5 expression after induction of skeletal muscle atrophy was tested. Skeletal muscle atrophy accompanies many chronic illnesses, sepsis, myopathies and dystrophies (Thomas, D. R., 2007). It is characterized by a decrease in muscle mass, muscle strength and fatigue resistance, and has the clinical consequence of severe deterioration of life-quality of the patients (Fanzani A. *et al*., 2012; Bonaldo P. and Sandri M., 2013). Although in the past years a lot has been reported about the different signaling pathways triggering skeletal muscle atrophy, changes in subcellular trafficking pathways during muscle atrophy remain unknown. Therefore mRNA and protein expression of SNX5 was tested in two different atrophy mouse models, denervation and starvation, as well as atrophied C2C12 myotubes. Denervation- and starvation- induced muscle atrophy was confirmed by a decreased muscle weight and an increased gene expression of *Trim63* and *Fbxo32*, which are strongly induced in disuse atrophy (Bodine S.C. *et al.*, 2001; Gomes M.D. *et al.*, 2001). *Snx5* mRNA expression and SNX5 protein content were significantly increased 7, 14, and 21 days after denervation compared to the controls. A small increase in *Snx5* mRNA expression was observed after 24 h but not after 48 h of starvation. Moreover, no significant change in SNX5 protein content was observed during starvation-induced atrophy. Also, no change in SNX5 protein content was observed in atrophied C2C12 myotubes after 24 h or 48 h of dexamethasone treatment. According to these results it was not possible to conclude with certainty that inducing atrophy had an effect on SNX5 expression.

The up-regulation of SNX5 as a result of denervation can be explained by the fact that after nerve injury, cell intrinsic mechanisms of neuronal regeneration in the peripheral nervous system, such as long-distance retrograde signaling, are activated. This process depends on retrograde signaling from the axonal lesion site to cell body in order to provide accurate and timely information on the nature and extent of axonal damage, and to modulate and coordinate a regenerative response to the injury in the cell body. This is based on local axonal synthesis of critical carrier proteins, including importins and vimentin that link diverse signaling molecules, such as transcription factors, to the dynein/dynactin retrograde motor

complex which moves toward the cell body along microtubules. The axonal signaling response to nerve injury induces alterations in cellular signaling, transcription, translation and post-translational modifications. For example, several kinases are activated in cell bodies in response to an injury event. Among these are the MAP kinases Erk1 and Erk2 and Jnk (Hanz S. and Fainzilber M., 2006; Rishal I. and Fainzilber M, 2010). As a protein which directly associates with the dynein/dynactin motor complex and contributes to retrograde minus-end transport pathways, SNX5 might be involved in axonal post-injury retrograde signaling. This could explain its upregulation in denervated muscle tissue, whereas no significant change in SNX5 expression was observed in mice after starvation, indicating that SNX5 upregulation was not due to induction of muscle atrophy but rather the denervation itself. This conclusion can be supported by the fact that SNX5 expression did not change in atrophied C2C12 myotubes, and that SILAC-MS analyses investigating up- and down-regulation of proteins during differentiation and atrophy did not show any enrichment or decrease in SNX5 content during atrophy.

Immobilization, aging and several inflammatory as well as other myopathies and dystrophies (e.g. critical illness myopathy) have been associated with disruption in GLUT4 pathway (Jensen E.B. *et al*., 2009; Hoshino S. *et al*., 2013; Weber-Carstens S. *et al*. 2013). Because SNX5 has been shown to play a role in GLUT4 translocation by binding to CHC22, it would be recommended to do further investigation regarding the role of SNX5 and also MuRF2 and MuRF3 in these conditions. Unfortunately, these mouse models and C2C12 mouse skeletal muscle cell line are not suitable because CHC22 only exists as a pseudogene in mice, which does not express the CHC22 protein (Vassilopoulos S. *et al.,* 2009). Also, C2C12 muscle cell line does not contain insulin-responsive intracellular compartments and dexamethasone-induced GLUT4 overexpression in C2C12 cells does not result in the formation of such compartments or lead to significant change in insulin-stimulated glucose transport (Tortorella L.L. and Pilch P.F., 2002).

4.11. Conclusions

This study showed for the first time the association of the two muscle specific E3 ligases MuRF2 and MuRF3 with the mammalian retromer subunit SNX5, a protein involved with subcellular trafficking pathways. SNX5 was identified as a novel interaction partner of MuRF3. SNX5 interacted physically and via its BAR-domain with MuRF3. SNX5 and MuRF3 co-localized and associated with early endosomes. SNX5 was also identified as a substrate of MuRF2. MuRF2 interacted with and ubiquitinated SNX5 *in vivo*, mediating its

degradation in a UPS-dependent manner. Interestingly, MuRF3 stabilized SNX5, inhibiting its MuRF2-mediated UPS-dependent degradation. SNX5 has been shown to directly associate with microtubules and to require an intact microtubule network for its function. The function of MuRF2 and MuRF3 as microtubule-stabilizers and the results of this study suggest a possible regulatory role of MuRF2 and MuRF3 in microtubule-dependent subcellular trafficking pathways. The better understanding of their regulatory function in specialized membrane trafficking pathways in muscle, such as GLUT4 pathway, may reveal new insights into diseases such as diabetes, and provide a better definition of processes critical for muscle development and repair.

5 References

Armstrong RB, 1996. Properties, distribution, and functions of mammalian skeletal muscle fibers. In: Exercise Bioenergetics and Gas Exchange, edited by Cerretelli P and Whipp BJ. Amsterdam: Elsevier/North-Holland Biomedical Press, p. 137–46.

Baehr, L. M., Furlow, J. D. and Bodine, S. C., 2011. Muscle sparing in muscle RING finger 1 null mice: response to synthetic glucocorticoids. *J. Physiol.* 589, 4759-4776.

Bananis E, Murray JW, Stockert RJ, Satir P, Wolkoff AW, 2000. Microtubule and motor-dependent endocytic vesicle sorting in vitro. J Cell Biol 151: 179–186

Bananis E, Nath S, Gordon K, Satir P, Stockert RJ, Murray JW, Wolkoff AW, 2004. Microtubule-dependent movement of late endocytic vesicles in vitro: requirements for Dynein and Kinesin. Mol Biol Cell 15: 3688–3697

Bansal D, Miyake K, Vogel SS,Groh S, Chen CC,Williamson R, McNeil PL, Campbell KP, 2003. Defective membrane repair in dysferlin-deficient muscular dystrophy. Nature 423:168–172.

Bissig C and Gruenberg J., 2013. Lipid sorting and multivesicular endosome biogenesis. Cold Spring Harb Perspect Biol. 5(10):a016816

Bodine, S.C., Latres A., Baumhueter S., Lai V.K., Nunez L., Clarke B.A., Poueymirou W.T., Panaro F.J., Na E., Dharmarajan K., *et al*., 2001. Identification of ubiquitin ligases required for skeletal muscle atrophy. *Science.* 294:1704–1708.

Bonifacino JS, Rojas R., 2006. Retrograde transport from endosomes to the trans- Golgi network. Nat Rev Mol Cell Biol 7: 568–579.

Bonifacino JS and Hurley JH, 2008. Retromer. Curr. Opin. Cell Biol. 20, 427-436.

Bonaldo P. and Sandri M., 2013. Cellular and molecular mechanisms of muscle atrophy. Disease Models and Mechanisms 6 (1):25-39

Borden K.L., 1998. RING fingers and B-boxes: zinc-binding protein-protein interaction domains. *Biochem. Cell Biol.* 76:351-358.

Boron WF and Boulpaep EL, 2009. Medical Physiology: A Cellular and Molecular Approach. Philadelphia, PA: Saunders/Elsevier.

Brodsky, F.M., Chen, C.Y., Knuehl, C., Towler, M.C., and Wakeham, D.E., 2001. Biological basket weaving: Formation and function of clathrin-coated vesicles. Annu. Rev. Cell Dev. Biol. *17,* 517–568.

Brown CL, Maier KC, Stauber T, Ginkel LM, Wordeman L, Vernos I, Schroer TA, 2005. Kinesin-2 is a motor for late endosomes and lysosomes. Traffic 6: 1114–1124

Bryant NJ, Govers R, James DE, 2002. Regulated transport of the glucose transporter GLUT4. Nat Rev Mol Cell Biol. (4):267-77.

Burd C. and Cullen P.J., 2014. Retromer: A Master Conductor of Endosome Sorting. Cold Spring Harb Perspect Biol. 6(2). pii: a016774.

Burden SJ. Building the vertebrate neuromuscular synapse, 2002. J Neurobiol. 53:501–511.

Carlton, J. G. *et al,* 2004. Sorting nexin‐1 mediates tubular endosome‐to‐TGN transport through co-incidence sensing of high curvature membranes and 3‐phosphoinositides. *Curr. Biol.* 14, 1791–1800

Carlton JG, *et al*, 2005. Sorting nexin-2 is associated with tubular elements of the early endosome, but is not essential for retromer-mediated endosome-to-TGN transport. J Cell Sci. 118:4527–4539.

Centner T., Yano J., Kimura E., McElhinny A.S., Pelin K., Witt C.C., Bang M.L., Trombitas K., Granzier H., Gregorio C.C. *et al*., 2001. Identification of muscle specific ring finger proteins as potential regulators of the titin kinase domain. *J. Mol. Biol.* 306:717–726.

Chavrier P, Parton RG, Hauri HP, Simons K, Zerial M, 1990. Localization of low molecular weight GTP binding proteins to exocytic and endocytic compartments. Cell 62: 317–329

Ciechanover A., Heller H., Elias S., Haas A. L., and Hershko A., 1980 a. ATP-dependent conjugation of reticulocyte proteins with the polypeptide required for protein degradation. Proc Natl Acad Sci USA *77*, 1365-1368.

Ciechanover A., Elias S., Heller H., Ferber S., Hershko A., 1980 b. Characterization of the heat-stable polypeptide of the ATP-dependent proteolytic system from reticulocytes. *J. Biol. Chem.* 255, 7525-7528.

Ciechanover, A., and Iwai, K. 2004. The ubiquitin system: from basic mechanisms to the patient bed. IUBMB Life 56:193-201.

Clark KA, McElhinny AS, Beckerle MC, Gregorio CC, 2002. Striated muscle cytoarchitecture: an intricate web of form and function. Annu Rev Cell Dev Biol. 18:637–706.

Clarke, B. A., Drujan, D., Willis, M. S., Murphy, L. O., Corpina, R. A., Burova, E., Rakhilin, S. V., Stitt, T. N., Patterson, C., Latres, E. et al., 2007. The E3 Ligase MuRF1 degrades myosin heavy chain protein in dexamethasone-treated skeletal muscle. *Cell Metab.* 6, 376-385.

Cohen, S., Brault, J. J., Gygi, S. P., Glass, D. J., Valenzuela, D. M., Gartner, C., Latres, E. and Goldberg, A. L., 2009. During muscle atrophy, thick, but not thin, filament components are degraded by MuRF1-dependent ubiquitylation. *J. Cell Biol.* 185, 1083-1095.

Cox J, Mann M., 2008. MaxQuant enables high peptide identification rates, individualized p.p.b.-range mass accuracies and proteome-wide protein quantification. Nat Biotechnol. 26(12):1367-72.

Cozier GE *et a.l*, 2002. The phox homology (PX) domain-dependent, 3 phosphoinositide-mediated association of sorting nexin-1 with an early sorting endosomal compartment is required for its ability to regulate epidermal growth factor receptor degradation. J Biol Chem. 277:48730– 48736.

Cruz-Jentoft AJ, Baeyens JP, Bauer JM, Boirie Y, Caderholm T, Landi F, et al., 2010. People EWGoSiO. Sarcopenia: European consensus on definition and diagnosis: report of the European Working Group on sarcopenia in older people. Age Ageing. 39:412-23.

Cullen PJ, 2008. Endosomal sorting and signalling: an emerging role for sorting nexins. Nat Rev Mol Cell Biol. 9:574–582.

Cullen PJ and Korswagen HC, 2013. Sorting nexins provide diversity for retromer-dependent trafficking events. Nat Cell Biol. 14(1): 29–37.

Dai K.S. and Liew C.C., 2001. A novel human striated muscle RING zinc finger protein, SMRZ, interacts with SMT3b via its RING-domain. *J Biol Chem* 276:23992-23999

de Bie P. and Ciechanover A., 2011. Ubiquitination of E3 ligases: self-regulation of the ubiquitin system via proteolytic and non-proteolytic mechanisms. Cell Death Differ. 18(9):1393-402

Deshaies, R.J., and Joazeiro, C.A., 2009. RING domain E3 ubiquitin ligases. Annu Rev Biochem. 78:399-434.

Driskell OJ, Mironov A, Allan VJ, Woodman PG, 2007. Dynein is required for receptor sorting and the morphogenesis of early endosomes. Nat Cell Biol 9: 113–120

Emoto M., S.E. Langille, and M.P. Czech. 2001. A role for kinesin in insulin-stimulated GLUT4 glucose transporter translocation in 3T3-L1 adipocytes. J. Biol. Chem. 276:10677-10682.

Ennion, S., Sant'ana Pereira, J., Sargeant, A. J., Young, A. & Goldspink, G., 1995. Characterization of human skeletal muscle fibres according to the myosin heavy chains they express. *Journal of Muscle Research and Cell Motility* 16, 35–43.

Esk C, Chen C, Johannes L, Brodsky FM., 2010. The clathrin heavy chain isoform CHC22 functions in a novel endosomal sorting step. J Cell Biol 188: 131–144.

Fanzani A, Conraads VM, Penna F, Martinet W, 2012. Molecular and cellular mechanisms of skeletal muscle atrophy: an update. J Cachexia Sarcopenia Muscle. 3(3):163-79

Fearon K, Strasser F, Anker SD, Bosaeus I, Bruera E, Fainsinger RL, et al., 2011. Definition and classification of cancer cachexia: an international consensus. Lancet Oncol. 12: 489-95.

Fielitz, J., van Rooij, E., Spencer, J. A., Shelton, J. M., Latif, S., van der Nagel, R., Bezprozvannaya S., de Windt L., Richardson J.A., Bassel-Duby, R., Olson, E. N., 2007 a. Loss of muscle-specific RING-finger 3 predisposes the heart to cardiac rupture after myocardial infarction. *Proceedings of the National Academy of Sciences*, *104*(11), 4377–4382.

Fielitz, J., Kim, M.S., Shelton, J. M., Latif, S., Spencer, J. A., Glass, D. J., Richardson J.A., Bassel-Duby R., Olson, E. N., 2007 b. Myosin accumulation and striated muscle myopathy result from the loss of muscle RING finger 1 and 3. *Journal of Clinical Investigation*, *117*(9), 2486–2495.

Finley D., 2009. Recognition and Processing of Ubiquitin-Protein Conjugates by the Proteasome. *Annual Review of Biochemistry*, *78*(1), 477–513.

Fletcher L.M., Welsh G.I., Oatey P.B., and Tavare J.M., 2000. Role for the microtubule cytoskeleton in GLUT4 vesicle trafficking and in the regulation of insulin-stimulated glucose uptake. Biochem. J. 352:267-276.

Galan JM, Peter M., 1999. Ubiquitin-dependent degradation of multiple F-box proteins by an autocatalytic mechanism. Proc Natl Acad Sci USA. 96: 9124–9129.

Galvez T, Gilleron J, Zerial M, O'Sullivan GA, 2012. Snap Shot: mammalian Rab proteins in endocytic trafficking. Cell 151:234–42.

Garvey, W.T., L. Maianu, J.H. Zhu, G. Brechtel-Hook, P. Wallace, and A.D. Baron., 1998. Evidence for defects in the trafficking and translocation of GLUT4 glucose transporters in skeletal muscle as a cause of human insulin resistance. *J. Clin. Invest.* 101:2377–2386.

Glass D. J., 2005. Skeletal muscle hypertrophy and atrophy signaling pathways. *The International Journal of Biochemistry & Cell Biology*, *37*(10), 1974–1984.

Glickman M. H., Ciechanover A., 2002. The ubiquitin-proteasome proteolytic pathway: destruction for the sake of construction. *Physiological Reviews*, *82*(2), 373–428.

Gokool S, Tattersall D, Seaman MN, 2007. EHD1 interacts with retromer to stabilize SNX1 tubules and facilitate endosome-to-Golgi retrieval. Traffic 8:1873–1886.

Gomes, M. D., Lecker, S. H., Jagoe, R. T., Navon, A. and Goldberg, A. L., 2001. Atrogin-1, a muscle-specific F-box protein highly expressed during muscle atrophy. *Proc. Natl. Acad. Sci. USA* 98, 14440-14445.

Gomez TS, Billadeau DD, 2009. A FAM21-containing WASH complex regulates retromer-dependent sorting. Dev Cell 17:699–711.

Gotthardt, M., Hammer R.E., Hubner N., Monti J., Witt C.C., McNabb M., Richardson J.A., Granzier H., Labeit S., Herz J., 2003. Conditional expression of mutant M-line titins results in cardiomyopathy with altered sarcomere structure. *J. Biol. Chem.* 278:6059–6065.

Grant BD, Donaldson JG., 2009. Pathways and mechanisms of endocytic recycling. Nat Rev Mol Cell Biol 10: 597–608.

Gregorio CC, Trombitas K, Centner T, Komerer, Stier G, Kunke K, Suzuki K, Obermayr F, Hermann B, Granzier H, Sorimachi H and Labeit S, 1998. The NH2 terminus of titin spans the Z-disc: its interaction with a novel 19-kDa ligand (T-cap) is required for sarcomeric integrity. *J Cell Biol*. 143: 1013-1027.

Gregorio CC, Perry CN, McElhinny AS, 2005. Functional properties of the titin/connectin-associated proteins, the muscle-specific RING finger proteins (MURFs), in striated muscle. J Muscle Res Cell Motil 26: 389-400.

Gruenberg J and Howell KE, 1989. Membrane traffic in endocytosis: insights from cell-free assays. Annu Rev Cell Biol. 5:453–81.

Gruenberg J., 2001. The endocytic pathway: a mosaic of domains. Nat Rev Mol Cell Biol. 10:721-30.

Guilherme A, Emoto M, Buxton JM, Bose S, Sabini R, Theurkauf WE, Leszyk J, Czech MP, 2000. Perinuclear localization and insulin responsiveness of GLUT4 requires cytoskeletal integrity in 3T3-L1 adipocytes. J Biol Chem. 8;275(49):38151-9.

Gundersen, G., Khawaja, S., Bulinski, J.C., 1989. Generation of a stable, posttranslationally modified microtubule array is an early event in myogenic differentiation. J. Cell Biol. 109, 2275–2288.

Gundersen K., 2010. Excitation-transcription coupling in skeletal muscle: the molecular pathways of exercise. *Biological Reviews*, *86*(3), 564–600.

Hanz S. and Fainzilber M., 2006. Retrograde signaling in injured nerve – the axon reaction revisited. *Journal of Neurochemistry*. 99, 13–19

Hara, S., Kiyokawa, E., Iemura, S., Natsume, T., Wassmer, T., Cullen, P.J., Hiai, H., and Matsuda, M., 2008. The DHR1 domain of DOCK180 binds to SNX5 and regulates cation-independent mannose 6-phosphate receptor transport. Mol. Biol. Cell 19, 3823–3835.

Harbour ME, *et al*., 2010. The cargo-selective retromer complex is a recruiting hub for protein complexes that regulate endosomal tubule dynamics. J Cell Sci 123:3703–3717.

Hershko, A., Heller, H., Elias, S., and Ciechanover, A., 1983. Components of ubiquitin-protein ligase system. Resolution, affinity purification, and role in protein breakdown. J Biol Chem. *258*, 8206-8214.

Hershko A. and Ciechanover A., 1998. The ubiquitin system. *Annu. Rev. Biochem., 67*, 425-427.

Hierro A *et al.,* 2007. Functional architecture of the retromer cargo-recognition complex. Nature. 449:1063–1067.

Hirokawa N, Noda Y, Tanaka Y, Niwa S, 2009. Kinesin superfamily motor proteins and intracellular transport. Nat Rev Mol Cell Biol 10: 682–696

Hoepfner S, Severin F, Cabezas A, Habermann B, Runge A, Gillooly D, Stenmark H, Zerial M, 2005. Modulation of receptor recycling and degradation by the endosomal kinesin KIF16B. Cell 121: 437–450

Hong, Z., Yang, Y., Zhang, C., Niu, Y., Li, K., Zhao, X. and Liu, J. J., 2009. The retromer component SNX6 interacts with dynactin p150(Glued) and mediates endosome-to-TGN transport. Cell Res. 19, 1334-1349.

Hoshino S, Sakamoto K, Vassilopoulos S, Camus SM, Griffin CA, Esk C, Torres JA, Ohkoshi N, Ishii A, Tamaoka A, Funke BH, Kucherlapati R, Margeta M, Rando TA, Brodsky FM, 2013. The CHC22 clathrin-GLUT4 transport pathway contributes to skeletal muscle regeneration. PLoS One. 8(10):e77787.

Hou, J.C., and J.E. Pessin. 2007. Ins (endocytosis) and outs (exocytosis) of GLUT4 trafficking. *Curr. Opin. Cell Biol.* 19:466–473.

Howes MT, Kirkham M, Riches J, Cortese K, Walser PJ, Simpson F, *et al.*, 2010. Clathrin-independent carriers form a high capacity endocytic sorting systemat the leading edge of migrating cells. J Cell Biol 190:675–91.

Hsu VW and Prekeris R., 2010. Transport at the recycling endosome. Curr Opin Cell Biol. 22:528–34.

Huang, S., and M.P. Czech., 2007. The GLUT4 glucose transporter. *Cell Metab.* 5:237–252.

Hunt SD, Townley AK, Danson CM, Cullen PJ, Stephens DJ, 2013. Microtubule motors mediate endosomal sorting by maintaining functional domain organization. J Cell Sci. 126(Pt 11):2493-501.

Huotari J and Helenius A, 2011. Endosome maturation. EMBO J 30:3481–500.

Im SK, Jeong H, Jeong HW, Kim KT, Hwang D, Ikegami M, Kong YY, 2013. Disruption of sorting nexin 5 causes respiratory failure associated with undifferentiated alveolar epithelial type I cells in mice. PLoS One. 8(3):e58511.

Ishiki M, Klip A., 2005. Minireview: recent developments in the regulation of glucose transporter-4 traffic: new signals, locations, and partners. Endocrinology.146(12):5071-8.

Jackman, R.W., and Kandarian S.C., 2004. The molecular basis of skeletal muscle atrophy. Am J Physiol Cell Physiol 287:C834-843.

Jagoe R.T., Lecker S.H., Gomes M., Goldberg A.L., 2002. Patterns of gene expression in atrophying skeletal muscles: Response to food deprivation. *FASEB J., 16*, 1697-1712.

Jensen EB, Zheng D, Russell RA, Bassel-Duby R, Williams RS, Olson AL, Dohm GL, 2009. Regulation of GLUT4 expression in denervated skeletal muscle. *Am J Physiol Regul Integr Comp Physiol.* 296(6):R1820-8.

Johannes L and Popoff V., 2008. Tracing the retrograde route in protein trafficking. Cell. 135:1175–1187.

Jovic M, Sharma M, Rahajeng J, Caplan S, 2010. The early endosome: a busy sorting station for proteins at the crossroads. Histol Histopathol 25: 99–112

Joazeiro CA, Weissman AM, 2000. "RING finger proteins: mediators of ubiquitin ligase activity". *Cell* 102 (5): 549–52.

Kaisto T, Rahkila P, Marjomaki V, Parton RG, Metsikko K, 1999. Endocytosis in skeletal muscle fibers. Exp Cell Res. 253:551–560.

Kandarian, S.C., and Stevenson, E.J., 2002. Molecular events in skeletal muscle during disuse atrophy. Exerc Sport Sci Rev 30:111-116.

Karagounis LG, Hawley JA, 2010. Skeletal muscle: increasing the size of the locomotor cell. Int J Biochem Cell Biol. 42(9):1376-9.

Kedar, V., McDonough H., Arya R., Li H.H., Rockman H.A., Patterson C., 2004. Muscle-specific RING finger 1 is a bona fide ubiquitin ligase that degrades cardiac troponin I. *Proc. Natl. Acad. Sci. U. S. A.* 101:18135–18140.

Kedra, D., Peyrard, M., Fransson, I., Collins, J.E., Dunham, I., Roe, B.A., and Dumanski, J.P., 1996. Characterization of a second human clathrin heavy chain polypeptide gene (*CHL-22*) from chromosome 22q11. Hum. Mol. Genet. *5,* 625–631.

Kee, A.J., Combaret, L., Tilignac, T., Souweine, B., Aurousseau, E., Dalle, M., Taillandier, D., and Attaix, D., 2003. Ubiquitin-proteasome-dependent muscle proteolysis responds slowly to insulin release and refeeding in starved rats. J Physiol 546:765-776.

Kerr MC, Lindsay MR, Luetterforst R, Hamilton N, Simpson F, Parton RG, Gleeson PA and Teasdale RD, 2006. Visualisation of macropinosome maturation by the recruitment of sorting nexins. J. Cell Sci. 119, 3967-3980.

Korthuis RJ**,** 2011**.** Skeletal Muscle Circulation. San Rafael (CA): Morgan & Claypool Life Sciences; 2011. Integrated Systems Physiology: from Molecule to Function to Disease.

Koumandou VL *et al*, 2011. Evolutionary reconstruction of the retromer complex and its function in Trypanosoma brucei. J Cell Sci. 124:1496–1509.

Laemmli, U.K. 1970. Cleavage of structural proteins during the assembly of the head of bacteriophage T4. Nature 227:680-685.

Lamb CA, Yoshimori T, Tooze SA, 2013. The autophagosome: origins unknown, bio-genesis complex. Nat Rev Mol Cell Biol 14:759–74.

Lange S, Xiang F, Yakovenko A, Vihola A, Hackman P, *et al*., 2005. The kinase domain of Titin controls muscle gene expression and protein turnover. Science 308: 1599-1603.

Langhans C, Weber-Carstens S, Schmidt F, Hamati J, Kny M, Zhu X, Wollersheim T, Koch S, Krebs M, Schulz H, Lodka D, Saar K, Labeit S, Spies C, Hubner N, Spranger J, Spuler S, Boschmann M, Dittmar G, Butler-Browne G, Mouly V, Fielitz J, 2014. Inflammation-induced acute phase response in skeletal muscle and critical illness myopathy. PLoS One. 9(3):e92048.

Li Y, Gazdoiu S, Pan ZQ, Fuchs SY, 2004. Stability of homologue of Slimb F-box protein is regulated by availability of its substrate. J Biol Chem. 279: 11074–11080.

Lim, J. P., Wang, J. T., Kerr, M. C., Teasdale, R. D. and Gleeson, P. A., 2008. A role for SNX5 in the regulation of macropinocytosis. BMC Cell Biol. 9, 58.

Lim JP, Teasdale RD, Gleeson PA, 2012. SNX5 is essential for efficient macropinocytosis and antigen processing in primary macrophages. Biol Open. 1(9):904-14

Liu, H., Liu, Z.Q., Chen, C.X., Magill, S., Jiang, Y., and Liu, Y.J., 2006. Inhibitory regulation of EGF receptor degradation by sorting nexin 5. Biochem. Biophys. Res. Commun. 342, 537–546.

Liu SH, Towler MC, Chen E, Chen CY, Song W, Apodaca G, Brodsky FM, 2001. A novel clathrin homolog that co-distributes with cytoskeletal components functions in the trans-Golgi network. EMBO J. 20:272–284.

Long, K.R., Trofatter, J.A., Ramesh, V., McCormick, M.K., and Buckler, A.J., 1996. Cloning and characterization of a novel human clathrin heavy chain gene (CLTCL). Genomics *35,* 466–472.

Lorick, K. L. *et al.,* 1999. RING fingers mediate ubiquitin-conjugating enzyme (E2)-dependent ubiquitination. *Proc. Natl Acad. Sci. USA* 96, 11364–11369.

Loubery S, Wilhelm C, Hurbain I, Neveu S, Louvard D, Coudrier E, 2008. Different microtubule motors move early and late endocytic compartments. Traffic 9: 492–509

Luzio JP, Pryor PR, Bright NA, 2007. Lysosomes: fusion and function. Nat Rev MolCell Biol 8:622–32.

Maianu, L., S.R. Keller, and W.T. Garvey., 2001. Adipocytes exhibit abnormal subcellular distribution and translocation of vesicles containing glucose transporter 4 and insulin-regulated aminopeptidase in type 2 diabetes mellitus: implications regarding defects in vesicle trafficking. *J. Clin. Endocrinol. Metab.* 86:5450–5456.

Maruyama K, Matsubara R, Natori Y, Nonomura S and Kimura S, 1977. Connectin, an elastic protein of muscle. *J Biochem.* 82: 317-337.

Mathews KD, Moore SA, 2003. Limb-girdle muscular dystrophy. *Current Neurology and Neuroscience Reports* 3 (1): 78–85.

Mayor S, Pagano RE, 2007. Pathways of clathrin-independent endocytosis. Nat Rev Mol Cell Biol. 8:603–612.

Maxfield FR, McGraw TE, 2004. Endocytic recycling. Nat Rev Mol Cell Biol 5: 121–132.

McComas AJ, 1996. Skeletal Muscle: Form and Function. Champaign, Ill: Human Kinetics.

McElhinny, A.S., Kakinuma, K., Sorimachi, H., Labeit, S., and Gregorio, C.C., 2002. Muscle-specific RING finger-1 interacts with titin to regulate sarcomeric M-line and thick filament structure and may have nuclear functions via its interaction with glucocorticoid modulatory element binding protein-1. *J. Cell Biol.* 157:125–136.

McElhinny, A.S., Perry C.N., Witt C.C., Labeit, S., and Gregorio, C.C., 2004. Muscle-specific RING finger-2 (MURF-2) is important for microtubule, intermediate filament and sarcomeric M-line maintenance in striated muscle development. *J. Cell Sci.* 117:3175–3188.

Merino-Trigo, A., Kerr, M.C., Houghton, F., Lindberg, A., Mitchell, C., Teasdale, R.D., and Gleeson, P.A., 2004. Sorting nexin 5 is localized to a subdomain of the early endosomes and is recruited to the plasma membrane following EGF stimulation. J. Cell Sci. 117, 6413–6424.

Mues A, van der Ven PF, Young P, Fürst DO and Gautel M, 1998. Two immunoglobulin-like domains of the Z-disc portion of titin interact in a conformation-dependent way with telethonin. *FEBS Lett* 428:111-114.

Mukherjee, S. & Maxfield, F. R., 2000. Role of membrane organization and membrane domains in endocytic lipid trafficking. *Traffic* 1, 203–211

Murray JW, Bananis E, Wolkoff AW, 2000. Reconstitution of ATP dependent movement of endocytic vesicles along microtubules in vitro: an oscillatory bidirectional process. Mol Biol Cell 11: 419–433

Musa H, Meek S, Gautel M, Peddie D, Smith AJ *et al*., 2006. Targeted homozygous deletion of M-band titin in cardiomyocytes prevents sarcomere formation. J Cell Sci 119: 4322-4331.

Nielsen E, Severin F, Backer JM, Hyman AA, Zerial M, 1999. Rab5 regulates motility of early endosomes on microtubules. Nat Cell Biol 1: 376–382

Norwood SJ *et al*., 2011. Assembly and solution structure of the core retromer protein complex. Traffic. 12:56–71.

Obermann WM, Gautel M, Weber K and Fürst DO, 1997. Molecular structure of the sarcomeric M band: mapping of titin and myosin binding domains in myomesin and the identification of a potential regulatory phosphorylation site in myomesin. *EMBO J* 16: 211-220

Ochala J, Gustafson A-M, Lano Diez M, Renaud G, Li M, Aare S, Qaisar R, Banduseela VC, Hedstrom Y, Tang X, Dworkin B, Ford GC, Nair S, Perera S, Gautel M, Larsson L, 2011. Preferential skeletal muscle myosin loss in response to mechanical silencing in a novel rat intensive care unit model: underlying mechanisms. J Physiol 589:2007–2026

Olson A.L., Trumbly A.R., Gibson G.V., 2001. Insulin-mediated GLUT4 translocation is dependent on the microtubule network. J. Biol. Chem. 276:10706-10714.

Otsuki T, Kajigaya S, Ozawa K, Liu JM, 1999. SNX5, a new member of the sorting nexin family, binds to the Fanconi anemia complementation group A protein. *Biochem. Biophys. Res. Commun*. 265, 630-635

Patki V., J. Buxton, A. Chawla, L. Lifshitz, K. Fogarty, W. Carrington, R. Tuft, and S. Corvera, 2001. Insulin action on GLUT4 traffic visualized in single 3T3-L1 adipocytes by using ultra-fast microscopy. Mol. Biol. Cell 12:129-141.

Perera S., Holt M.R., Mankoo B.S., Gautel M., 2011. Developmental regulation of MURF ubiquitin ligases and autophagy proteins nbr1, p62/ SQSTM1 and LC3 during cardiac myofibril assembly and turnover. Dev Biol 351: 46–61.

Perera S., Mankoo B., Gautel M., 2012. Developmental regulation of MURF E3 ubiquitin ligases in skeletal muscle. J Muscle Res Cell Motil 33: 107–122.

Peter BJ *et al*., 2004. BAR domains as sensors of membrane curvature: the amphiphysin BAR structure. Science. 303:495–499.

Pickart C.M., 2000. Ubiquitin in chains. *Trends in Biochemical Sciences*, *25*(11), 544–548.

Pickart C.M., 2001. Ubiquitin enters the new millennium. Mol Cell. 8:499-504

Pickart, C.M. 2004. Back to the future with ubiquitin. Cell 116:181-190.

Pizon V, Iakovenko A, van der Ven PF, Kelly R, Fatu C, Fürst DO, Karsenti E, Gautel M, 2002. Transient association of titin and myosin with microtubules in nascent myofibrils directed by the MURF2 RING-finger protein. J Cell Sci 115: 4469-4482.

Pizon V, Rybina S, Gerbal F, Delort F, Vicart P, Baldacci G, Karsenti E, 2013. MURF2B, a Novel LC3-Binding Protein, Participates with MURF2A in the Switch between Autophagy and Ubiquitin Proteasome System during Differentiation of C2C12 Muscle Cells. PLoS ONE 8(10): e76140.

Plowman SA and Smith DL, 1997. Exercise Physiology for Health, Fitness, and Performance. Boston, Mass: Allyn & Bacon; 1997:433.

Polge C, Heng AE, Jarzaguet M, Ventadour S, Claustre A, Combaret L, Bechet D, Matondo M, Uttenweiler-Joseph S, Monsarrat B, *et al*., 2011. Muscle actin is polyubiquitinylated *in vitro* and *in vivo* and targeted for breakdown by the E3 ligase MuRF1. *FASEB J* **25**, 3790 - 3802.

Predmore JM, Wang P, Davis F, Bartolone S, Westfall MV, Dyke DB et al. (Mar 2010). "Ubiquitin proteasome dysfunction in human hypertrophic and dilated cardiomyopathies". *Circulation* 121 (8): 997–1004.

Raposo G and Stoorvogel W, 2013. Extracellular vesicles: exosomes, microvesicles, and friends. J Cell Biol 200:373–83.

Rappsilber J, Ishihama Y, Mann M, 2003. Stop and go extraction tips for matrix-assisted laser desorption/ionization, nanoelectrospray, and LC/MS sample pretreatment in proteomics. Anal Chem. 75(3):663-70.

Rink J, Ghigo E, Kalaidzidis Y, Zerial M, 2005. Rab conversion as a mechanism of progression from early to late endosomes. Cell 122: 735–749

Rishal I. and Fainzilber M., 2010. Retrograde signaling in axonal regeneration. Exp Neurol. (1):5-10.

Rojas R, van Vlijmen T, Mardones GA, Prabhu Y, Rojas AL, Mohammed S, *et al*., 2008. Regulation of retromer recruitment to endosomes by sequential action ofRab5 and Rab7. J Cell Biol 183:513–26.

Rudich A and Klip A, 2003. Push/pull mechanisms of GLUT4 traffic in muscle cells. Acta Physiol Scand. 178:297–308.

Sandri M., 2011. New findings of lysosomal proteolysis in skeletal muscle. Curr Opin Clin Nutr Metab Care. 2011 (3):223-9.

Sanes JR, Lichtman JW, 1999. Development of the vertebrate neuromuscular junction. Annu Rev Neurosci. 22:389–442.

Schiaffino, S., Dyar, K. A., Ciciliot, S., Blaauw, B., & Sandri, M., 2013. Mechanisms regulating skeletal muscle growth and atrophy. *FEBS Journal*, n/a–n/a. doi:10.1111/febs.12253

Schiaffino, S. & Reggiani, C., 1996. Molecular diversity of myofibrillar proteins: gene regulation and functional significance. *Physiological Reviews* 76, 371–423.

Schiaffino, S., and Reggiani, C., 2011. Fiber types in mammalian skeletal muscles. Physiol Rev 91:1447-1531.

Schill NJ, Hedman AC, Choi S and Anderson RA, 2014. Isoform 5 of PIPKIγ regulates the endosomal trafficking and degradation of E-cadherin. J Cell Sci. 127(Pt 10):2189-203

Schmidt F, Kny M, Zhu X, Wollersheim T, Persicke K, Langhans C, Lodka D, Kleber C, Weber-Carstens S, Fielitz J, 2014. The E3 ubiquitin ligase TRIM62 and inflammation-induced skeletal muscle atrophy. Crit Care. 18(5):545.

Schmidt, M., & Finley, D., 2013. Regulation of proteasome activity in health and disease. *Biochimica et Biophysica Acta (BBA)-Molecular Cell Research*. Biochim Biophys Acta. 1843(1):13-25.

Scott CC and Gruenberg J, 2011. Ion flux and the function of endosomes and lysosomes: pH is just the start: the flux of ions across endosomal membranes influencesendosome function not only through regulation of the luminal pH. Bioessays. 33:103–10.

Scott CC, Vacca F, Gruenberg J, 2014. Endosome maturation, transport and functions. Semin Cell Dev Biol (31):2-10.

Scott, W., Stevens, J., and Binder-Macleod, S.A. 2001. Human skeletal muscle fiber type classifications. Phys Ther 81:1810-1816.

Seaman MN, Marcusson EG, Cereghino JL, Emr SD., 1997. Endosome to Golgi retrieval of the vacuolar protein sorting receptor, Vps10p, requires the function of the VPS29, VPS30, and VPS35 gene products. J Cell Biol 137: 79–92.

Seaman MN, McCaffery JM, Emr SD., 1998. A membrane coat complex essential for endosome-to-Golgi retrograde transport in yeast. J Cell Biol 142: 665–681.

Seaman MN, 2005. Recycle your receptors with retromer. *Trends Cell Biol.* 15, 68-75.

Seaman MN, 2007. Identification of a novel conserved sorting motif required for retromer-mediated endosome-to-TGN retrieval. J Cell Sci. 120:2378–2389.

Seaman MN, Harbour ME, Tattersall D, Read E, Bright N., 2009. Membrane recruitment of the cargoselective retromer subcomplex is catalysed by the small GTPase Rab7 and inhibited by the Rab- GAP TBC1D5. J Cell Sci. 122:2371–2382.

Seaman MN, 2012. The retromer complex – endosomal protein recycling and beyond. J Cell Sci 125:4693–702.

Sirotkin, H. *et al.,* 1996. Isolation of a new clathrin heavy chain gene with muscle-specific expression from the region commonly deleted in velo-cardiofacial syndrome. Hum. Mol. Genet. *5,* 617–624.

Shigematsu S, Khan AH, Kanzaki M, Pessin JE, 2002. Intracellular insulin-responsive glucose transporter (GLUT4) distribution but not insulin-stimulated GLUT4 exocytosis and recycling are microtubule dependent. Mol Endocrinol. 16(5):1060-8.

Smerdu, V., Karsch-Mizrachi, I., Campione, M., Leinwand, L. & Schiaffino, S., 1994. Type IIx myosin heavy chain transcripts are expressed in type IIb fibers of human skeletal muscle. *American Journal of Physiology* 267, C1723–C1728.

Soppina V, Rai AK, Ramaiya AJ, Barak P, Mallik R, 2009. Tug-of-war between dissimilar teams of microtubule motors regulates transport and fission of endosomes. Proc Natl Acad Sci USA 106: 19381–19386

Spencer J.A., Eliazer S., Ilaria R.L. Jr., Richardson J.A., and Olson E.N., 2000. Regulation of microtubule dynamics and myogenic differentiation by MURF, a striated muscle RING-finger protein. *J. Cell Biol.* 150:771–784.

Strochlic TI, Setty TG, Sitaram A, Burd CG, 2007. Grd19/Snx3p functions as a cargo specific adapter for retromer-dependent endocytic recycling. J Cell Biol. 177:115–125.

Sun Y, Hedman AC, Tan X, Schill NJ, Anderson RA, 2013. Endosomal type IγPIP 5-Kinase controls EGF receptor lysosomal sorting. Developmental Cell. 25(2):144-55.

Teasdale, R. D., Loci, D., Houghton, F., Karlsson, L. & Gleeson, P. A, 2001. A large family of endosome-localized proteins related to sorting nexin 1. *Biochem. J.* 358, 7–16.

Temkin P, *et al.,* 2011. SNX27 mediates retromer tubule entry and endosome-to-plasma membrane trafficking of signalling receptors. Nat Cell Biol. 13:717–723.

Thomas, D. R., 2007. Loss of skeletal muscle mass in aging: Examining the relationship of starvation, sarcopenia and cachexia. *Clinical Nutrition*, *26*(4), 389–399.

Tortorella LL and Pilch PF, 2002. C2C12 myocytes lack an insulin-responsive vesicular compartment despite dexamethasone-induced GLUT4 expression. Am J Physiol Endocrinol Metab. 283(3):E514-24.

Towbin, H., Staehelin, T., and Gordon, J. 1979. Electrophoretic transfer of proteins from polyacrylamide gels to nitrocellulose sheets: procedure and some applications. Proc Natl Acad Sci U S A 76:4350-4354.

Towler M.C., Kaufman S.J. and Brodsky F.M., 2004 a. Membrane Traffic in Skeletal Muscle. *Traffic*, 2004. 5: 129–139

Towler, M.C., P.A. Gleeson, S. Hoshino, P. Rahkila, V. Manalo, N. Ohkoshi, C. Ordahl, R.G. Parton, and F.M. Brodsky, 2004 b. Clathrin isoform CHC22, a component of neuromuscular and myotendinous junctions, binds sorting nexin 5 and has increased expression during myogenesis and muscle regeneration. *Mol. Biol. Cell.* 15:3181–3195.

Ullrich O, Horiuchi H, Bucci C, Zerial M, 1994. Membrane association of Rab5 mediated by GDP-dissociation inhibitor and accompanied by GDP/GTP exchange. Nature 368: 157–160

van Weering JR, Verkade P, Cullen PJ, 2010. SNX-BAR proteins in phosphoinositide-mediated, tubular based endosomal sorting. Semin Cell Dev Biol 21:371–380.

van Weering JR, Sessions RB, Traer CJ, Kloer DP, Bhatia VK, Stamou D, Carlsson SR, Hurley JH, Cullen PJ., 2012a. Molecular basis for SNX-BAR-mediated assembly of distinct endosomal sorting tubules.EMBOJ 31: 4466–4480.

van Weering JR, Verkade P, Cullen PJ., 2012b. SNX-BAR mediated endosome tubulation is co-ordinated with endosome maturation. Traffic 13: 94–107.

Vandervoort AA, 2002. Aging of the human neuromuscular system. Muscle Nerve. 25:17-25

Vassilopoulos S, Esk C, Hoshino S, Funke BH, Chen CY, et al., 2009. A role for the CHC22 clathrin heavy-chain isoform in human glucose metabolism. Science 324: 1192–1196.

Wakeham, D.E., L. Abi-Rached, M.C. Towler, J.D. Wilbur, P. Parham, and F.M. Brodsky., 2005. Clathrin heavy and light chain isoforms originated by independent mechanisms of gene duplication during chordate evolution. *Proc. Natl. Acad. Sci. USA*. 102:7209–7214.

Wang, J. T., Kerr, M. C., Karunaratne, S., Jeanes, A., Yap, A. S. and Teasdale, R.D., 2010. The SNX-PX-BAR family in macropinocytosis: the regulation of macropinosome formation by SNX-PX-BAR proteins. PLoS ONE 5, e13763.

Wang K, McClure J, and Tu A, 1979. Titin: major myofibrillar components of striated muscle. *Proc Natl Acad Sci USA*. 76:3698-3702.

Wassmer T, Attar N, BujnyMV, Oakley J, Traer CJ, Cullen PJ, 2007. A loss-of-function screen reveals SNX5 and SNX6 as potential components of the mammalian retromer. J Cell Sci 120: 45–54.

Wassmer T, *et al.,* 2009. The retromer coat complex coordinates endosomal sorting and dynein-mediated transport, with carrier recognition by the trans-Golgi network. Dev Cell. 17:110–122.

Weber-Carstens S, Schneider J, Wollersheim T, Assmann A, Bierbrauer J, Marg A, Al Hasani H, Chadt A, Wenzel K, Koch S, Fielitz J, Kleber C, Faust K, Mai K, Spies CD, Luft FC, Boschmann M, Spranger J, Spuler S, 2013. Critical illness myopathy and GLUT4: significance of insulin and muscle contraction. Am J Respir Crit Care Med.187(4):387-96

Weinmaster G, Fischer JA, 2011. Notch ligand ubiquitylation: what is it good for? Dev Cell 21: 134–144.

Weissman AM, 2001. Themes and variations on ubiquitylation. Nat Rev Mol Cell Biol. 2:169-78.

Weissman A.M., Shabek N., Ciechanover A., 2011. The predator becomes the prey: regulating the ubiquitin system by ubiquitylation and degradation. Nat Rev Mol Cell Biol. 12(9):605-20.

Wilkinson, K. D., 2000. Ubiquitination and deubiquitination: Targeting of proteins for degradation by the proteasome. *Seminars in Cell & Developmental Biology*, *11*(3), 141–148.

Willis, M.S., Ike C., Li L., Wang D., Glass D.J. and Patterson C., 2007. Muscle ring finger 1, but not muscle ring finger 2, regulates cardiac hypertrophy in vivo. *Circ. Res*. 100:456–459.

Witt, S.H., Granzier, H., Witt, C.C., and Labeit, S., 2005. MURF-1 and MURF-2 target a specific subset of myofibrillar proteins redundantly: towards understanding MURF-dependent muscle ubiquitination. *J. Mol. Biol.* 350:713–722.

Worby, C. A. and Dixon, J. E., 2002. Sorting out the cellular functions of sorting nexins. Nat. Rev. Mol. Cell Biol. 3, 919-931.

Wray, C.J., Mammen, J.M., Hershko, D.D., and Hasselgren, P.O., 2003. Sepsis upregulates the gene expression of multiple ubiquitin ligases in skeletal muscle. Int J Biochem Cell Biol 35:698-705.

Yoo KW, Kim EH, Jung SH, Rhee M, Koo BK, *et al*., 2006. Snx5, as a Mind bomb-binding protein, is expressed in hematopoietic and endothelial precursor cells in zebrafish. FEBS Lett 580: 4409–4416.

6 Appendix

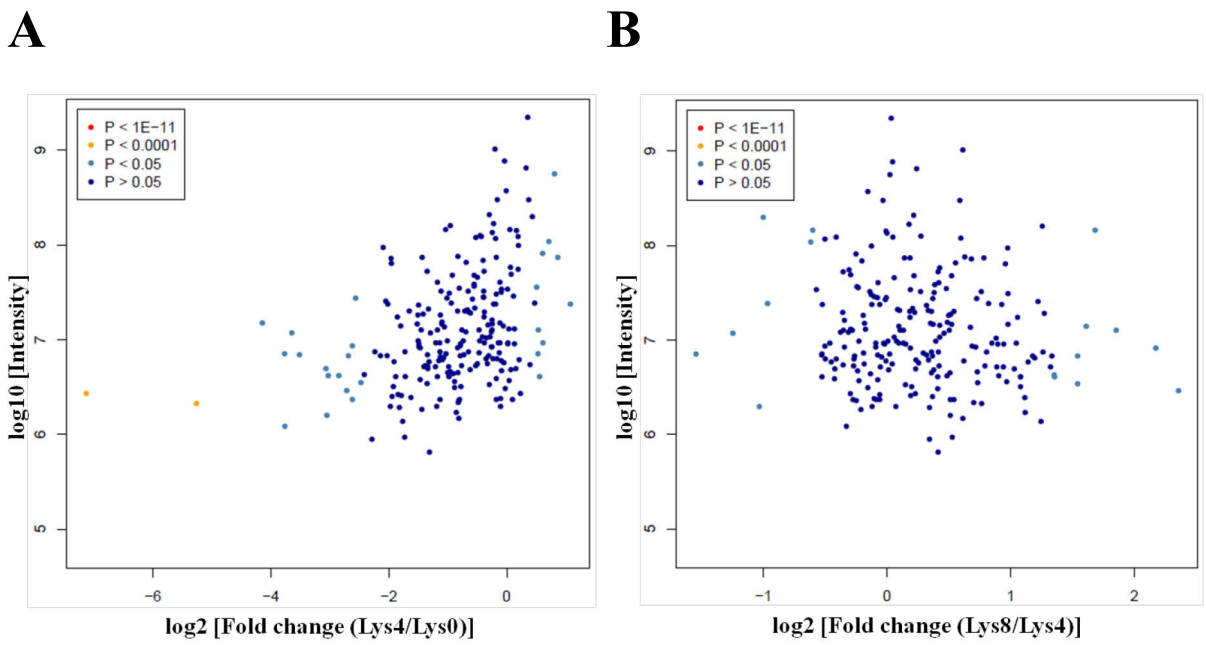

Appendix-Figure 1: Distribution of significantly up- or down-regulated proteins during differentiation and atrophy of C2C12 cells overexpressing MuRF1. The significance of each protein was determined as the intensity vs. the ratio representing the abundance change during myocyte differentiation **(A)** or atrophy of myotubes **(B)**. The legend refers to p-values from the Benjamini-Hochberg False Discovery Rate. Error rate was set to 0.05.

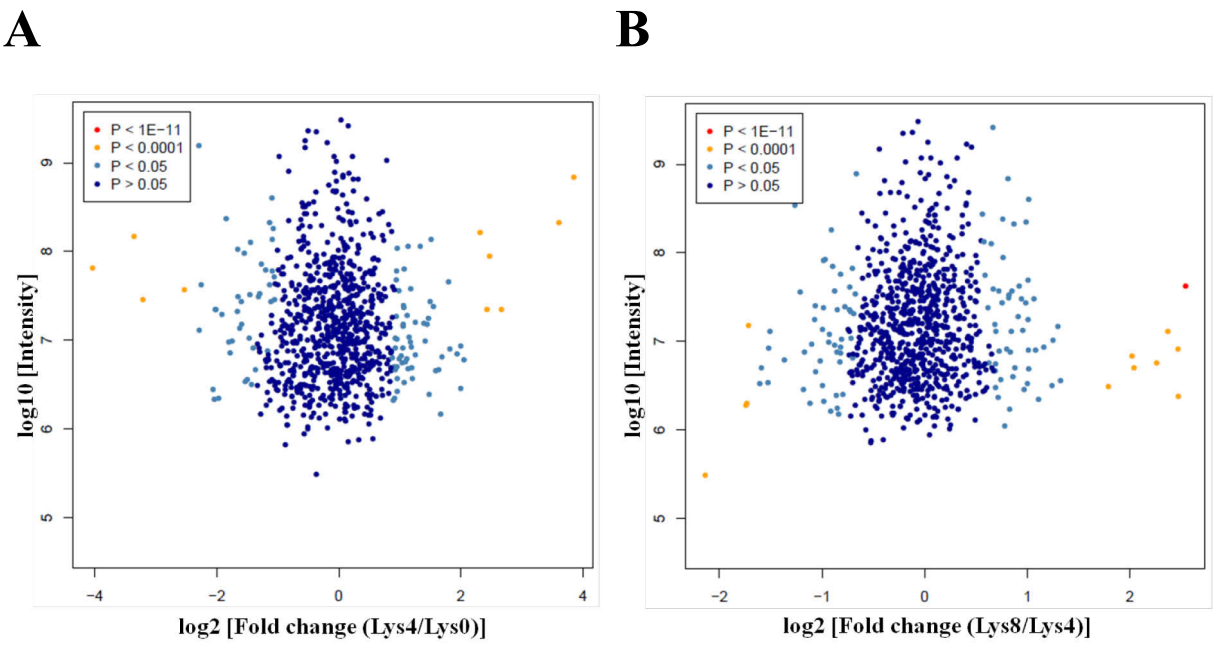

Appendix-Figure 2: Distribution of significantly up- or down-regulated proteins during differentiation and atrophy of C2C12 cells overexpressing MuRF2. The significance of each protein was determined as the intensity vs. the ratio representing the abundance change during myocyte differentiation **(A)** or atrophy of myotubes **(B)**. The legend refers to p-values from the Benjamini-Hochberg False Discovery Rate. Error rate was set to 0.05.

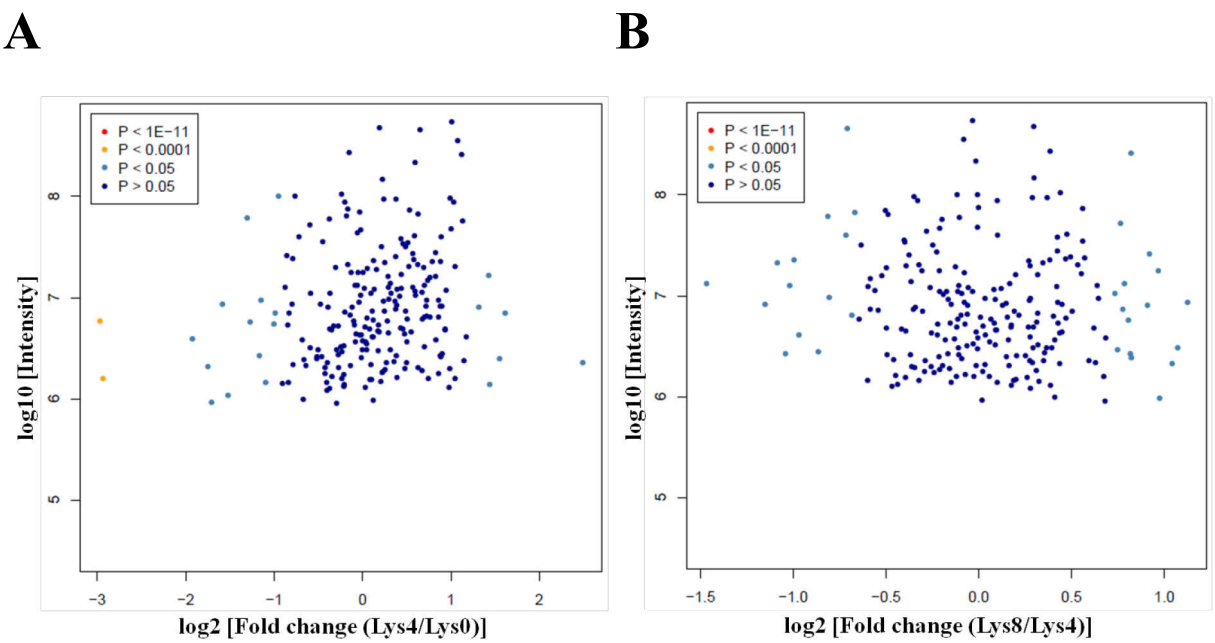

Appendix-Figure 3: Distribution of significantly up- or down-regulated proteins during differentiation and atrophy of C2C12 cells overexpressing MuRF3. The significance of each protein was determined as the intensity vs. the ratio representing the abundance change during myocyte differentiation **(A)** or atrophy of myotubes **(B)**. The legend refers to p-values from the Benjamini-Hochberg False Discovery Rate. Error rate was set to 0.05.

Appendix-Table 1: Mass spectrometric data of proteins with a significant abundance difference during differentiation of myocytes overexpressing MuRF1. A total of 658 proteins were detected in this screen, of which 78 were proteins whose abundance has significantly changed as a result of MuRF1-overexpression, which make approx. 11.8%. 51 proteins were significantly up-regulated and 27 proteins were significantly down-regulated. Significance was set to p-value < 0.05.

Protein	Log2 (fold change)	Significance p-value<0.05	Biological process	Molecular function	Cellular component
	Up-regulated				
Actin	2.0	0,0046718	Muscle contraction	ATP binding	Cytoskeleton, cytoplasm
Heat shock 70kDa protein 9 (Mortalin)	1.9	0,034041	Protein folding, protein export from nucleus	ATP binding, protein binding	Cytoplasm, nucleus, mitochondria, exosome
Heat shock 60kDa protein 1 (Chaperonin)	1.9	0,039306	*de novo* protein folding	DNA, RNA and p53 binding	Cytoplasm, mitochondria
JNK/SAPK associated protein	1.5	0,046261	MAPK, JUN kinase activation, retrograde transport	JUN kinase, kinesin binding	Cytoplasm, plasma membrane

Heat shock 70kDa protein 1B	1.2	0,00034963	Protein folding	Protein binding	Cytoplasm, mitochondria
Heme oxygenase 1	1.0	0,011908	Angiogenesis, cell prolifiration	Signal transduction	Nucleus, ER
	Down-regulated				
Tubulin, Beta 4	-3.8	0,0011174	Mitotic cell cycle, protein folding	Cytoskeleton component, GTPase activity	Microtubule, cytoplasm, plasma membrane
Ribosomal protein S25	-2.3	0,0071287	Translational initiation and elongation	Ribosome component, RNA binding	Cytoplasm, ribosome
Eukaryotic translation Termination factor 1	-1.4	0,030171	Translational termination, protein methylation	RNA and protein binding	Cytoplasm
Plectin	-1.0	0,049824	Apoptosis, cell junction assembly	Actin binding, Ankyrin binding	Cytoplasm, cytoskeleton, plasma membrane

Appendix-Table 2: Mass spectrometric data of proteins with a significant abundance difference during atrophy of myotubes overexpressing MuRF1. A total of 657 proteins were detected in this screen, of which 95 were proteins whose abundance has significantly changed as a result of MuRF1-overexpression, which make approx. 14.5%. 64 proteins were significantly up-regulated and 31 proteins were significantly down-regulated. Significance was set to p-value < 0.05.

Protein	Log2 (fold change)	Significance p-value<0.05	Biological process	Molecular function	Cellular component
	Up-regulated				
Coenzyme A transferase	2.1	0,010076	Metabolic process	Coenzyme transferase activity	Mitochondria
Heat shock 60kDa protein 1 (Chaperonin)	2.1	0,043389	*de novo* protein folding	DNA, RNA and p53 binding	Cytoplasm, mitochondria
Carbonic anhydrase III	1.7	0,0050979	Oxidative stress response	Zinc ion binding, catalytic activity	Cytosol
Thioredoxin	1.6	0,045609	Cell redox homeostasis	Cytalytic activity	Endoplasmic reticulum
Annexin A5	1.5	0,044924	Signal transduction	Calcium ion binding	Cytoplasm

	Down-regulated				
Nucleoside diphosphate kinase	-2.4	0,0010896	GTP, UTP, CTP biosynthetic process	nucleotide binding	Nucleus, cytoplasm, mitochondria
Argininosuccinate synthase 1	-2.1	0,0013749	Urea cycle, metabolic process	ATP, nucleotide binding	Cytoplasm, exosome, mitochondria
Calcium/calmodulin dependent Protein kinase II delta	-2.0	0,022441	Regulation of cell growth	Protein kinase activity	Cytoplasm, nucleus, membrane
Ataxin-2	-1.5	0,021206	regulation of translation and EGFR endocytosis	RNA, EGFR, protein binding	Cytoplasm, nucleus, TGN
CHIP E3 ubiquitin protein ligase	-1.4	0,027007	ubiquitin-dependent proteolysis	Ubiquitin protein-ligase activity	Cytoplasm, nucleus
Glutaredoxin (thioredoxin-like)	-1.0	0,049793	cell redox homeostasis, cardiac hypertrophy	Protein binding	Cell cortex, Z disc

Appendix-Table 3: Mass spectrometric data of proteins with a significant abundance difference during differentiation of myocytes overexpressing MuRF2. A total of 691 proteins were detected in this screen, of which 88 were proteins whose abundance has significantly changed as a result of MuRF2-overexpression, which make approx. 12.7%. 45 proteins were significantly up-regulated and 43 proteins were significantly down-regulated. Significance was set to p-value < 0.05.

Protein	Log2 (fold change)	Significance p-value<0.05	Biological process	Molecular function	Cellular component
	Up-regulated				
Carbonic anhydrase III	4.5	0,00056515	Oxidative stress response	Zinc ion binding, catalytic activity	Cytosol
Annexin A2	3.0	1,4512E-11	Angiogenesis, membrane raft assembly	Calcium ion binding	Cytoplasm, EEs
S100 calcium binding Protein A10	2.7	1,1357E-10	Membrane raft assembly and budding	Calcium ion binding	Plasma membrane, exosome
Annexin A6	2.1	0,000017506	Calcium ion transport, muscle contraction	Calcium ion binding	Plasma membrane, exosome

Ras suppressor protein 1	2.1	1,9487E-06	Ras signal transduction	Protein binding	Cytosol, exosome
Myosin heavy chain 10	2.1	0,0034534	Plasma membrane repair	Actin binding, motor activity	Cytoplasm, stress fiber
Myosin 1c	1.8	0,0058731	Protein targeting, transport	Actin binding, motor activity	Nucleus
Glutathione S-transferase Mu1	1.1	0,0044456	Glutathione metabolic process	Glutathione transferase activity	cytoplasm
	Down-regulated				
S100 calcium binding protein A6	-5.3	6,2426E-09	Signal transduction	Tropomyosin, calcium and zinc binding	Nucleus, cytoplasm
S100 calcium binding protein A4	-4.2	1,0058E-06	NF-kappaB signaling	Actin binding, calcium ion binding	Nucleus, cytoplasm, exosome
S100 calcium binding protein A11	-4.2	2,6253E-06	Signal transduction	Calcium ion binding	Nucleus, cytoplasm, exosome
Vimentin	-1.6	0,0052722	Immune response	Cytoskeleton component	Cytoplasm
Heat shock 70kDa protein 9 (Mortalin)	-1.1	0,012485	Protein folding, protein export from nucleus	ATP binding, protein binding	Cytoplasm, nucleus, mitochondria, exosome

Appendix-Table 4: Mass spectrometric data of proteins with a significant abundance difference during atrophy of myotubes overexpressing MuRF2. A total of 690 proteins were detected in this screen, of which 81 were proteins whose abundance has significantly changed as a result of MuRF2-overexpression, which make approx. 11.7%. 35 proteins were significantly up-regulated and 46 proteins were significantly down-regulated. Significance was set to p-value < 0.05.

Protein	Log2 (fold change)	Significance p value<0.05	Biological process	Molecular function	Cellular component
	Up-regulated				
Myosin 1c	2.4	0,0032281	Protein targeting, transport	Actin binding, motor activity	Nucleus
Stathmin 1	1.8	0,016501	Signal transduction, microtubule depolymerization	Tubulin binding, signal transducer	Cytoplasm, microtubule, membrane

Exportin (tRNA)	**1.7**	**0,03329**	**tRNA export from nucleus**	**tRNA and Ran GTPase binding**	**Cytoplasm, nucleus**
Myosin heavy chain 9	**1.5**	**0,044093**	**Angiogenesis, cell differentiation**	**Actin binding, motor activity**	**Nucleus, stress fiber**
Glutathione S-transferase Mu1	**1.2**	**0,0051187**	**Glutathione metabolic process**	**Glutathione transferase activity**	**Cytoplasm**
Annexin A1	**0.9**	**0,0054213**	**Inflammatory response, cell cycle**	**Calcium ion binding**	**Cytoplasm, nucleus**
	Down-regulated				
Heme oxygenase 1	**-3.3**	**0,0044642**	**Angiogenesis, cell prolifiration**	**Protein binding, signal transducer**	**Nucleus, ER**
Heat shock 70kDa protein 1B	**-1.8**	**0,012008**	**Cell proliferation, gene expression, mRNA catabolic process**	**ATP and ubiquitin ligase binding**	**Cytoplasm, ER, nucleus, mitochondria**
Endoplasmic reticulum protein 44	**-1.7**	**0,00057456**	**Protein folding, cell redox homeostasis**	**Calcium ion binding**	**ER, exosome**
Acyl-CoA thioesterase 9	**-1.4**	**0,027103**	**Acyl-CoA metabolic process**	**Acetyl-CoA hydrolase activity**	**Mitochondria**
Calcium/calmodulin dependent Protein kinase II delta	**-1.3**	**0,014109**	**Regulation of cell growth**	**Protein kinase activity**	**Cytoplasm, nucleus, membrane**
Peroxiredoxin 4	**-1.3**	**0,000044232**	**Oxidation-reduction process**	**Protein binding**	**Cytoplasm, mitochondria, exosome**
Nedd4	**-0.8**	**0,0055331**	**Protein mono-ubiquitination**	**Ubiquitin ligase activity**	**Nucleus, cytoplasm, Golgi**

Appendix-Table 5: Mass spectrometric data of proteins with a significant abundance difference during differentiation of myocytes overexpressing MuRF3. A total of 606 proteins were detected in this screen, of which 61were proteins whose abundance has significantly changed as a result of MuRF3-overexpression, which make approx. 10%. 37 proteins were significantly up-regulated and 24 proteins were significantly down-regulated. Significance was set to p-value < 0.05.

Protein	Log2 (fold change)	Significance p value<0.05	Biological process	Molecular function	Cellular component
	Up-regulated				
Clathrin heavy chain 17 (CHC17)	2.8	0,032746	Intracellular transport, endocytosis	Protein binding	Cytosol, plasma membrane
Acyl-CoA Thioesterase 2	2.4	0,0003882	Acyl-CoA metabolic process	Acyl-CoA hydrolase activity	Mitochondria
Proteasome subunit, beta 1	2.3	0,027817	Protein poly-ubiquitination	Protein binding	Cytosol, proteasome complex
Heat Shock 60kDa Protein 1 (Chaperonin)	2.3	0,016259	*de novo* protein folding	DNA, RNA and p53 binding	Cytoplasm, mitochondria
Proteasome subunit, alpha 5	2.1	0,037052	Protein poly-ubiquitination	Endopeptidase activity	Nucleus, cytoplasm
Proteasome subunit, alpha 4	2.0	0,035291	Protein poly-ubiquitination	Endopeptidase activity	Nucleus, cytoplasm
Proteasome subunit, alpha 6	2.0	0,041525	Protein poly-ubiquitination	RNA binding, endopeptidase activity	Nucleus, cytoplasm, mitochondria
Heme oxygenase 1	1.9	0,00073758	Angiogenesis, cell proliferation	Protein binding, signal transducer	Nucleus, ER
Heat Shock 70kDa Protein 1B	1.7	0,000061457	Cell proliferation	ATP, dsRNA and ubiquitin ligase binding	Nucleus, ER, cytoplasm, mitochondria
Glutathione S-transferase Mu1	1.6	0,010408	Gene expression	Glutathione transferase activity	Cytoplasm
Heat shock protein 90kDa, Beta 1	1.3	0,04642	Glutathione metabolic process	RNA, ATP and calcium ion binding	Cytosol, ER
Heat shock 70kDa protein 5	1.0	0,036495	Protein folding, response to stress	Calcium ion binding, ATPase activity	Nucleus, ER
Calumenin	1.0	0,014676	Cell morphogenesis	Calcium ion binding	Golgi, ER
Carbonic anhydrase XIII	1.0	0,035849	Platelet degranulation Bicarbonate transport	Zinc ion binding	Cytosol

	Down-regulated				
S100 calcium binding protein A6	-3.7	0,00093536	Signal transduction	Tropomyosin, calcium and zinc binding	Nucleus, cytoplasm
Tubulin, Beta 4	-3.6	0,001636	Microtubule-based process, protein folding	Cytoskeleton component, GTAase activity	Cytoplasm, microtubule, plasma membrane
Coatomer protein complex Subunit delta (Archain 1)	-2.7	0,00045282	Intracellular protein transport	Protein binding	Cytoplasm, Golgi, ER
Ribosomal protein L9	-2.0	0,03379	Translation	RNA binding	Cytoplasm, ribosome
Importin Alpha 4	-1.4	0,03346	Protein import into nucleus	Protein transporter activity	Cytoplasm, nucleus
Eukaryotic Translation Initiation Factor 4A1	-1.1	0,018036	Translation, gene expression	Nucleic acid binding	Nucleus, cytosol
Importin Alpha 1	-1.0	0,0011136	Protein import into nucleus	Protein transporter activity	Cytoplasm, nucleus

Appendix-Table 6: Mass spectrometric data of proteins with a significant abundance difference during atrophy of myotubes overexpressing MuRF3. A total of 605 proteins were detected in this screen, of which 74 were proteins whose abundance has significantly changed as a result of MuRF3-overexpression, which make approx. 12.2%. 39 proteins were significantly up-regulated and 35 proteins were significantly down-regulated. Significance was set to p-value < 0.05.

Protein	Log2 (fold change)	Significance p value<0.05	Biological process	Molecular function	Cellular component
	Up-regulated				
ISG15 Ubiquitin-Like modifier	1.8	0,00018428	Cell-cell signaling	Protein binding	Cytoplasm
EH-Domain containing 2	1.8	0,018334	Endocytosis, endocytic recycling	ATP,calcium ion binding, GTPase activity	Nucleus, endosome and plasma membrane
Actin, Alpha 2	1.7	0,0017045	Muscle contraction	ATP binding	Cytoplasm, cytoskeleton
Transgelin	1.5	0,000013291	Muscle organ development	Actin binding	Cytoplasm
Calponin 3	1.5	0,0025479	Cytoskeleton organization	Actin, microtubule binding	Postsynaptic density
Leiomodin 1	1.4	0,0028993	Muscle contraction	Actin, tropomyosin binding	Cytoplasm, cytoskeleton, membrane

Palladin, cytoskeletal-associated protein	**1.2**	**0,014803**	**Cytoskeleton organization**	**Actin, alpha-actinin binding**	**Nucleus, Z-disc, actin-filament**
Biglycan	**1.0**	**0,0052346**	**Extracellular matrix organization**	**Extracellular matrix binding**	**Extracellular matrix, Golgi, cell surface**
Ubiquitin Fusion Degradation 1 Like	**1.0**	**0,035656**	**Ubiquitin-dependent proteaolysis**	**Ubiquitin-specific protease activity**	**Cytoplasm, nucleus**
Annexin A5	**1.0**	**0,044483**	**Signal transduction**	**Calcium ion binding**	**Cytoplasm**
Actinin, Alpha 1	**0.9**	**0,018551**	**Cell junction assembly, extracellular matrix organization**	**Actin, integrin, calcium ion, binding**	**Cytoplasm, nucleus**
Fermitin family member 2	**0.9**	**0,0044141**	**Cell-matrix adhesion**	**PIP_3 binding, Protein binding**	**Nucleus, cytoplasm, stress fiber**
	Down-regulated				
Cystathionase (Cystathionine Gamma-Lyase)	**-2.2**	**1,2004E-09**	**Metabolic process, bio-synthetic process**	**Protein, calmodulin binding**	**Cytoplasm, nucleus, exosome**
Argininosuccinate synthase 1	**-1.5**	**0,00061098**	**Urea cycle, metabolic process**	**ATP, nucleotide binding**	**Cytoplasm, exosome, mitochondria**
Platelet-Activating Factor Acetylhydrolase 1b, Regulatory Subunit 1	**-1.5**	**0,0019577**	**Microtubule cytoskeleton organization**	**Microtubule binding, hydrolase activity**	**Cytoplasm, nucleus, microtubules**

Abbreviations

ADP	**Adenosine diphosphate**
AP	**Affinity purification**
APS	**Ammonium persulfate**
ARR	**Acidic rich region**
ATP	**Adenosine triphosphate**
BAR	**Bin/Amphiphysin/Rvs domain**
BMI	**Body mass index**
BSA	**Bovine serum albumin**
C2C12	**Mouse myoblast cell line**
CCD	**Coiled coil domain**
cDNA	**Complementary DNA**
CHC	**Clathrin heavy chain**
CHF	**Chronic heart failure**
CHX	**Cycloheximide**
CI-MPR	**Cation-independent mannose 6-phosphate receptor**
CKD	**Chronic kidney disease**
CLC	**Clathrin light chain**
COPD	**Chronic obstructive pulmonary disease**
COS7	**African green monkey kidney cell line**
CSC	**Cargo selective complex**
DCTN1	**Dynactin subunit 1**
DMEM	**Dulbecco's modified eagle medium**
DMSO	**Di-Methyl-Sulfoxide**
DANN	**Desoxyribonucleic acid**
DUBs	**Deubiquitinating enzymes**
E.coli	***Escherichia coli***
ECM	**Extracellular matrix**
ECV	**Endosomal carrier vesicle**
EDL	***M. Extensor digitorum longus***
EDTA	**Ethylenediaminetetraacetic acid**
EE	**Early endosome**
EEA1	**Early endosome antigen 1**
EGFR	**Epidermal growth factor receptor**
FANCA	**Fanconi anemia complementation group A protein**
FBS	**Fetal bovine serum**
FHL2	**Four-and-a-half LIM domain protein 2**
GAPDH	**Glyceraldehyde 3-phosphate dehydrogenase**
GLUT4	**Glucose transporter type 4**
GP	***M. Gastrocnemius-plantaris***
GSC	**GLUT4 storage compartment**
GST	**Glutathione S-transferase**
HDAC5	**Histone Deacetylase 5**
HECT	**Homologous to E6 associated protein C- terminus**
HEK293	**Human embryonic kidney 293 cell line**
ICC	**Immunocytochemistry**
IGF2R	**Insulin-like growth factor II receptor**
ILV	**Intraluminal vesicle**

IPTG	**Isopropyl β-D-1-Thiogalactopyranoside**
LAMP1	**Lysosomal-associated membrane protein 1**
LE	**Late endosome**
MAFbx	**Muscle atrophy F-box**
MB	**Myoblast**
MBP	**Maltose binding protein**
MFC	**MuRF-family conserved domain**
MHC	**Myosin heavy chain**
Mib1	**Mind bomb-1**
Mm	***Mus musculus***
mRNA	**Messenger RNA**
MS	**Mass spectrometry**
MT	**Myotubue**
MTA	**Atrophied myotube**
MTJs	**Myotendinous junctions**
MTOC	**Microtubule organizing center**
MuRF	**Muscle RING-finger**
MVB	**Multivesicular body**
NEM	***N*-Ethylmaleimide**
PBS	**Phosphate buffered saline**
PCR	**Polymerase chain reaction**
PEI	**Polyethylenimine**
PKD2	**Protein kinase D2**
PMSF	**Phenylmethanesulfonyl fluoride**
PX	**Phox-homology**
qRT-PCR	**Quantitative real - time PCR**
RBCC	**RING-B-box-coiled-coil**
RE	**Recycling endosome**
RIPA	**Radioimmunoprecipitation assay**
RING	**Really interesting new gene**
RNA	**Ribonucleic acid**
RT	**Room temperature**
SCF	**Skp-Cullin-F-box**
SDS	**Sodium dodecyl sulphate**
SDS-PAGE	**SDS polyacrylamide gel electrophoresis**
SILAC	**Stable Isotope Labeling by Amino acids in Cell culture**
SNX	**Sorting nexin**
SOC	**Super optimal broth**
Sol	***M. Soleus***
TA	***M. Tibialis-anterior***
TAE	**Tris-acetate-EDTA**
TCEP	***tris*(2-carboxyethyl) phosphine**
TGN	***trans*-Golgi network**
TRIM	**Tripartite motif containing**
UPS	**Ubiquitin proteasome system**
Vps	**Vacuolar protein sorting**
WB	**Western blot**

Acknowledgments

I would like to express my appreciation and thanks to PD Dr. med. Jens Fielitz for giving me the opportunity to work at his laboratory and be a part of a very interesting field of research.

I would like to acknowledge Dr. Gunnar Dittmar, Ph.D. and Dr. Rick Scavetta, Ph.D. for their collaboration and highly appreciated work.

Special thanks to my fellow labmates at the Fielitz lab for making my stay there a very pleasant one.

Statement of authorship/ Selbstständigkeitserklärung

I, Jida Hamati, hereby declare that I am the sole writer of this thesis. I have fully acknowledged and referenced the ideas and work of others, whether published or unpublished, and I did not use any other sources or aid other than those mentioned in the reference list.

Hiermit erkläre ich, die vorliegende Arbeit selbstständig und nur unter Zuhilfenahme der angegebenen Quellen und Hilfsmittel verfasst zu haben.
Ich erkläre, mich nicht anderwärtig um einen Doktorgrad beworben zu haben bzw. keinen entsprechenden Doktorgrad zu besitzen.
Ich habe die dem Verfahren zugrunde liegende Promotionsordnung der Mathematisch-Naturwissenschaftlichen Fakultät I der Humboldt-Universität zu Berlin zur Kenntnis genommen.

Berlin, June 2015 Jida Hamati